



NOVEL CONTACT SENSOR FOR LANDMINE  
DETECTION

by

Hussein Fouad Mohamed Ali

A Thesis Submitted to the  
Graduate School of Innovative Design Engineering,

Egypt-Japan University of Science and Technology (E-JUST)

In Partial Fulfillment of the Requirements for the Degree of  
Doctor of Philosophy

in

Mechatronics and Robotics Engineering

March 2016

# NOVEL CONTACT SENSOR FOR LANDMINE DETECTION

by

Hussein Fouad Mohamed Ali

For The Degree of

Doctor of Philosophy

in

Mechatronics and Robotics Engineering

## Supervisor Committee

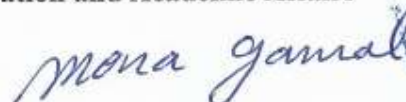
Name, Title	Affiliation	Signature, Date
1. Prof. Said M. Megahed (Main Supervisor)	Cairo University, Faculty of Engineering, Egypt	
2. Assoc. Prof. Ahmed M. R. Fath El-Bab (Co-Supervisor)	Egypt-Japan University of Science and Technology (E-JUST), Egypt	
3. Assoc. Prof. Zakarya A. Zyada (Co-Supervisor)	Tanta University, Egypt. Universiti Teknologi Malaysia, Malaysia.	

## Examination Committee

Name, Title	Affiliation	Approved, Date
1. Prof. Ahmed Elassal (Chief Examiner - External)	Banha University, Faculty of Engineering, Egypt	
2. Prof. Sohair Fathy Rezeka (External Examiner)	Alexandria University, Faculty of Engineering, Egypt	
3. Prof. Said M. Megahed (Main Supervisor)	Cairo University, Faculty of Engineering, Egypt	
4. Assoc. Prof. Ahmed M. R. Fath El-Bab (Co-Supervisor)	Egypt-Japan University of Science and Technology (E-JUST), Egypt	

Acting Vice President for Education and Academic Affairs

Prof. Mona Gamal Alddin





## **Declaration and Certificate of Originality**

I certify that in the preparation of this thesis, I have observed the provisions of E-JUST Code of Ethics dated 8 September 2013. Further; I certify that this work is free of plagiarism and all materials appearing in this thesis have been properly quoted and attributed.

I certify that all copyrighted material incorporated into this thesis is in compliance with the international copyright law and that I have received written permission from the copyright owners for my use of their work, which is beyond the scope of the law.

I agree to indemnify and save harmless E-JUST from any and all claims that may be asserted or that may arise from any copyright violation.

I hereby certify that the research work in this thesis is my original work and it does not include any copied parts without the appropriate citation.

Hussein Fouad Mohamed Ali

Signature: .....

Date: / /2016

## SUMMARY

Many places in the world are heavily contaminated with landmines, which cause that many resources are not utilized. Much recent research acknowledges that the contact sensors have promising potential for landmine detection. To guarantee reliable landmine sensing system, deep analysis and many test cases are required. The proposed concept is based on application of 1kPa external constant pressure (lower than the landmine activation pressure) to the sand surface. The resultant contact pressure distribution is dependent on the imbedded object characteristics (type and depth). Then Neural Networks (NN) is trained to find the inverse solution of the sand-landmine problem. In other words when the contact pressure is known, NN can estimate the imbedded object type and depth. In this work, using finite element modeling, the existence of landmines in sand is modeled, and analyzed. The resultant contact pressure distribution for five objects in sand at different depths is used in training NN. Three NN are developed to estimate the landmine characteristics. The 1st one is perceptron type which classifies the introduced objects in sand. The other two feed-forward-NNs are developed to estimate the depth of two landmine types. The NN detection rates of Anti-tank and Anti-personnel landmines are 100% and 67% in training, and 95% and 70% in validation, respectively. As test cases, the detection rates of the NN in case of landmine inclination angles ( $0^{\circ}$ - $30^{\circ}$ ) and random noises 10%-20% of the average signal are studied.

Also, this work introduces a new concept for landmine detection with contact sensor. The sensor main principle is based on the concept of 2-DOF vibration absorber system (two springs and two masses), to detect the existence of an object (ex: landmine) in sand which is modeled as a 3<sup>rd</sup> spring in the 2-DOF vibration absorber system. The sand stiffness (the 3<sup>rd</sup> spring stiffness  $k_o$ ) can be acquired as a function of the vibration absorber mode frequency  $\omega_{Abs}$  (the frequency at which the 2<sup>nd</sup> mass has the lowest amplitude (mathematically proven: zero)). When the sand stiffness changed due to the presence of the landmine, the vibration absorber frequency  $\omega_{Abs}$  changes, and consequently the landmine can be detected. The mathematical derivation of the ( $\omega_{Abs}$ - $k_o$ ) relation is verified by simulations with Matlab and finite element COMSOL Multi-physics. The system is succeeded to measure the sand stiffness up to 2 MN/m. A prototype for the sensor is developed with sensitivity 7.58 (N/m)/Hz at range of 200 N/m. Also, design procedure for the contact stiffness sensor for landmine detection is developed for selecting and optimizing the sensor parameters (masses and springs). Finally, feasibility study is developed for sensor fabrication with MEMS technology, including design and fabrication process.

To...  
My Father's Soul,  
My Mother,  
My Wife and My Sons  
Abd-Allah, Abd-Alrahman and Fatemah,  
My Brothers.

To...  
Prof. Ahmed Abo-Ismael Soul.

## ACKNOWLEDGMENT

First of all, and the foremost, **countless thanks to ALLAH.**

Secondly, I would like to give a heartfelt, special thanks to my supervisors Assoc. Prof. Ahmed Fath El-Bab, and Assoc. Prof. Zakarya Zyada. Their support, deep insights, patience, flexibility, genuine caring and concern, and faith in me enabled me to go ahead through-out the research. I am sure that whatever I have learned while working with them, will be very useful in my future endeavors.

Thirdly, I would like to express my deep sense of gratitude towards my supervisor Prof. Said Megahed for his expert guidance and constant support throughout the research.

Thanks for his fruitful advice relevant to my research.

Fourthly, Thanks to all my professors and colleagues in MTR Department E-JUST for useful discussion and cooperation through the lectures and the weekly seminars and all other issues.

Finally, I wish to express my grateful thanks to EJUST for supporting this research by this PhD scholarship.

Hussein Fouad

# TABLE OF CONTENTS

<b>CHAPTER 1 : INTRODUCTION</b>	<b>1</b>
1.1 Motivation	1
1.2 Problem Statement and Thesis Objectives	5
1.3 The Proposed System	6
1.4 Thesis Organization	6
<b>CHAPTER 2 : LITERATURE REVIEW</b>	<b>7</b>
2.1 The Landmine Problem in Brief	7
2.2 Robotic Research for Demining	7
2.3 Contact Sensors for Landmine Detection	8
<b>CHAPTER 3 : LANDMINE DETECTION BY MEASURING SURFACE PRESSURE DISTRIBUTION</b>	<b>15</b>
3.1 Background and Problem Definition	15
3.2 Material and Methods	17
3.2.1 The Landmine Activation Pressure	18
3.2.2 Finite Element Model	19
3.2.3 Neural Networks	20
3.2.4 The Simulation Work Procedure	21
3.3 Simulations and Results	23
3.3.1 Test Cases 1: Inclined Landmine	29
3.3.2 Test Cases 2: Noise Effect on Detection	35
<b>CHAPTER 4 : SENSOR DYNAMIC MODELING</b>	<b>37</b>
4.1 Vibration Analysis of Difference Sensor Architecture	38
4.1.1 Single DOF Sensor System	38
4.1.2 Two DOF Sensor System	39
4.1.3 Comparison between Single DOF and Two DOF Sensor Systems	46
4.2 Novel Sensor Description	47
4.3 Mathematical Derivation	48
4.4 Measuring Range of Sand-Landmine Problem	49

4.5	Parameters Selection Criterion Based on Vibration Absorber System	50
4.6	Modeling and Simulation	51
4.6.1	Mathematical Model	51
4.6.2	Finite Element model (with COMSOL Multiphysics)	53
4.6.2.1	The COMSOL Model	54
<b>CHAPTER 5 : SIMULATION RESULTS AND PARAMETER OPTIMIZATION</b>		<b>57</b>
5.1	Simulation Results	57
5.2	Parameter Optimization	59
5.3	Sensor Behavior with Optimum Parameter	61
5.4	Design Procedure of the Sensor	63
<b>CHAPTER 6 : EXPERIMENTAL RESULTS</b>		<b>65</b>
6.1	The Need of a Prototype	65
6.2	Sensor Prototype	66
6.3	Experimental Setup	67
6.4	Position Sensor Calibration	68
6.5	Specimens Preparations	71
6.6	Experiment #3	74
6.7	Experiment #4	78
<b>CHAPTER 7 : STUDY SENSOR FABRICATION WITH MEMS TECHNOLOGY</b>		<b>83</b>
7.1	Miniaturization Advantages	83
7.2	MEMS Design	84
7.3	Fabrication Process	85
<b>CHAPTER 8 : CONCLUSIONS AND FUTURE WORK</b>		<b>89</b>
8.1	Conclusions	89
8.2	Future Work	91
<b>REFERENCES</b>		<b>93</b>
<b>APPENDIX A: SENSORS TECHNOLOGIES COMPARISON</b>		<b>99</b>
<b>LIST OF PUBLICATIONS</b>		<b>103</b>



## LIST OF TABLES

<b>Table 3.1</b>	Landmines activation pressure calculations .....	19
<b>Table 3.2</b>	Perceptron NN (classification) training data analysis .....	27
<b>Table 3.3</b>	Perceptron NN (classification) validation data analysis .....	28
<b>Table 3.4</b>	Feed forward NN training and validation, Root mean Square of Error .....	29
<b>Table 3.5</b>	Inclination effect on alarm rate .....	32
<b>Table 3.6</b>	LM01 inclination effect on depth detection .....	33
<b>Table 3.7</b>	LM02 inclination effect on depth detection .....	34
<b>Table 3.8</b>	Perceptron NN (classification) validation data analysis plus random noises 10%, 20% of each signal average .....	35
<b>Table 3.9</b>	Inclination effect on alarm rate with signal noises 5%, 10%, 20% .....	36
<b>Table 4.1</b>	Comparison between 1 DOF and 2 DOF sensor systems .....	46
<b>Table 4.2</b>	Typical values of Young's modulus for granular material (MPa).....	50
<b>Table 4.3</b>	Typical values of Young's modulus for cohesive material (MPa).....	50
<b>Table 5.1</b>	Parameter $k_l$ changes effect on sensitivity and linearity .....	60
<b>Table 6.1</b>	Calibration results .....	69
<b>Table 6.2</b>	Experiment #3 –Specimens stiffness calculations .....	72
<b>Table 6.3</b>	1 <sup>st</sup> resonance frequency change with stiffness $k_o$ .....	76
<b>Table 6.4</b>	Vibration absorber frequency change with stiffness $k_o$ .....	76
<b>Table 6.5</b>	2 <sup>nd</sup> resonance frequency change with stiffness $k_o$ .....	77
<b>Table 6.6</b>	Objects test.....	78
<b>Table 7.1</b>	Cantilever dimensions options to satisfy stiffness $k_l=1.14 \times 10^5$ N/m .....	85
<b>Table A.1</b>	Summary of the Detection Technologies Reviewed .....	99

## LIST OF FIGURES

<b>Figure 1.1</b>	Anti-Tank Landmine [1].....	1
<b>Figure 1.2</b>	Human deminer tools [4].....	2
<b>Figure 1.3</b>	Sensor fusion concept [4, 6] .....	3
<b>Figure 1.4</b>	Robotic Systems used in demining research .....	3
<b>Figure 1.5</b>	The proposed 2-DOF vibration absorber system for stiffness detection .....	6
<b>Figure 2.1</b>	Robotic systems prototype designed to mimic human deminer main movement .	8
<b>Figure 2.2</b>	Configuration of a Pogo-Stick ground-contacting vibrometer [35] .....	10
<b>Figure 2.3</b>	Structure of a prototype of prodder and modeling of Anti-Personnel landmine and prodder (no-soil model) [37].....	11
<b>Figure 2.4</b>	The ground as a single-DOF system. Input force by Electrodynamic shaker [42] .....	12
<b>Figure 3.1</b>	Rolling Cylinder with pressure mat.....	16
<b>Figure 3.2</b>	Finite element models of sand-landmine.....	17
<b>Figure 3.3</b>	Anti-tank MK7 noted as ‘LM01’, Anti-Personnel noted as ‘LM02’, TIN200, ROCK200, and sandonly .....	18
<b>Figure 3.4</b>	Flowchart of forward and inverse approaches.....	21
<b>Figure 3.5</b>	Surface pressure (Pa) Sand only plus random noise with 5% of the average, repeated for same number.....	24
<b>Figure 3.6</b>	Surface pressure (Pa) when LM01 at depths: (from 5 mm to 205 mm with step 5mm).....	24
<b>Figure 3.7</b>	Surface pressure (Pa) when LM02 at depths: (from 5 mm to 205 mm with step 5mm).....	25
<b>Figure 3.8</b>	Surface pressure (Pa) when TIN 200 at depths: (from 5 mm to 205 mm with step 5mm).....	25
<b>Figure 3.9</b>	Surface pressure (Pa) when Rock 200 at depths: (from 5 mm to 205 mm with step 5mm).....	26
<b>Figure 3.10</b>	Perceptron NN: Designed to detect the object type.....	27
<b>Figure 3.11</b>	Feed forward NN: Designed to detect the object depth.....	28
<b>Figure 3.12</b>	Inclined Landmine effect for LM01 and LM02 .....	30
<b>Figure 3.13</b>	Inclined Landmine effect for LM01 .....	33
<b>Figure 3.14</b>	Inclined Landmine effect for LM02 .....	34
<b>Figure 4.1</b>	Single DOF sensor System .....	38

<b>Figure 4.2</b> Two DOF sensor system.....	39
<b>Figure 4.3</b> Accerlation Amplitudes and ratio versus at higher excitation frequency range 550-950 Hz and at $K_1 = 4$ MN/m and $m_1 = 4$ gm .....	41
<b>Figure 4.4</b> Accerlation Amplitudes and ratio versus at lower excitation frequency range 50-550 Hz and at $K_1 = 4$ MN/m and $m_1 = 40$ gm.....	42
<b>Figure 4.5</b> Accerlation Amplitudes and ratio versus at lower range of $k_1$ with excitation frequency 50 Hz and at $K_2 = 4$ MN/m and $m_1 = 40$ gm.....	43
<b>Figure 4.6</b> Accerlation Amplitudes and ratio versus at higher range of $k_1$ with excitation frequency 50 Hz and at $K_2 = 4$ MN/m and $m_1 = 40$ gm.....	44
<b>Figure 4.7</b> Accerlation Amplitudes and ratio versus at lower range of $k_1$ with excitation frequency 380 Hz and at $K_1 = 400$ kN/m (softer), $K_2 = 4$ MN/m(harder) and $m_1 = 40$ gm.....	45
<b>Figure 4.8</b> Sensor physical model and free body diagram.....	47
<b>Figure 4.9</b> Indentation model parameters. ....	49
<b>Figure 4.10</b> Flow chart of the mathematical model algorithm.....	51
<b>Figure 4.11</b> Frequency response of $x_2, x_1$ at certain ground stiffness $k_o$ values, and the corresponding vibration absorber frequency $\omega_{Abs}$ .....	52
<b>Figure 4.12</b> Frequency response at certain ground stiffness $k_o$ values, and the corresponding vibration absorber frequency $\omega_{Abs}$ . ....	52
<b>Figure 4.13</b> Piezo-electric version of the proposed sensor .....	53
<b>Figure 4.14</b> Finite element COMSOL model 2D beam model, load and boundary constrains .....	54
<b>Figure 5.1</b> Linearity of the relation between $\omega_{Abs}$ - $k_o$ (finite element model) $k_o$ range (0 – 2 MN/m) at ( $n = 1, k_1=1.78$ kN/m). ....	58
<b>Figure 5.2</b> Sensor frequencies when changing stiffness $k_o$ at ( $n=1, k_1=1.78$ kN/m).....	58
<b>Figure 5.3</b> Optimization based on the sensor stiffness $k_1$ . ....	60
<b>Figure 5.4</b> Optimum Sensor frequencies change when changing stiffness $k_o$ Range (0-2 MN/m) at ( $n = 4, k_1=1.14 \times 10^5$ N/m).....	61
<b>Figure 5.5</b> Finite element COMSOL model responses at ground stiffness $k_o = 10^5$ N/m and ( $n = 4, k_1=1.14 \times 10^5$ N/m).....	62
<b>Figure 5.6</b> Optimum design comparison between the theoretical results and finite element results for stiffness $k_o$ range (0 – 2 MN/m) at ( $n = 4, k_1=1.14 \times 10^5$ N/m).....	63
<b>Figure 6.1</b> PIEZO SYSTEMS: D220-A4-503YB and T434-A4-201 .....	65
<b>Figure 6.2</b> Sensor Prototype.....	66
<b>Figure 6.3</b> Experimental setup .....	67

<b>Figure 6.4</b>	Calibration experimental setup .....	68
<b>Figure 6.5</b>	Eddy current position sensor calibration curve .....	70
<b>Figure 6.6</b>	Universal Laser Cutting Machine.....	71
<b>Figure 6.7</b>	Twenty specimens fabricated with widths from 2.5 mm to 22.5 mm, with step 2.5 mm. ....	73
<b>Figure 6.8</b>	5mm width specimen fixed in the final stiffness sensor setup .....	73
<b>Figure 6.9</b>	Oscilloscope output no excitation exist, noise only exist.....	74
<b>Figure 6.10</b>	Oscilloscope output at $k_o=0$ , and with excitation at 1 <sup>st</sup> resonance mode.....	75
<b>Figure 6.11</b>	Experiment #3, all the specimens are form same fabrication conditions .....	77
<b>Figure 6.12</b>	Test object 1, Sponge.....	78
<b>Figure 6.13</b>	Test object 2, leafs .....	79
<b>Figure 6.14</b>	Test object 3, Anti-Personnel (LM02).....	79
<b>Figure 6.15</b>	Test object 4, Sand from the sea coast.....	80
<b>Figure 6.16</b>	Test object 5, Sand and metal on the surface .....	80
<b>Figure 6.17</b>	Test object 6, Clay from Borg Alarab .....	81
<b>Figure 6.18</b>	Test object 1, Metal part below clay.....	81
<b>Figure 7.1</b>	Layout 1 of the proposed sensor in MEMS.....	84
<b>Figure 7.2</b>	Layout of the proposed sensor in MEMS with dimensions.....	86
<b>Figure 7.3</b>	Schematic representation proposed sensor in MEMS. ....	86
<b>Figure 7.4</b>	Fabrication process flow of stiffness sensor based on vibration absorber .....	87

## NOMENCLATURE

$d$	The indentation depth inside certain material, mm
$E$	The Young's Modulus of certain material, Pa
$f_u$	The applied force to the second mass, N
$F_u$	The amplitude of the applied force, N
$h$	The height of certain material, mm
$L_c$	The length of a cantilever, mm
$k_o$	The stiffness coefficient of sensed object, N/m
$k_1$	The first stiffness coefficient of the sensor, N/m
$k_2$	The second stiffness coefficient of the sensor, N/m
$m_1$	The first mass of the sensor, kg
$m_2$	The second mass of the sensor, kg
$t$	The height (thickness) of a cantilever, mm
$w$	The width of a cantilever, mm
$\nu$	The Poisson's ratio of certain material,
$\omega$	The applied frequency to the second mass, Hz
$\omega_1$	The first natural frequency, Hz
$\omega_2$	The second natural frequency, Hz
$\omega_{11}$	$\sqrt{k_1/m_1}$ , Hz
$\omega_{22}$	$\sqrt{k_2/m_2}$ , Hz
$\omega_{Abs}$	The frequency at which that vibration absorption phenomenon occurs, Hz

## ABBREVIATIONS

<b>APL</b>	<b><u>A</u>nti-<u>P</u>ersonnel <u>L</u>andmines</b>
<b>ATL</b>	<b><u>A</u>nti-<u>T</u>ank <u>L</u>andmines</b>
<b>COTS</b>	<b><u>C</u>ommercial <u>O</u>ff-<u>T</u>he-<u>S</u>helf</b>
<b>DOF</b>	<b><u>D</u>egree <u>O</u>f <u>F</u>reedom</b>
<b>ERW</b>	<b><u>E</u>xplosive <u>R</u>emnants of <u>W</u>ar</b>
<b>FDTD</b>	<b><u>F</u>inite <u>D</u>ifference <u>T</u>ime <u>D</u>omain</b>
<b>FFNN</b>	<b><u>F</u>eed <u>F</u>orward <u>N</u>eural <u>N</u>etworks</b>
<b>GICHD</b>	<b><u>G</u>eneva <u>I</u>nternational <u>C</u>enter for <u>H</u>umanitarian <u>D</u>emining</b>
<b>GPR</b>	<b><u>G</u>round <u>P</u>enetration <u>R</u>adar</b>
<b>HW</b>	<b><u>H</u>ard<u>w</u>are</b>
<b>IMAS</b>	<b><u>I</u>nternational <u>M</u>ine <u>A</u>ction <u>S</u>tandards</b>
<b>MD</b>	<b><u>M</u>etal <u>D</u>etector</b>
<b>NN</b>	<b><u>N</u>eural <u>N</u>etworks</b>
<b>Pk-Pk</b>	<b><u>P</u>ea<u>k</u> to <u>P</u>ea<u>k</u> amplitude</b>
<b>PNN</b>	<b><u>P</u>erceptron <u>N</u>eural <u>N</u>etworks</b>
<b>REST</b>	<b><u>R</u>emote <u>E</u>xplosive <u>S</u>cent <u>T</u>racing</b>
<b>RMSE</b>	<b><u>R</u>oot <u>M</u>ean <u>S</u>quare <u>E</u>rror</b>
<b>SW</b>	<b><u>S</u>oft<u>w</u>are</b>
<b>UXO</b>	<b><u>U</u>ne<u>X</u>ploded <u>O</u>rdnances</b>
<b>UNDHA</b>	<b><u>U</u>nited <u>N</u>ation <u>D</u>epartment of <u>H</u>uman <u>A</u>ffairs</b>
<b>UNDP</b>	<b><u>U</u>nited <u>N</u>ations <u>D</u>evelopment <u>P</u>rogramme</b>

# CHAPTER 1 : INTRODUCTION

## 1.1 Motivation

According to the International Campaign to Ban Landmines and the Civil Right Organization: “a Landmine is some object placed on or under the ground or any surface, conceived for exploding by the simple fact of the presence, the proximity or the contact of a person or a vehicle”[1]. As an example: Anti-Tank landmine is shown in Figure 1.1.

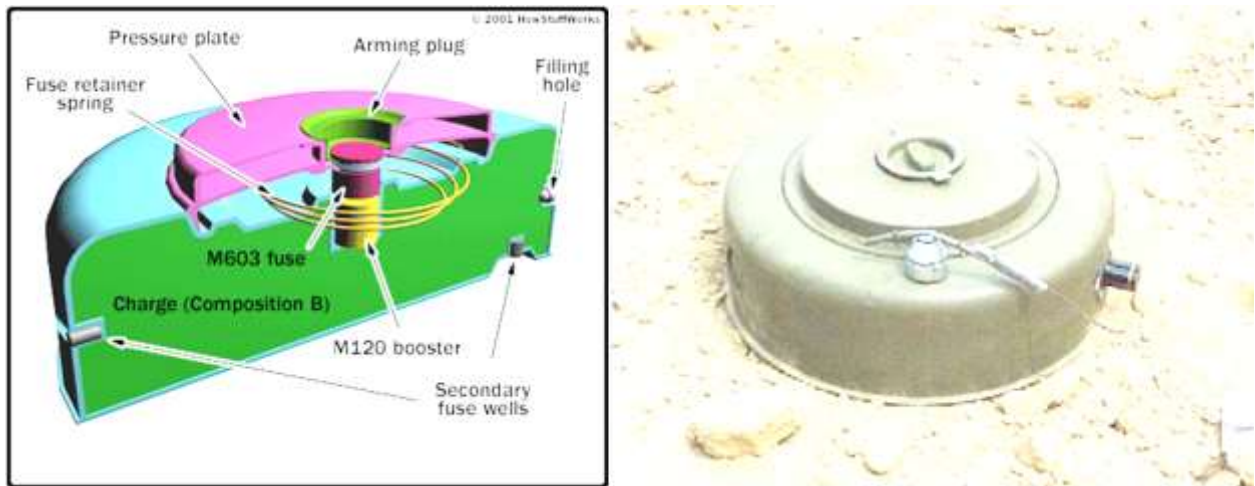


**Figure 1.1:** Anti-Tank Landmine [1]

Landmines cause major problems, waste life and money. Many places in the world are heavily contaminated with landmines, which cause that many resources are not utilized. This makes landmine detection and removal are challenging subjects for research. Much recent research acknowledges that the contact sensors have promising potential. In the last few years, the landmine problem becomes one of the hottest research areas. Through decades of wars spread in the world, huge areas are infected with Landmines, ERW and UXO. Egypt is considered one of the most infected countries. It is infected with about 21% of the landmines in the world [2].

Today’s demining is based mainly on deminers (humans). Every detected signal takes unpredictable duration. Some manual demining tools is shown in Figure 1.2. Deminer interacts very close to the examined object, because the manual demining is the only reliable technique. And with regular, difficult deminers training and good supervision, it is still not

safe method because of the limited equipment. Also, its basic limitation is the difficulty and the time-consuming, caused by the high amount of metal elements in the soil. These facts, together with the possibility that deminers may find no landmine for days and weeks which may induce tiredness, inattention, boredom and also mistakes. But all these factors are besides demining highly undesirable [2].

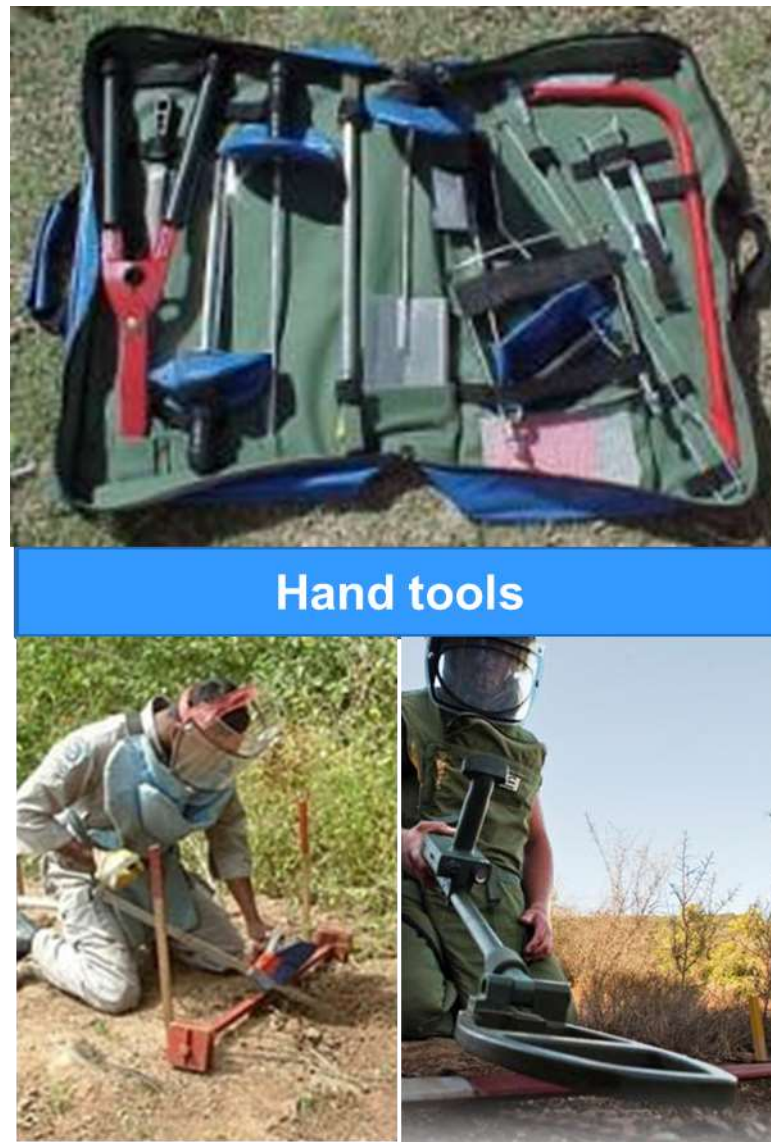


**Figure 1.2:** Human deminer tools [4]

The landmine detection sensors are the most costive and critical issue in the demining process and research [3, 4]. Each sensor has its operating principles, strengths, limitations, and potential for humanitarian landmine detection. Many experts studied the advantages and disadvantages of the sensors technologies. Result that the Acoustic/seismic sensor and contact sensors have promising potential for Humanitarian Demining [5].



The most well-known technologies are based on the electromagnetic waves (Electromagnetic induction Metal Detector (MD), Magnometers, Ground Penetration Radar (GPR)) [4, 5, 6]. Two main directions in demining research:

1st: is the detection technique: GPR, MD, Gas Sensor, etc. Each sensor has detection capability and limitation. The integration between the good capabilities (sensor fusion), as shown in Figure 1.3, can give higher detection and lower false alarm rate. Due to the problem complexity, many researches are conducted to gain the best of each sensor and consider in the final decision. This technique is named sensors fusion. Sensor fusion methods can be classified to hardware sensor fusion and software sensor fusion [7].

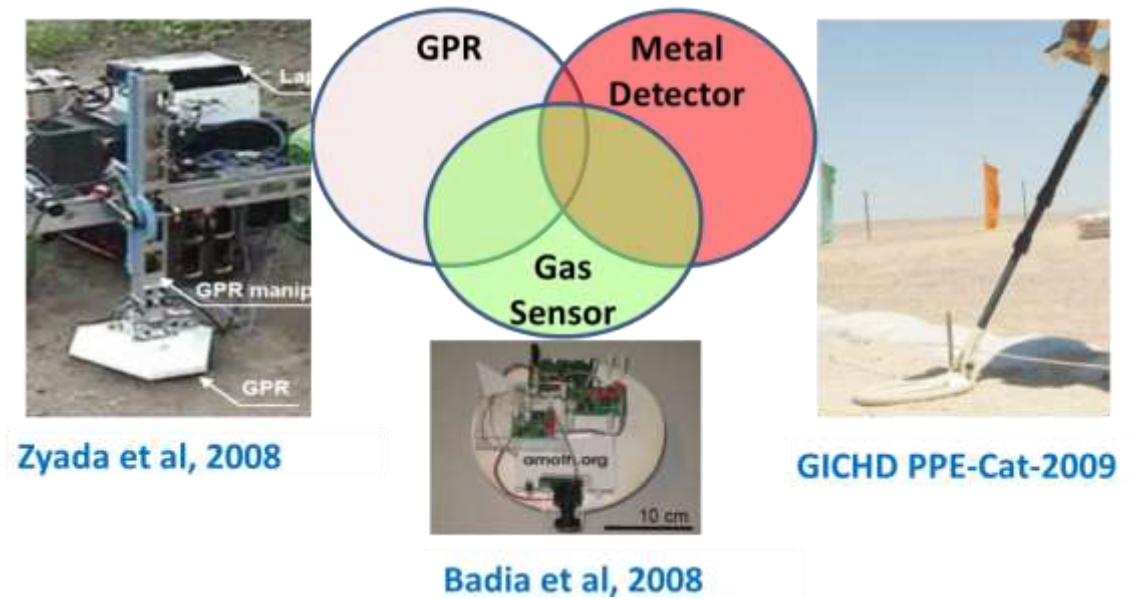


**Figure 1.3:** Sensor fusion concept [4, 6]

2nd: is the vehicle contact pressure with the ground, (minimizing the weight of the moving part and maximizing the contact area if there is a contact). This is dramatically impact the design of the Locomotion system: mobile robot, snake robot, balloon, quad-rotor, etc. as shown in Figure 1.4.



**Figure 1.4:** Robotic Systems used in demining research

The Humanitarian Demining Standards for clearance success must satisfy 99.6% at 200 mm depth (according to United Nation Department of Human Affairs (UNDHA)) and 100% (according to International Mine Action Standards (IMAS)). To satisfy high grade, until now, this relies on manual procedure (that uses 'prodding' or 'probing' excavation tool) [6]. This is why, Acoustic/Seismic and smart prodding are considered of the most promising technologies as they have low false alarm, properties feedback [5].

## 1.2 Problem Statement and Thesis Objectives

The literature review in landmine detection shows that, the main problem can be defined as there are many uncertainties in the environment which significantly impact the detection possibility with certain type of sensors. It is important for a multi-sensor system to utilize the benefit of each sensor to gain the information (presence of a Landmine and not any other metal scrape or rocks). In order to satisfy the Humanitarian Demining Standards manual demining is mandatory. In literature, it is found that the smart 'prodding' or 'probing' tools are promising as they have Low false alarm, and properties feedback. This research focuses on contact sensors modeling and design and experimental analysis. A Novel contact sensor design is presented to detect the stiffness of the object based on shock absorber like model (2 masses 3 springs).

Firstly, literature review and survey about the demining complications, the landmine detectors will be done. Then sensor selection based on the criteria justified in the literature survey. Secondly, finite element analysis will be executed for sand-landmine model. Thirdly, sensors models based on vibration response will be investigated. Fourth, a comparison will be held between simulation and experimental validation of the proposed sensor model. Finally, Feasibility study about developing a micro scale sensor by MEMS technology.

The primary objectives of this thesis research are:

- 1- Survey and review the detection technologies and the working principle. Select the high potential sensors set appropriate in research.
- 2- Development of Finite Element analysis for sand-Landmine model using COMSOL when applying static loading (constant pressure).
- 3- Neural Networks training for different Landmine parameters, e.g.: type and depth in sand.
- 4- Design Procedure for Landmine sensor using tactile sensor or the Surface-Contacting Vibration based.
  - Contact sensor models comparison based on vibration response.
  - Propose contact sensor model based on vibration absorber like (2 masses 3 springs).
- 5- Sensor model testing with the sand-Landmine model with finite element using COMSOL.
- 6- Design, fabrication and testing of the sensor.
- 7- Experimental measurements for different sand-landmine situations using macro scale sensor prototype.
- 8- Study the development of a micro scale sensor by MEMS technology.

### 1.3 The Proposed System

In this thesis a new contact sensor is presented and investigated in static loading and dynamic loading analytically, numerically with finite element method and experimentally. A Neural Networks is used to detect the landmine type. Also inclined landmines and added noises are investigated. The thesis presents novel contact stiffness sensor has been introduced with a detailed design procedure for landmine detection, based on the concept of 2-DOF vibration absorber system. It consists of two springs and two masses, to detect a third spring (landmine presence in sand) as shown in Figure 1.5. The goal was to model and design contact sensor for landmine detection precisely in a cheap way.

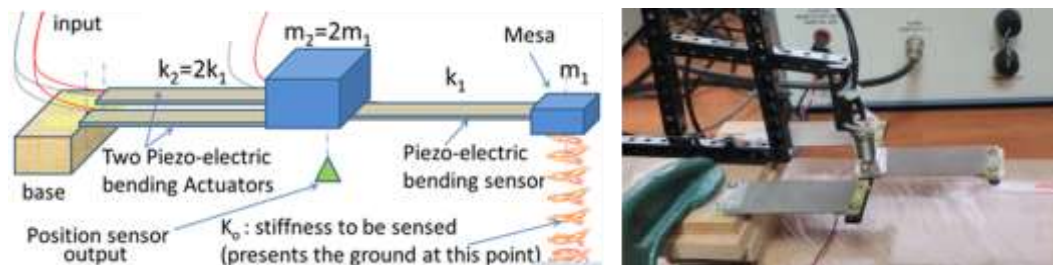


**Figure 1.5:** The proposed 2-DOF vibration absorber system for stiffness detection

### 1.4 Thesis Organization

**Chapter 1** introduces the Landmine problem. The main problem statement and thesis objectives are also listed followed by thesis organization. **Chapter 2** presents an overview of the problem standard solutions and similar research work in the literature. **Chapter 3** describes the Sand-landmine model, when applying static loading (constant pressure to the surface) in some situations. The resultant pressure distribution at the ground surface is used in NN training and validation, to classify the buried object and detect its depth. **Chapter 4** studies the application of dynamic loading (sinusoidal input). It compares the mathematical relation of the ground stiffness  $k_0$  in two case single DOF sensor model and two DOF sensor model. Also it presents a Novel Contact Sensor Prototype using 2-DOF Vibration Absorber for Landmine Detection model. Mathematical derivation, theoretical simulations (using Matlab) and finite element studies (using COMSOL Multi-physics) are also included in this chapter. **Chapter 5** presents the results and parameter optimization processes for the proposed sensor model presented in chapter 4. **Chapter 6** presents the details of the experimental prototype system used in this work for the verification and validation of the proposed sensor model presented in chapter 4. **Chapter 7** presents the MEMS design for the proposed sensor in chapter 4. **Chapter 8** concludes the thesis with the suggestion for the future works.

## **CHAPTER 2 : LITERATURE REVIEW**

### **2.1 The Landmine Problem in Brief**

Landmines have very harmful effect on many regions in the world, as they limit the development and increase the danger in such regions. More than 100 countries are affected by Landmines, Unexploded Ordnances (UXO), and Explosive Remnants of War (ERW). About 20 countries are heavily-affected, like that in Egypt from World War II (1939-1945) [2]. Sensors are the most critical and costive issue in the landmine detection process [3]. Many sensing technologies and studies were introduced. The most mature technologies are based on the electromagnetic waves [4] (like Electromagnetic induction metal detector (MD), magnometers, and Ground Penetration Radar (GPR)) [5]. Due to the problem complexity, many research works are conducted to gain the benefit from more than one sensor and consider in the final decision, through their fusion. Sensor fusion methods can be classified into hardware fusion and software fusion [6]. For that, two studies are considered with fuzzy logic principles in order to select suitable sensors for the sand-landmine case [7]. Most of the presented sensors are contactless sensors. However, it is expected that, through the advances in MEMS, light-weight ground-contact sensors will be introduced to detect landmines.

### **2.2 Robotic Research for Demining**

Sensor should be operated remotely due to the field dangers. Dawson-Howe and Williams [8] introduced a new approach to detect of anti-personnel landmines in a similar way to that employed by human deminers. Their approach is based on the physical detection of landmines using a sharp ended probe. The proposed solution is a robot capable of performing the probing task. The probe is connected to a force sensor which is connected to a linear actuator which is connected to the XY table using a 30 degree angle bracket. This system is capable to position the probe over the experiment area. Furihata and Hirose [9] proposed two mechanical master-slave hands to remove landmines. Mine Hand-1 (with 7 DOFs) is simple to operate but heavy, and Mine Hand-2 (with 5 DOFs) is light weight, simple design and robust for average landmines. The contact here is also based on force

sensor. Megahed and Ali [10 ,7] developed mobile robot prototype with arm for remote demining operations. The arm is designed to mimic the basic movements of human deminers (3 DOFs: RPP), and a wireless camera with (4 DOFs: RPRR), as shown in Figure 2.1. They used metal detector at first.



**Figure 2.1:** Robotic systems prototype designed to mimic human Deminer main movement

### **2.3 Contact Sensors for Landmine Detection**

Prodding is one of the most common methods used by deminers to distinguish the main cause of detected signal by a metal detector or any other systems [3]. Different sensing techniques are utilized, for example: accelerometric, piezoelectric, acoustic and ultrasonic.

Some Prodders sensing techniques are based on acceleration measurements. A system with multiple probes is introduced, where each one is equipped with a spring and an accelerometer to directly measure vibrations deriving from contact with objects [11].

Also Prodders with piezoelectric transducers are also utilized for material recognition. In the approach developed by the University of Catania a tactile piezoelectric sensor touches the surface of a material so it can be detect a response signal related to the physical

characteristics of the stimulated material. Experimental prototypes have been developed, and evaluated for different materials like stone, glass, iron, wood and plastic [12, 13, 14].

Acoustic sensing prodders are based on acoustic microphone. In this case the microphone is employed as sensor for registering vibrations coming from the tip contact with the material. When the prodder tip touches the object, the vibrations generated are acquired by the microphone, and recorded using a PC sound card. The acoustic microphone has been integrated in a simple prodder as sensor so that a waveguide for transmitting the pulse is unnecessary. The experiments were performed evaluating four different materials: wood, plastic, iron, and stone [15, 16]. Based on this principle, is the first version of SmartProbe™ [17]. Improved versions including force sensors as feedback elements have been developed as the Instrumented Prodder by HF Research Inc. , that provided good results [18] , However extensive tests conducted by TNO-FEL have shown that the identification is not reliable when test conditions change [19, 20]. In the patents [21] and [22] the acoustic prodder is instrumented with a force feedback mechanism. Other researches involved the development of rotary prodders to improve penetration into the soil, or prodder equipped via a microphone to give feedback of the contact sound to the operator [23], [24], or prodder that give a sound to the operator when the force is exceeding a given threshold [25].

In Ultrasonic based prodders, which augment ultrasonic sensor (as a recognition strategy), the prodder tip is considered a guide for both transmitting the ultrasonic wave and receiving reflected energy from the contact point with the buried target material. The experimental tests were held with different materials (steel, stone, plastic) and acquired data were divided into two sets: one for “training” and the other for “testing” in order to train and validate the classifier [26], [27].

Contact accelerometers are utilized to detect vibration of soil-mine system excited by an acoustic source (airborne excitation like a loudspeaker). Contact sensor type MMA7260QT has been chosen considering the high sensitivity and the z-axis frequency response. By the spectral analysis of the soil acceleration signals is possible to estimate features characteristic of the vibration of a compliant case and possibly to distinguish from the presence of non-compliant objects compliant (i.e. stone, root or debris) [28].

Donskoy et al. [29-32] studied the nonlinear response of the 2-DOF model of the soil-mine system. The perturbation method used in the model introduces for the derived analytical solution to describe both quadratic and cubic acoustic interactions at the soil-mine interface. This solution has been compared with actual field measurements to obtain the nonlinear parameters of the buried mines, which have been analyzed with respect to mine types and

burial depths. It was found that the cubic nonlinearity could be a significant contributor to the nonlinear response. This effect has led to develop a new intermodulation detection algorithm based on dual-frequency excitation.

Many concepts have been introduced based on contact Acoustic/Seismic sensor. Schröder et al. [33] studied the elastic-wave interactions with landmines using finite difference method. Martin et al. [34-36] also studied the elastic-wave interactions with landmines and investigated 2-DOF model of surface-contacting vibrometer. Ground excitation is based on remote source while the moving vibrometer measures the associated ground surface motion, which is affected by the buried landmine when exists. Experimental model and surface-contacting vibrometer for seismic landmine are produced, as shown in Figure 2.2. The main limitation is that the elastic-wave decays exponentially with the sensor distance from the excitation source.

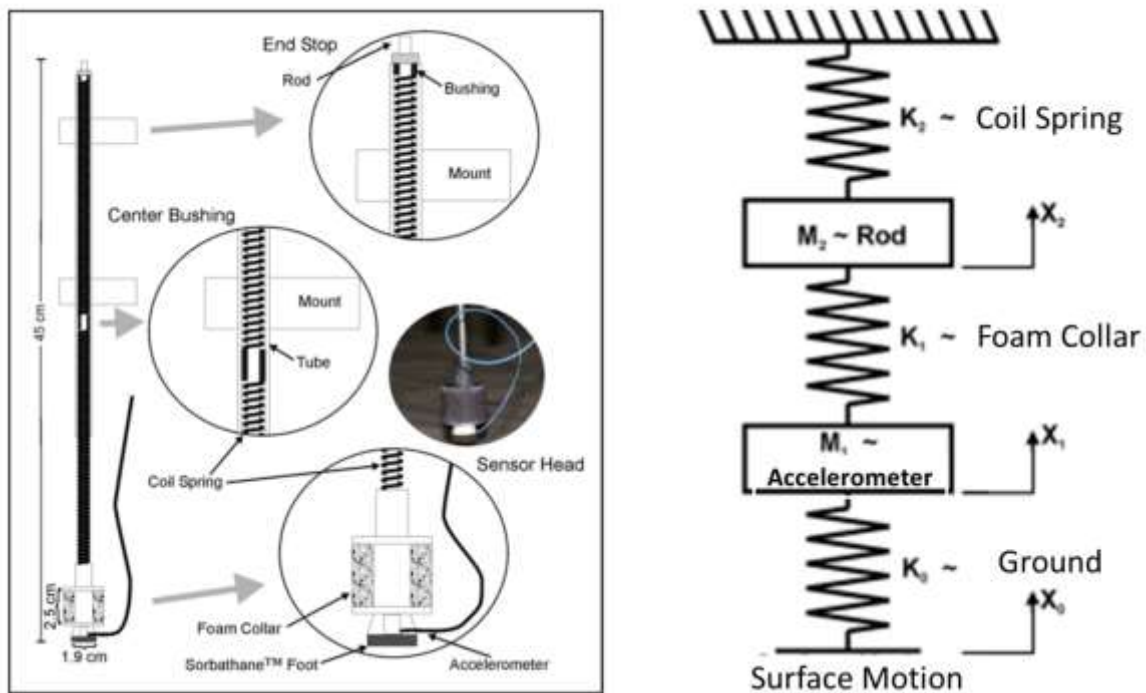


**Figure 2.2:** Configuration of a Pogo-Stick ground-contacting vibrometer [35]

Ishikawa and Iino [37] have proposed active sensing prodder (2-DOF model as shown in Figure 2.3) that emits white Gaussian noise vibration to identify the object in front of the pointed tip of the prodder by the frequency response and discrete Fourier transform. The main complication that the parameters:  $k_2$ ,  $k_3$ ,  $d_2$ ,  $d_3$  must be estimated. The system could not distinguish clearly among brass, aluminum and some landmines, even though it has a good potential.



Baglio et al. [38] stated from the state of the art and several discussions made with demining agencies, that an intelligent prodder is a useful device. But the developed instrumented prodders are usually expensive with respect to the reliability level required in the demining process.

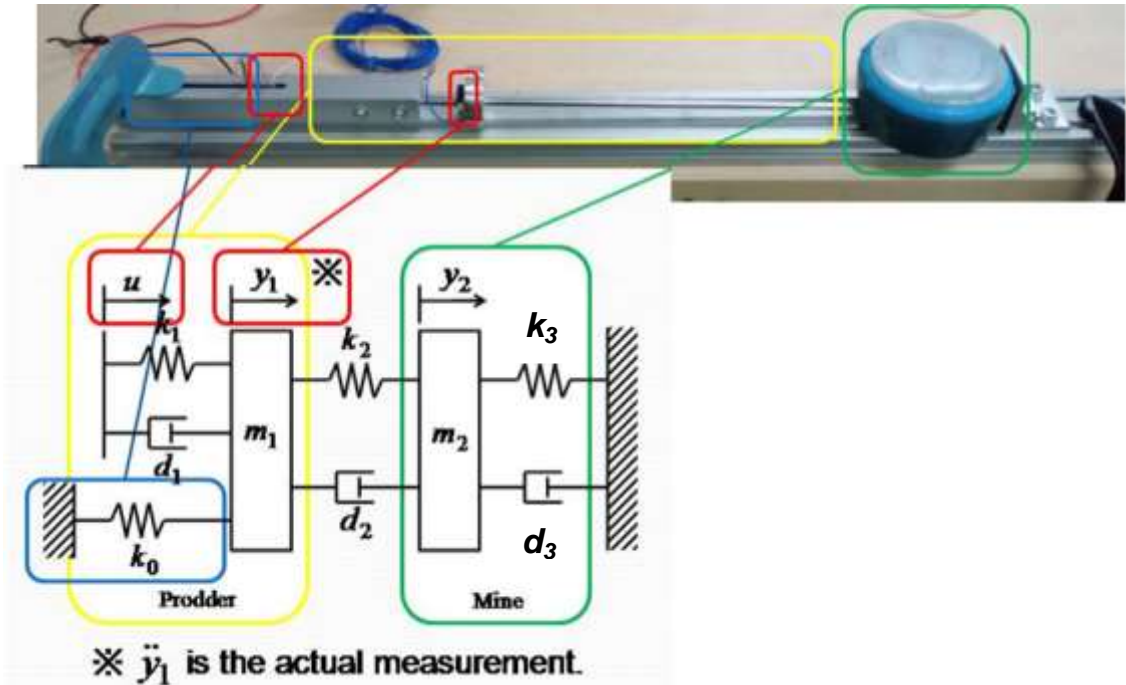


**Figure 2.3:** Structure of a prototype of prodder and modeling of Anti-Personnel landmine and prodder (no-soil model) [37].

Baglio et al.[39-41] introduced a novel smart prodder with sensor feedback. The surface of the object is excited and its response is measured with a pair of piezoelectric transducers. The system consists of four parts:

- 1) A sliding steel rod, chassis and other elements compose the mechanical system.
- 2) Two piezoelectric transducers, used for actuation and sensing.
- 3) A force sensor, used to monitor the applied force to solicit the objects.
- 4) An inclinometer, to monitor the angle at which the prodder is used.

To detect several materials, two different experimental prototypes of the tactile sensing system have been investigated and their performances have been characterized. A smart tactile measuring system, based on suitable signal processing strategies and fuzzy classification methodology, has been developed.

Muggleton et al. [42] explored point vibration measurements in order to detect shallow-buried objects. The ground itself is modeled as single DOF at low frequency as shown in Figure 2.4. A shaker is used to excite the ground vertically and has a built in

impedance head which senses both the applied force and the measured acceleration. They used the resonance frequency and acceleration to detect buried pipes. Mechanical fatigue could occur at resonance.

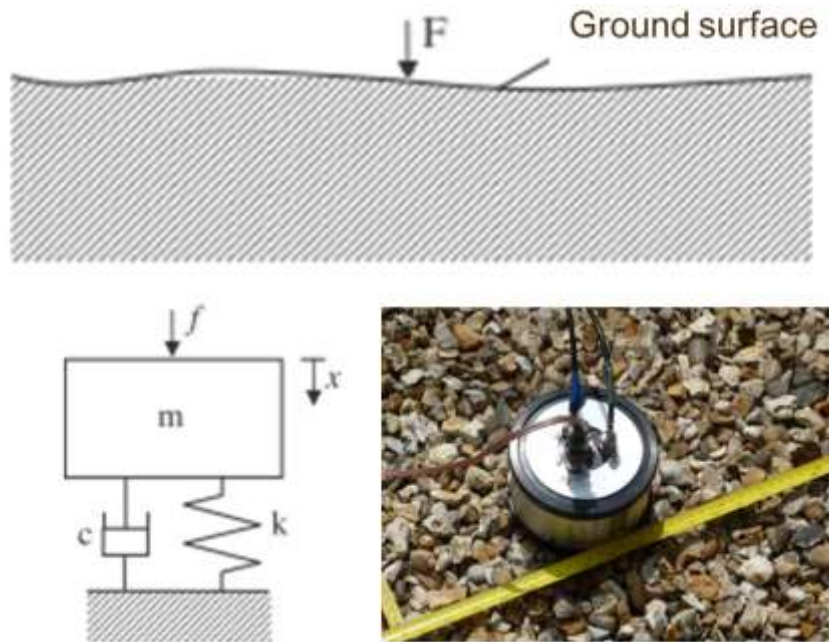


**Figure 2.4:** The ground as a single-DOF system. Input force by Electrodynamic shaker [42]

A finite element modelling tool, COMSOL Multi-physics has suitable user interface and capabilities to couple many physics with facilities. Contact pressure modelling with COMSOL is verified analytically [43]. The structural mechanics module supports contact boundary conditions using contact pairs. The contact boundary pair comprises a flat boundary and a curved boundary. A comparison with theoretical and experimental results is tabulated in [44]. In this work, 2D modelling for the sand-landmine is presented using COMSOL Multi-physics.

Artificial intelligent techniques such as Fuzzy Logic (FL), Particle Swarm Optimization (PSO) and Neural Networks (NN) can be used to extract nonlinear relations. The PSO algorithm is coupled to Finite Elements analysis to identify a buried object from its ElectroMagnetic Induction (EMI) signature [45]. Fuzzy logic is applied for automatic landmine detection based on the GPR volumetric data [46]. In this work, three NNs are trained and applied to detect landmines.

In the inverse problem solution of landmine presence using electromagnetic, several studies have been undertaken in the frequency domain [47, 48] as well as in the time domain [49, 50]. In [50] a separated GPR aperture sensor method is applied to detect buried targets by evaluating and comparing the electromagnetic coupling between the transmitting and

receiving antennas, by using Finite Difference Time Domain (FDTD) for electromagnetic simulation.

Most of the present research work in landmine detection is carried out while the landmine is in normal configuration, (without inclination). However, in a real situation, landmine position and inclination may be changed because of environmental conditions. Few works are available in the literature for examining landmines inclination angles effect on the detection rate. Nishimoto et al. [51] presented the effects of ground surface roughness, soil inhomogeneity and target inclination on the classification performance of landmines. However, the deteriorated results of inclined targets assure the need for more analysis. In this work, the landmine characteristics are modeled using finite element models and estimated using NN with test cases and analysis.



## **CHAPTER 3 :    LANDMINE DETECTION BY MEASURING SURFACE PRESSURE DISTRIBUTION**

This chapter presents an essential study of landmine presence inside sand through sand-landmine model affected by external pressure loading. The proposed concept is based on the application of 1 kPa external constant pressure (lower than the landmine activation pressure) to the sand surface. The resultant contact pressure distribution is dependent on the imbedded object characteristics (type and depth). Then Neural Networks (NN) is trained to find the inverse solution of the sand-landmine problem. In other words when the contact pressure is known, NN can estimate the imbedded object type and depth. In this work, using finite element modeling, the existence of landmines in sand is modeled, and analyzed. The resultant contact pressure distribution for five objects (1-Anti-tank, 2-Anti-Personnel, 3-Tin with diameter of 200mm and height of 200mm, 4-Spherical rock with 200mm diameter, and 5-Sand without any object) in sand at different depths is used in training NN. Three NN are developed to estimate the landmine characteristics. The 1<sup>st</sup> one is perceptron type which classifies the introduced objects in sand. The other two feed-forward-NNs are developed to estimate the depth of two landmine types.

### **3.1 Background and Problem Definition**

Landmines are spreading in many areas in the world. Due to landmines the development plan of such areas is canceled or postponed. Simple and cheap techniques for landmine detection with lower false alarms are needed. FDTD method is used to generate inverse solution to the landmine detection problem Based on GPR data [50]. The authors used finite element method to study the inclination angle effect on landmine detection [52]. Even so, possible detection properties based on direct contact still not utilized with many test cases.

In this work, the main concept is applying constant pressure (less than the activation pressure of any landmine) to the sand surface; then a pressure distribution is generated on the sand surface due to the difference between the Young's modulus of the sand and a landmine. In real case this pressure distribution can be measured by contact pressure sensor (ex: TekScan Pressure Mapping Sensor 9920), so that the landmine type and depth may be detected. Some measuring systems include processing software which export to Matlab or Excel is commercially available (ex: MatScan, source: [www.tekscan.com](http://www.tekscan.com)). The proposed

system carrying the sensor would be autonomously or remotely controlled. The experimental procedure could be as follows:

- 1- Rolling cylinder with fixable pressure mat fixed on its circumference, as shown in Figure 3.1, will be pushed to roll over the sand which is infected by landmines.
- 2- According to the sensed contact pressure by the flexible pressure mat, an indication could be acquired for the landmine existence.
- 3- Then by using the NN the characterization of the landmine (type and depth) can be determined.

To study the presence of landmine in sandy desert, a finite element model is presented with 2D model. First, a 3D model of a landmine inside sand is done, as shown in Figure 3.2.a. The main problems of the 3D models are the big size, HW requirements and long processing time. While faster and similar results can be presented with a 2D model. The 2D model of landmine inside sand 2m x 2m x 0.5m at different depths up to 205 mm is shown in Figure 3.2.b. The 2D models are done for two types of landmines, two other objects and only sand, at different depths.

Due to the differences in the pressure distributions profile with different landmines and different depths, the landmine type and depth can be determine by an artificial intelligent techniques as shown in the next section.

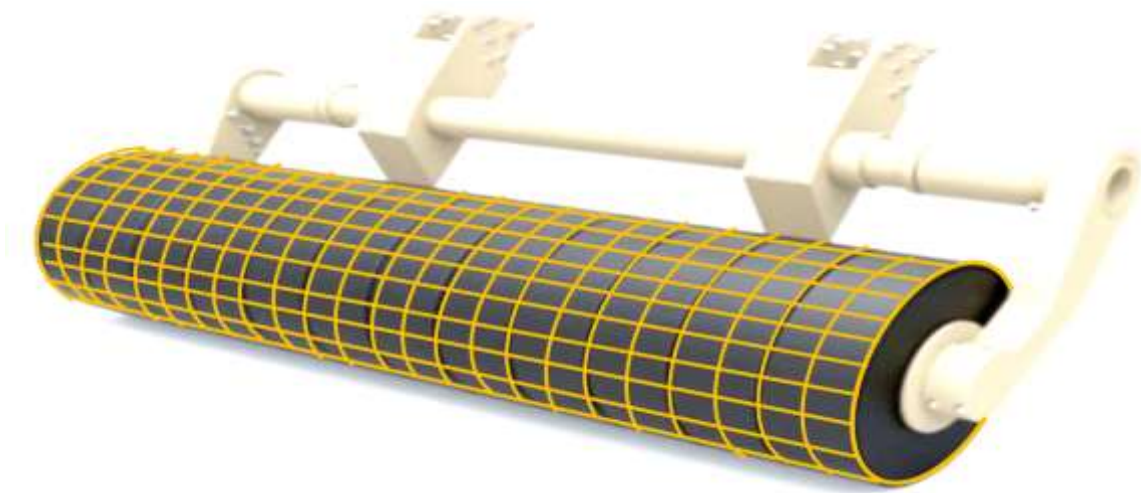
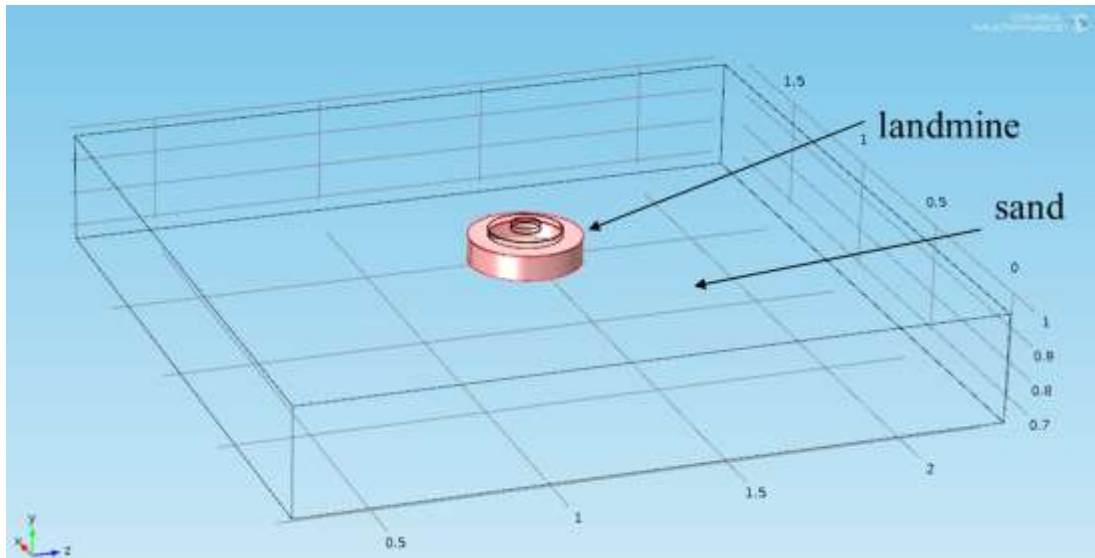
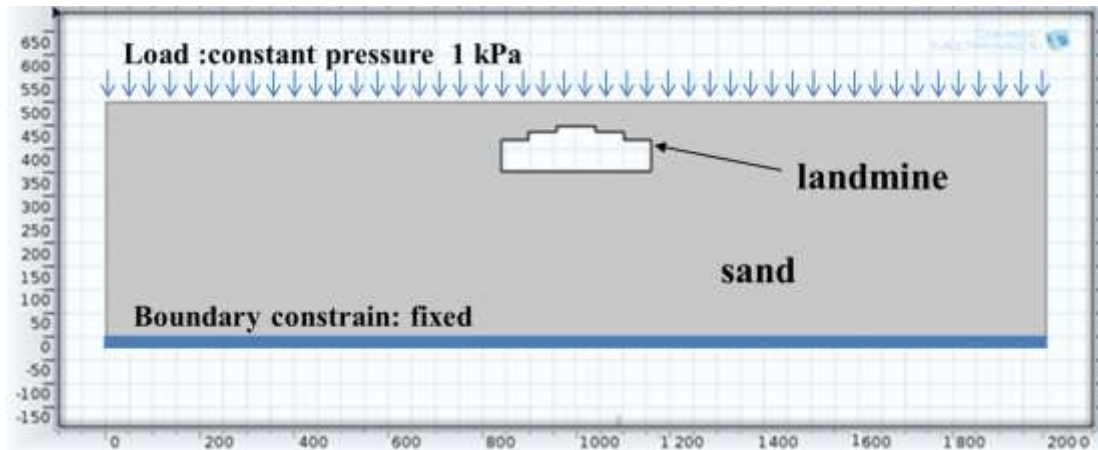


**Figure 3.1:** Rolling Cylinder with pressure mat



(a) 3D Finite element model of sand-landmine with COMSOL MULTIPHYSICS



(b) 2D Finite element model of sand-landmine with COMSOL MULTIPHYSICS

**Figure 3.2:** Finite element models of sand-landmine

### 3.2 Material and Methods

In this section two landmine types are used, the first one is noted as ‘LM01’ which is an anti-tank landmine MK7 (with diameter 325 mm and height 110 mm) and the other is noted as ‘LM02’ which is an anti-personnel landmine (with diameter 70 mm and height 70 mm). Also two different objects (not landmines) of an intermediate size (200 mm) comparing to the aforementioned landmines are considered. ‘TIN200’ is a food tin with diameter of 200 mm and height of 200 mm, ‘ROCK200’ is Rocky sphere with diameter of 200mm, and ‘SandOnly’ is free from any object, as shown in Figure 3.3.

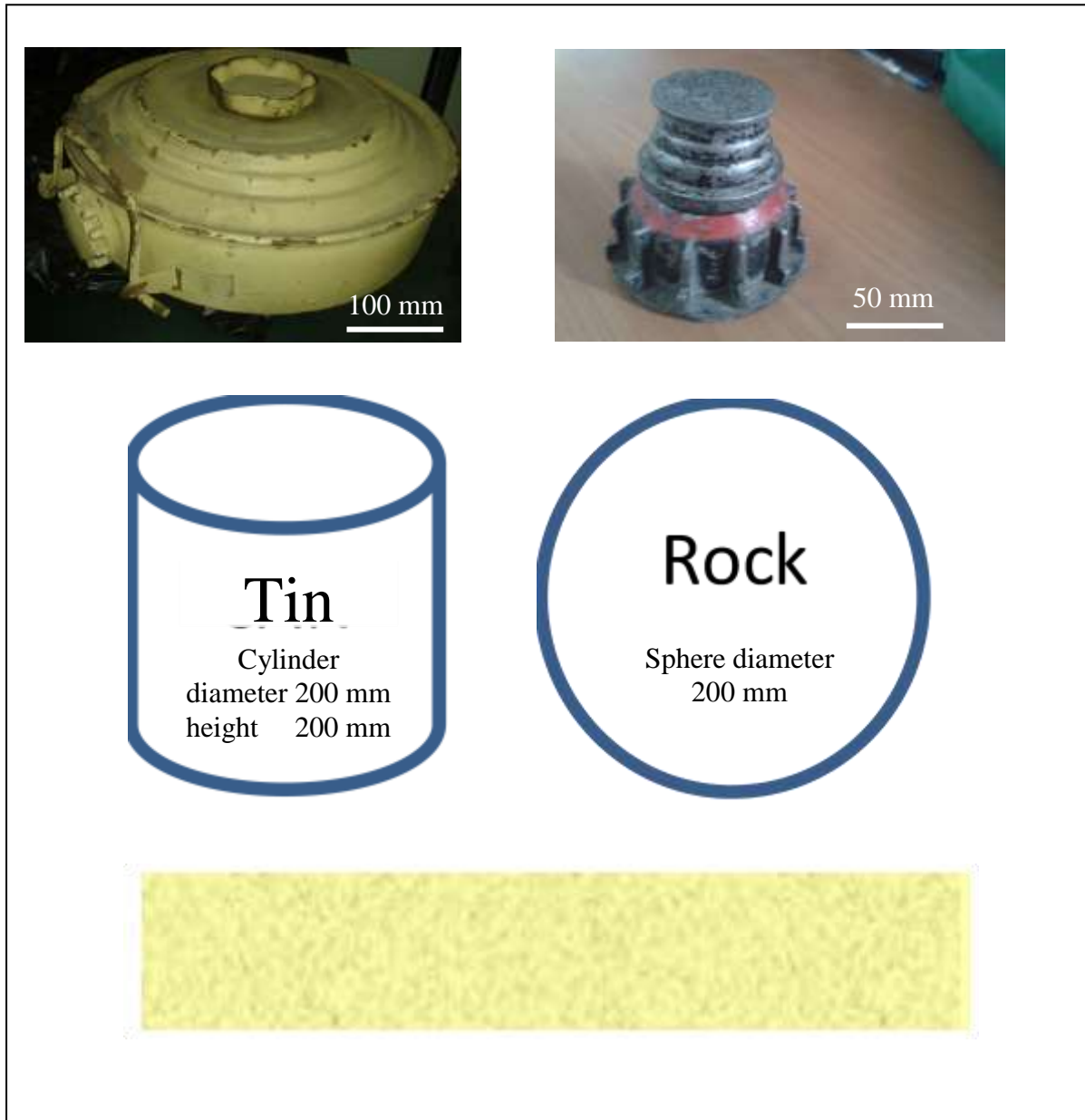


**Figure 3.3:** Anti-tank MK7 noted as ‘LM01’, Anti-Personnel noted as ‘LM02’, TIN200, ROCK200, and sandonly

### 3.2.1 The Landmine Activation Pressure

The activation pressure is one of the most important considerations in the demining studies. It is the loading pressure which causes the landmine explosion. Based on the, available online, information portals [53, 54] about the Landmines (dimensions and activation load [kg]), the activation pressure is calculated for each landmine, as shown in Table 3.1. From this table, the safe contact pressure threshold can be selected as 1.9 kPa.



Base on that and considering a factor of safety = 2, the simulation will be with a boundary pressure load of 1 kPa.

**Table 3.1:** Landmines activation pressure calculations.

Landmine Type	Dimensions (mm)	Activation load (kg)	activation pressure = Force/Area (kPa)
MK5 (AT)	Diam: 203	114.45	34.6
MK7 (AT) <sup>a</sup>	Diam: 325	150 - 275	17.7
Rieglmine43 (AT)	Length: 800 Width: 95	180 - 360	23.2
S mines (AP)	Diam: 102	3 - 5.5	3.5
Tellermine 35,42,43(AT)	Diam: 318	90- 180	11.1
B-2(AT),V-3, (like)TMB2	Diam: 273	11.5	1.9
M71 copy of TM46,	Diam: 30.5 cm	120–400	16
T79 copy of TS50, (AP)	9 cm	12.5	19.2

a. MK7 is the Anti-Tank landmine noted with ‘LM01’ in this paper

### 3.2.2 Finite Element Model

This section introduces 2D finite element model of the sand–landmine problem using COMSOL Multiphysics as show in Figure 3.2. The finite element model type is solid mechanics with static loading. A uniform pressure of 1 kPa is applied to the sand surface, the meshing is triangular type, extremely fine size (maximum: 20mm, minimum: 0.04mm) and regular refinement number is 3.

The work is carried out for each one of the four objects (LM01, LM02, TIN200, ROCK200) and free sand at different depths (starting from 5 mm to 205 mm with step 5mm). The materials are assumed to be homogeneous, isotropic, and linearly elastic. The Young’s modulus and Poison’s ratio for the “TIN” and the “mine” casing are (steel:  $E = 210$  GPa,  $\nu=0.3$ ). The sand Young’s modulus and Poison’s ratio are (sandstone:  $E = 10$  GPa,  $\nu=0.295$ ) and adhered to a rigid rock from bottom. The sand dimension is 2m x 2m x 0.5 m.

These pressure distribution cases are exported to excel file then a MATLAB programs are coded in order to unify the “spline interpolation” in the x-axis range (from 500 to1500 mm with step 5 mm) in order to be used in the next step (the neural network training).

### **3.2.3 Neural Networks**

The design of artificial Neural Networks (NN) is significantly affected by understanding the living nervous system biological mechanism and its structure. In the traditional structure of an NN, the weights represent the synapses in a biological neuron, while the activation function corresponds to the intracellular current conduction mechanism in the soma. This simplified model ignores many of the characteristics of its biological inspiration, e.g. it does not consider the time delays that affect the system dynamics but useful approximation[55].

The NN used for objects classification is perceptron neural networks (PNN) and the neural network used to detect the object depth is feed-forward neural networks (FFNN). It would show up that NN is promising in affording better solutions for estimating the landmine characteristics under the sand (type, depth). Three NNs are trained to determine the landmine characteristics, where the sand surface contact pressure charts were the NN inputs and the landmine characteristics were the desired outputs. The distinct features of the NN make this technique very helpful in situations where the functional correlation between the inputs and outputs is not clear. Some characteristics of the NN technique which were specifically beneficial for landmine detection in this study are as follows: The NN technique is efficient in representing non-linear relationships between the dependent and independent variables, by an approach similar to a ‘black box’. The NN technique has prediction and optimization capabilities and can be updated with new data. Also, after the models are trained, it can be used to predict the response for new experimental conditions. The PNN learning function is ‘learnp’, while for the FFNN; a back propagation algorithm is used for training purposes. The data is divided between training and validation, to check if the NN well understood the relation or not.

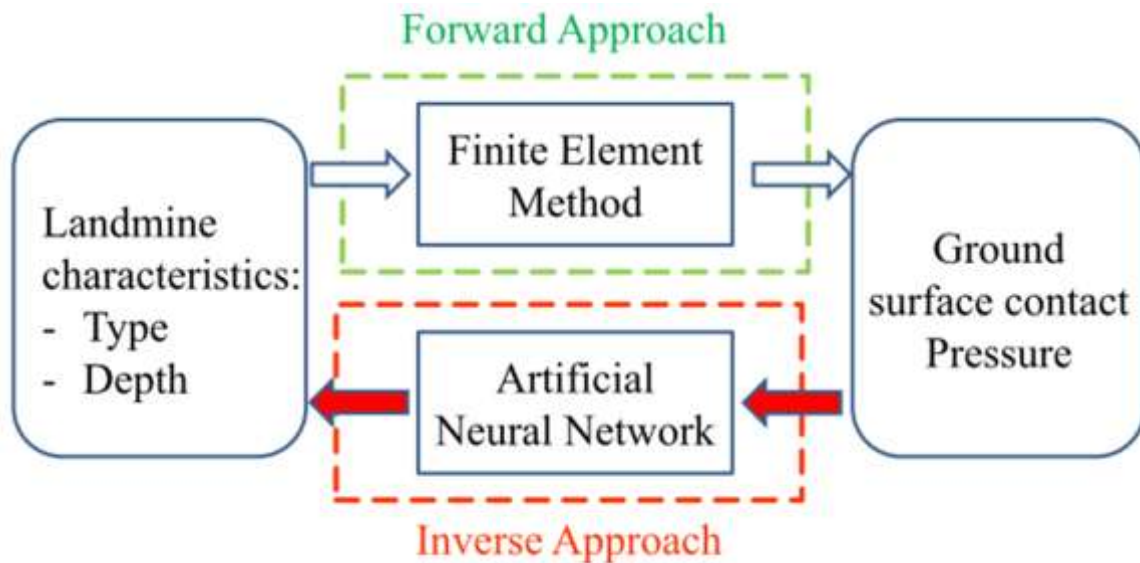


**Figure 3.4:** Flowchart of forward and inverse approaches

### 3.2.4 The Simulation Work Procedure

#### Using COMSOL:

- 1) Build 2D finite element model - FEM, type Solid mechanics with static pressure loading = 1 kPa.
- 2) Repeat the same FEM with each object type (LM01, LM02, TIN200, ROCK200, and SandOnly).
- 3) Repeat the same FEM at object depths (from 5 mm to 205 mm with step 5mm) below the sand surface.
- 4) Solve COMSOL model, generate the surface pressure distribution curve.
- 5) Export the contact pressure data to Microsoft Excel, and then read from Matlab.

#### Using Matlab (NN toolbox):

- 6) “spline interpolation” function is used to extract the contact pressure values at certain distances on the measurement span.
- 7) The extracted contact pressure values are used to build the training data set and validation data set, Ex: Odd order values is used for training and even order values is used for validation.
- 8) Train PNN (5 neurons to detect the 5 object types, ex: “10000” code for LM01, “00100” code for TIN200 and “00001” code for OnlySand).
- 9) Test the PNN with the validation data.
- 10) After determining the landmine type, train the FFNN (to detect the object depth) for the two landmine types LM01, and LM02. Then, test with the validation data

**Test case1:** Repeat NN tests at inclined landmines LM01, and LM02 in the COMSOL model with angles 0 to 30° with step 5°. Then, this is repeated at depths 50, 100, 150, 200mm.

**Test case2:** Repeat NN tests when adding noise to the interpolated pressure distribution curves generated from COMSOL models.

The simulation results will be presented in the next section.

### 3.3 Simulations and Results

The simulation is divided mainly into five parts: the finite element data generation, data preparation, neural networks training, neural networks validation, and error analysis. After that two test cases will be presented: inclined landmines and added noise. The forward approaches are utilized here to generate an artificial data using the finite element models. After that the inverse approaches are utilized by NN to detect the landmine characteristics: (type and depth) as shown in Figure 3.4.

Figures 3.5 to 3.9 shows the sand surface pressure distribution in cases of the different objects mentioned in section 3.2, and Figure 3.3, at depths (from 5 mm to 205 mm with step 5 mm) below the sand surface.

The data (205 models, 41 models for each case of the five) is as follows:

- 41 models of sand and Only sand plus random noise with 5% of the average as shown in Figure 3.5.
- 41 models of sand and LM01 at depths: (from 5 mm to 205 mm with step 5 mm), as shown in Figure 3.6.
- 41 models of sand and LM02 at depths: (from 5 mm to 205 mm with step 5 mm), as shown in Figure 3.7.
- 41 models of sand and TIN at depths: (from 5 mm to 205 mm with step 5 mm), as shown in Figure 3.8.
- And 41 models of sand and ROCK at depths: (from 5 mm to 205 mm with step 5 mm), as shown in Figure 3.9.

Figure 3.5 shows that the contact pressure distribution is nearly constant when no object impeded in the sand (OnlySand). The common issues in the Figure 3.6 to Figure 3.9 are the contact pressure has certain distribution due to existence of an object in the sand; the closer the object to the sand surface, the higher contact pressure distribution.

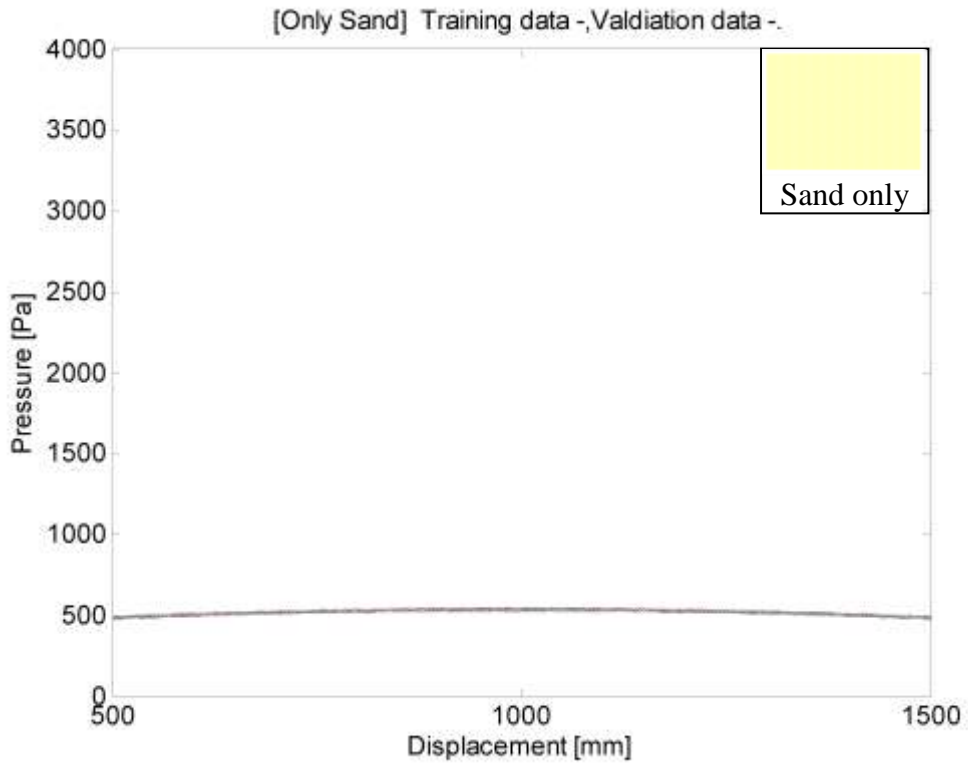


**Figure 3.5:** Surface pressure (Pa) Sand only plus random noise with 5% of the average, repeated for same number

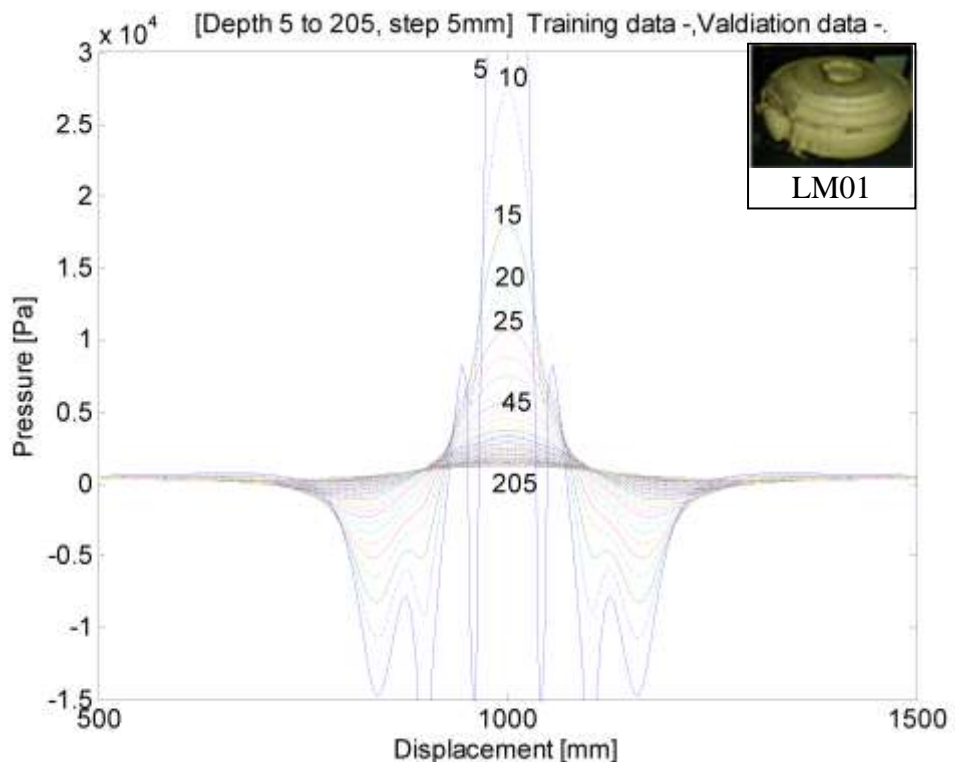


**Figure 3.6:** Surface pressure (Pa) when LM01 at depths: (from 5 mm to 205 mm with step 5mm)

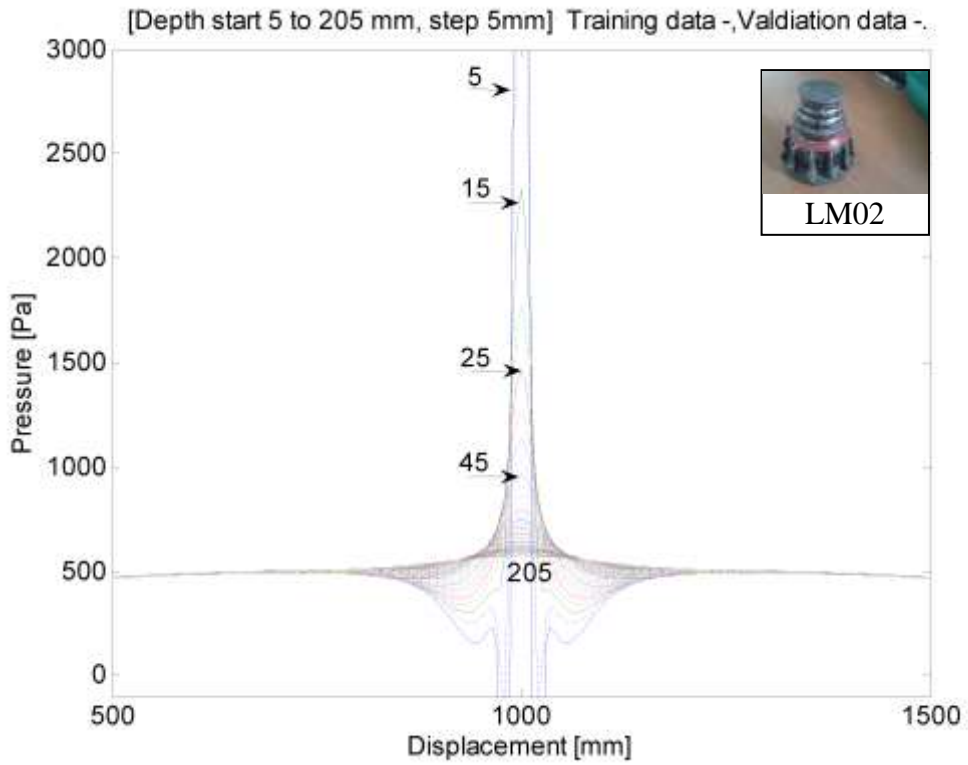


**Figure 3.7:** Surface pressure (Pa) when LM02 at depths: (from 5 mm to 205 mm with step 5mm)

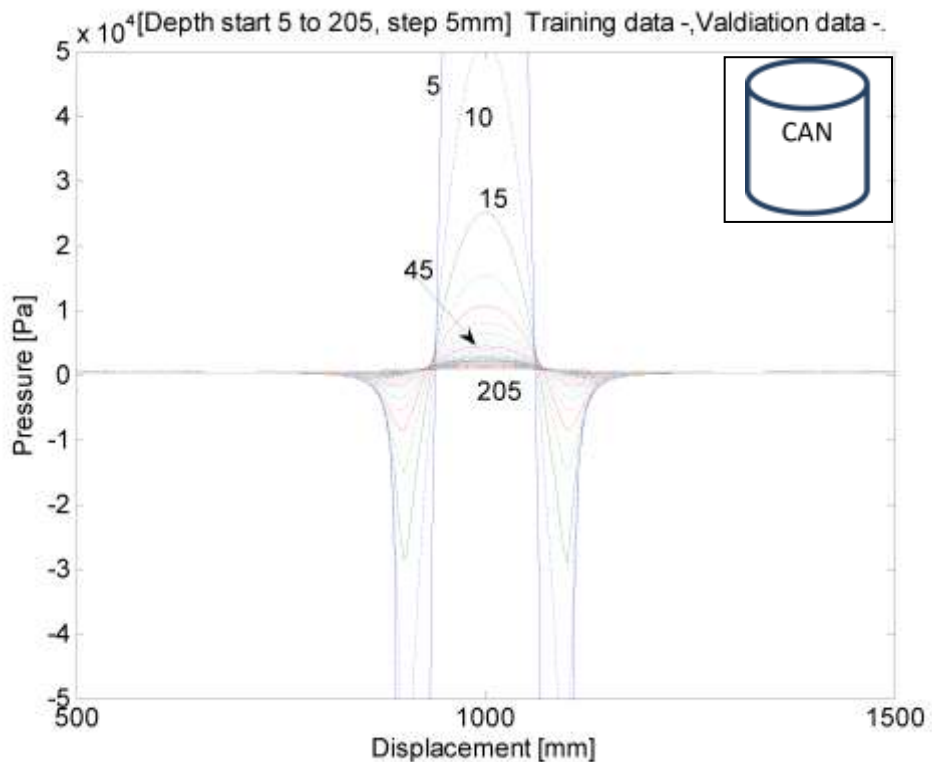


**Figure 3.8:** Surface pressure (Pa) when TIN 200 at depths: (from 5 mm to 205 mm with step 5mm)

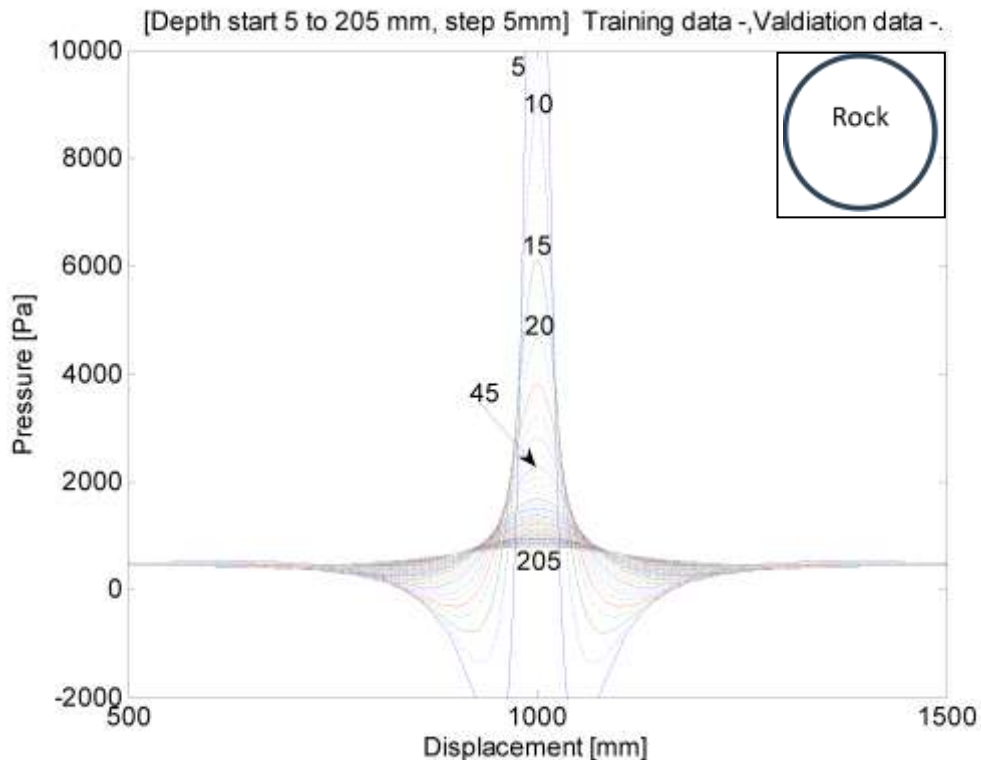


**Figure 3.9:** Surface pressure (Pa) when Rock 200 at depths: (from 5 mm to 205 mm with step 5mm)

Neural networks (NN) can extract some information from these pressure distribution curves. After exporting these curves to MATLAB, they are used to train NNs to do two tasks:

- 1<sup>st</sup> Task: To detect the object type {LM01, LM02, TIN200, ROCK200, or SandOnly}.
- 2<sup>nd</sup> Task: To detect the depth at which this object is existed {range 5- 205 mm}.

To do the first task (classification), two NN structures are investigated: Perceptron NN and Competitive NN. The Perceptron NN gave better results than the other because while training the required output target is introduced to the Perceptron NN many times (epochs) (supervised learning), but the other structure (Competitive NN) doesn't introduce the output target to the NN while training (unsupervised learning). The Perceptron NN consists of one layer with 5 neurons (each neuron detects the presence of certain object) as shown in Figure 3.10. After training, each neuron is required to give output 1 or 0 based on the object presence or not.

The data is divided into two parts, a part for training and another for validation, in order to ensure that the neural networks well acquired the whole relation not just the training data. Table 3.2 and Table 3.3 show true alarm percentage (correct detections) and the false alarm percentage (not correct detections) for the training data and validation data respectively. Table 3.2 shows that the LM01 (coded with PNN output 10000) is fully detect using (21



training set x 5 objects types), while the smaller landmine LM02 were harder to detect only 67% (to reach this percentage we had to assign two codes for LM02 01000 and 00000). False alarm is that the NN state there is an object but there is no object which is high for LM02 18%. Also, it is obvious that OnlySand (coded with PNN output 00001) is fully detected with no false alarm which is good (the NN will not indicate clear land unless it is really clear).

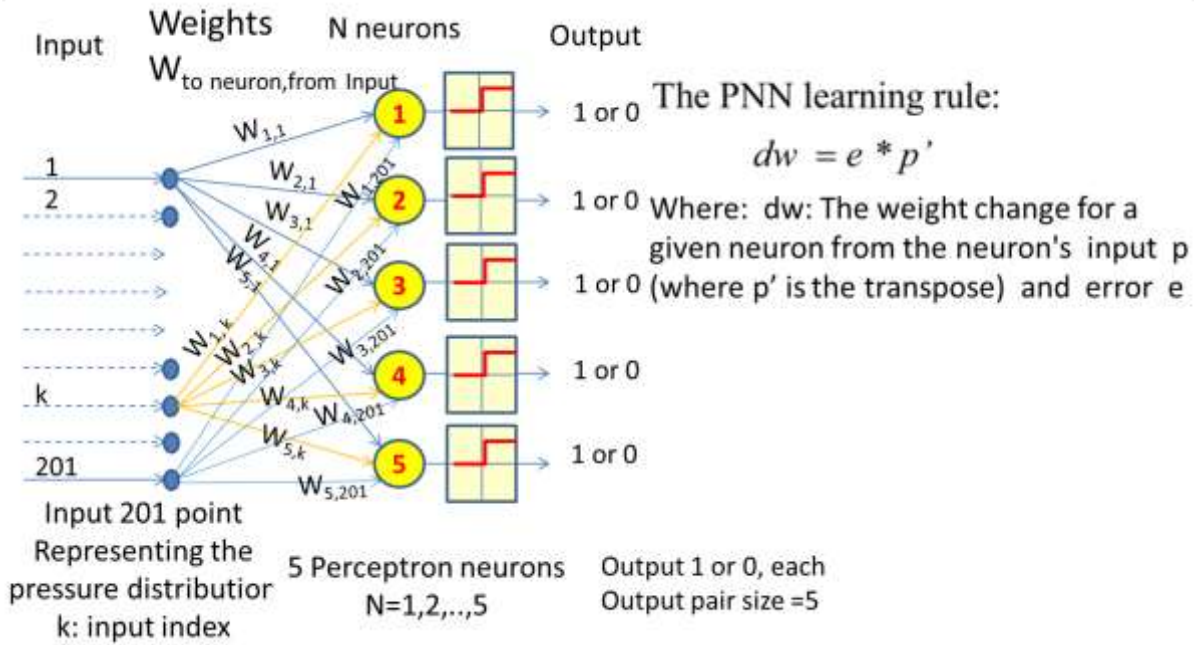


**Figure 3.10:** Perceptron NN: Designed to detect the object type

**Table 3.2:** Perceptron NN (classification) training data analysis

\ Detect Data from	LM01	LM02	TIN200	ROCK200	OnlySand
	10000	01000 00000	00100	00010	00001
<b>True alarm</b>	100%	67%	100%	52%	100%
<b>Not Detected</b>	0%	33%	0%	48%	0%
<b>False alarm</b>	0%	18%	0%	9%	0%

True alarm rate = number of correct detections / total number of the training data pair for certain object  
 True alarm rate + Not Detected = 100%  
 False alarm rate = number of detections which are not correct / total number of the training set (21x5=105)

Table 3.3 shows that the LM01 is detect with percentage 95% in the validation 20x5 data pairs, while the smaller landmine LM02 was harder to detect only 70%. False alarm for LM02 is 11%. Also, it is obvious that OnlySand (coded with PNN output 00001) is fully detected with no false alarm which is good (the NN will not indicate clear land unless it is really clear).

**Table 3.3:** Perceptron NN (classification) validation data analysis

\ Detect Data from	LM01	LM02	TIN200	ROCK200	OnlySand
	10000	01000 00000	00100	00010	00001
<b>True alarm</b>	95%	70%	100%	50%	100%
<b>Not Detected</b>	5%	30%	0%	50%	0%
<b>False alarm</b>	0%	11%	0%	17%	0%

True alarm rate = number of correct detections / total number of the validation data pair for certain object

True alarm rate + Not Detected = 100%

False alarm rate = number of detections which are not correct / total number of the validation set (20x5=100)

After the detection of the LM01 or LM02, the second task is the depth detection.

Another two Feed Forward NNs are used to detect the depth of the landmines under the sand, as shown in Figure 3.11. Each one of these two NNs is trained using the data of one of the two landmines.

The data is also divided into two parts, one part for training (21 data pair each) and the other for validation (20 data pair each). The FFNN design is repeated 50 times and the root mean square of error (RMSE) is calculated for the training set and validation set, in order to select the appropriate FFNN design with the lowest RMSE each in training and then in validation. This work is repeated for FFNN sizes 1, 2, 3, and 4 neurons and the lowest validation RMSE is accomplished by the FFNNs of size 2 neurons for both LM01 and LM02, as shown in Table 3.4.

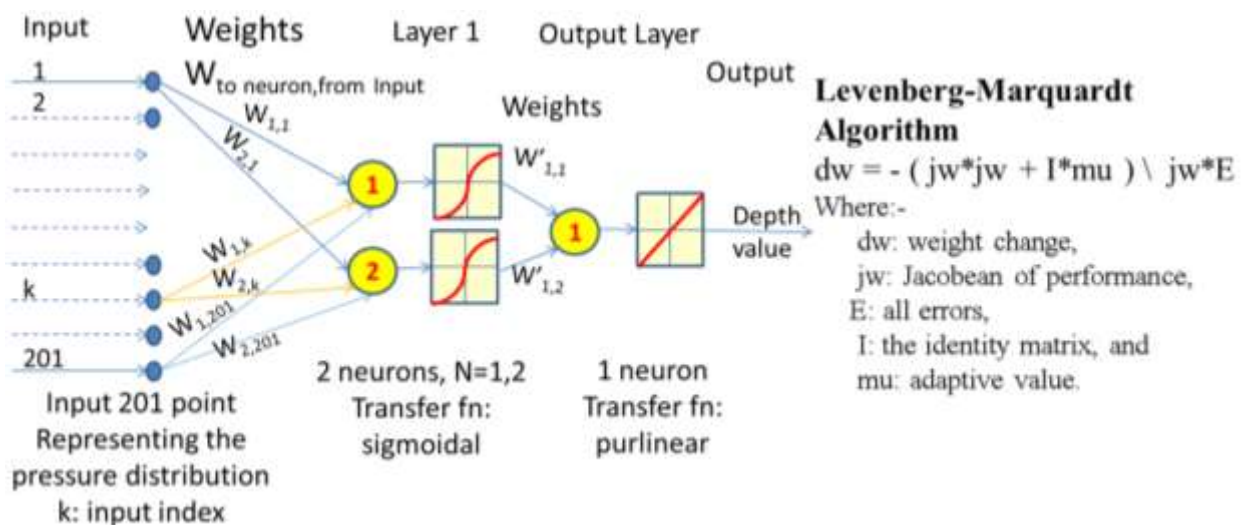


**Figure 3.11:** Feed forward NN: Designed to detect the object depth

**Table 3.4:** Feed forward NN training and validation, Root mean Square of Error (RMSE)

Number of neurons	LM01		LM02	
	Training	Validation	Training	Validation
1	0	0.057	0	0.214
<b>2</b>	<b>0</b>	<b>0.013</b>	<b>0</b>	<b>0.131</b>
3	0	0.020	0	0.139
4	0	0.032	0	0.180

### 3.3.1 Test Cases 1: Inclined Landmine

This section studies the case of inclined landmines with angles ( $0^\circ$ ,  $5^\circ$ ,  $10^\circ$ ,  $15^\circ$ ,  $20^\circ$ ,  $25^\circ$ , and  $30^\circ$ ); the pressure distribution is different from that when the landmine is horizontal. It can be clearly seen that, as the inclination angle increases, the distribution is twisted more to the landmine higher side. And also the deeper the landmine the smaller the effect of the inclination angle on the pressure distribution, as shown in Figure 3.12.

Finite element models are built to study the two landmines types at depths 50, 100, 150, and 200 mm and inclination angles ( $0^\circ$ ,  $5^\circ$ ,  $10^\circ$ ,  $15^\circ$ ,  $20^\circ$ ,  $25^\circ$ , and  $30^\circ$ ), and the surface pressure distribution curves are generated from each case as shown for LM01 and LM02 in Figure 3.12. The target of this simulation is to input these surface pressure curves to the PNN (designed as shown earlier in Figure 3.10) and to find the effect of inclination on the detection rates of the landmine types, and also to input the same surface pressure curves to the FFNN (designed for each LM01 and LM02 as shown earlier in Figure 3.11), in order to detect the depth. The results in Table 3.5, show that LM01 detection is 100% same as the horizontal LM02, but cross detections are found. Cross detection means that when landmine with certain type (Ex: LM01 code: 10000) is introduced to the NN, the resulted detection is the introduced landmine with a probability that at least one of the other objects assume ROCK200 may exist, (Ex: code:10010, means LM01 or ROCK200). LM02 is detected with 75% same as the horizontal LM02.

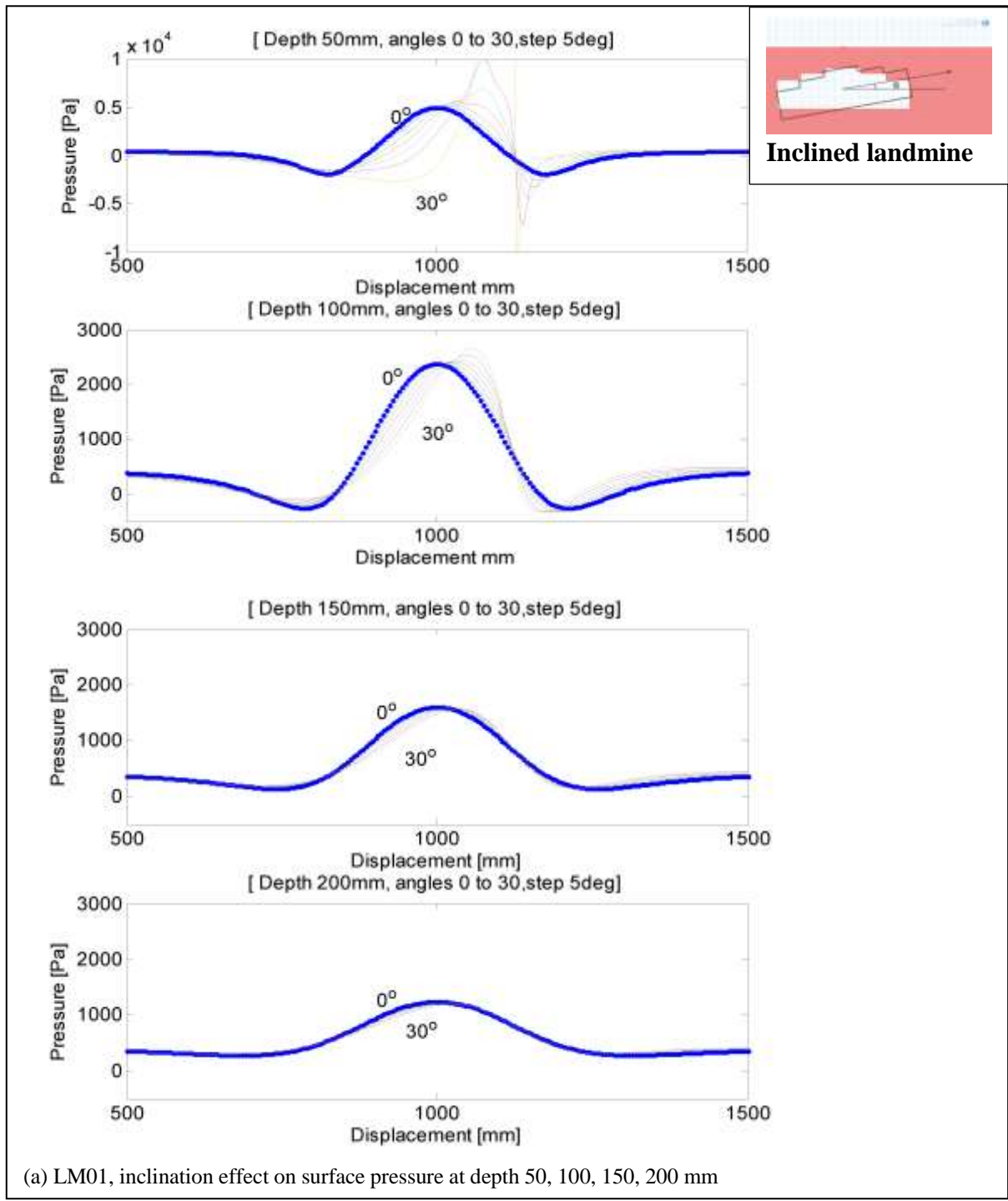


**Figure 3.12:** Inclined Landmine effect for LM01 and LM02

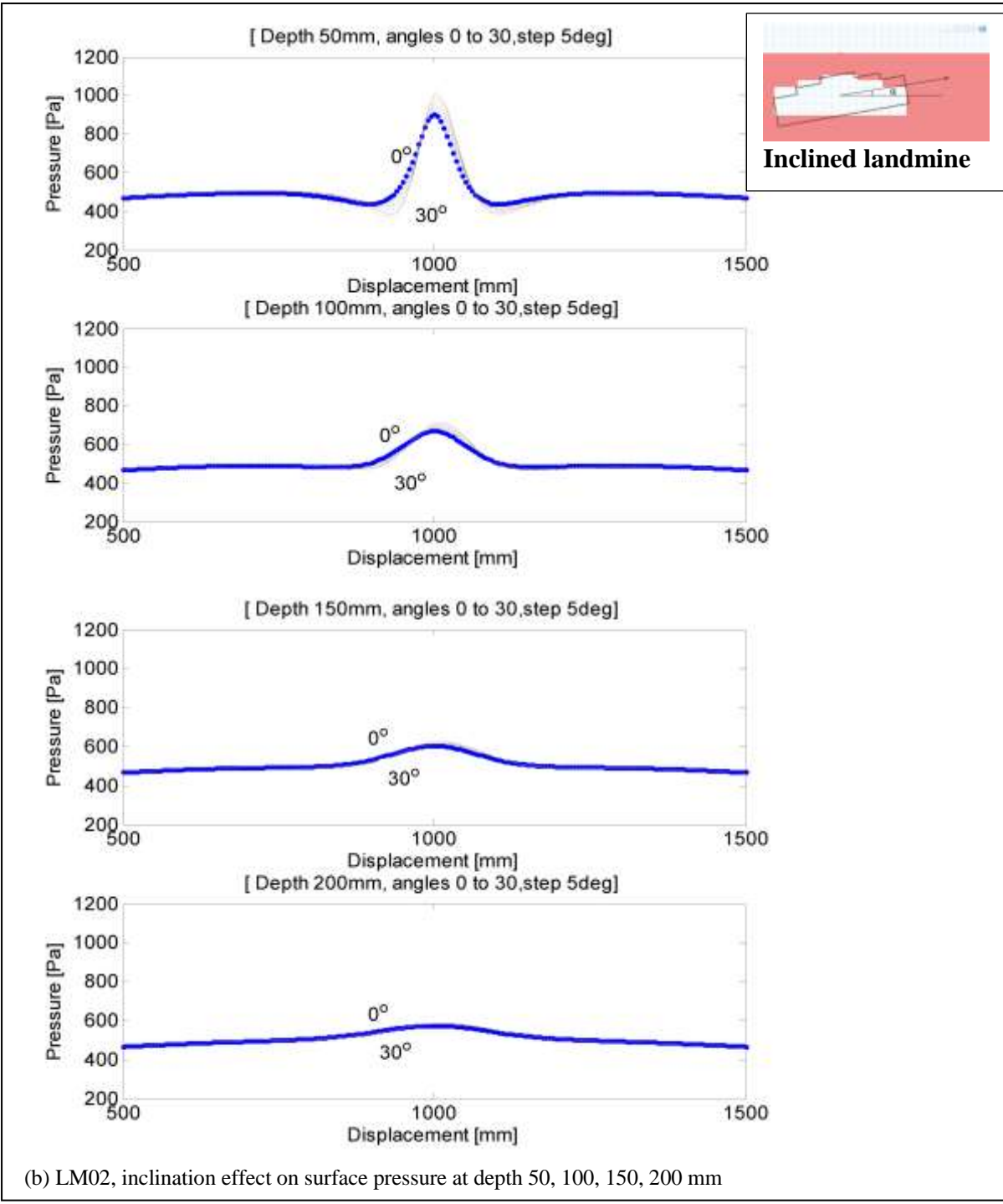


**Figure 3.12:** Inclined Landmine effect for LM01 and LM02

**Table 3.5: Inclination effect on alarm rate**

<b>Input Output</b>	<b>Data of LM01</b>	<b>Remarks</b>	<b>Data of LM02</b>	<b>Remarks</b>
<b>LM01</b>	100%	All detected	--	--
<b>LM02</b>	--	--	75%	Only 75%
<b>TIN200</b>	11%	Cross detection	0%	--
<b>ROCK200</b>	32%	Cross detection	25%	False detection
<b>Sand</b>	4%	Cross detection	0%	--

Table 3.6 and Table 3.7 show the error in depth detection using the FFNNs for LM01 and LM02 respectively; the exact depths are detected when the inclination angle is zero which is logical. The error increases when the inclination increases. Also when the object get deeper the error decreases. Figure 3.13 and Figure 3.14 show the depth detection error at different depths and inclination angles for LM01 and LM02 respectively. For LM01, the error increases as the inclination angle increases at all depths which is logical as shown in Figure 3.13.a. Also it indicates that the error decrease as the landmine depth increase. The reason is that the closer inclined object makes greater deformation to that pressure curve produced at inclination angle zero. In Figure 3.13.b the average error for all inclination angles also decrease as the landmine depth increases.

**Note1:** The positive error indicates the increase of the NN estimation more than the actual depth.

**Note2:** The logical justification for the little decrease at angle 25° and depth 50mm is the geometrical effect of the LM01 at this depth and inclination as shown in Figure 3.13, while the similar curve is smooth for the LM02 as stated in Figure 3.14.

**Table 3.6: LM01 inclination effect on depth detection**

Actual Depth angle(deg)	50 mm	Err.	100 mm	Err.	150 mm	Err.	200 mm	Err.
0	50	0%	100	0%	150	0%	200	0%
5	117	134%	160	60%	174	16%	207	3.5%
10	283	466%	247	147%	203	35.3%	216	8%
15	435	770%	339	239%	235	56.7%	227	13.5%
20	494	888%	413	313%	270	80%	241	20.5%
25	462	824%	466	366%	306	104%	259	29.5%
30	488	876%	502	402%	346	130.7%	280	40%
<b>Error average:</b>		<b>565.4%</b>		<b>218.1%</b>		<b>60.4%</b>		<b>16.4%</b>

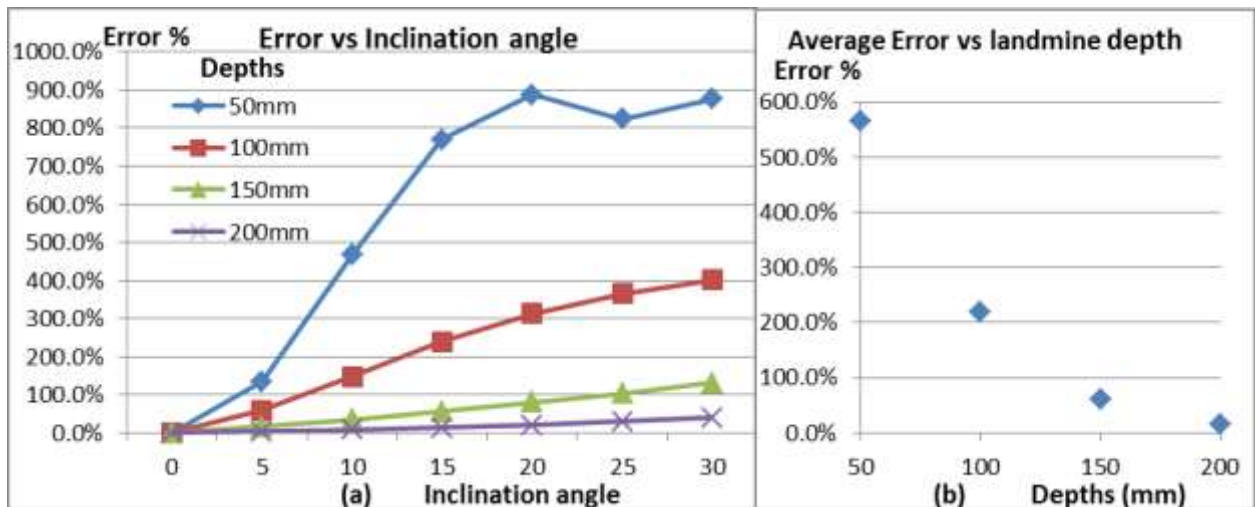


**Figure 3.13: Inclined Landmine effect for LM01**

In Figure 3.14.a for LM02, the absolute error increases as the inclination angle increases at all depths which is logical. Also Figure 3.14.a indicates that the absolute error decrease as the landmine depth increase. The reason is that the closer inclined object makes greater deformation to the pressure curve at inclination angle zero. In Figure 3.14.b the average absolute error for all inclinations also decreases as the landmine depth increase.

Note1: The negative error indicates that the decrease of the NN estimation less than the actual depth.

To sum up, the FFNN detecting the landmine depth has error= 0 at inclination angle 0°. This error increases as the inclination angle increases. And the effect of the inclination angle is dominant as the landmine is closer to the sand surface.

**Table 3.7:** LM02 inclination effect on depth detection

Actual Depth Angle(deg)	50 mm	Err.	100 mm	Err.	150 mm	Err.	200 mm	Err.
0	49.98	0.0%	99.99	0.0%	149.98	0.0%	200.04	0.0%
5	8.67	-82.7%	77.39	-22.6%	133.13	-11.2%	190.82	-4.6%
10	-10.06	-120.1%	49.8	-50.2%	123.97	-17.4%	189.6	-5.2%
15	-13.69	-127.4%	46.15	-53.9%	128.01	-14.7%	194.68	-2.7%
20	-16.65	-133.3%	42.32	-57.7%	129	-14.0%	197.5	-1.3%
25	-19.44	-138.9%	35.87	-64.1%	124.62	-16.9%	195.92	-2.0%
30	-21.75	-143.5%	27.76	-72.2%	115.11	-23.3%	189.66	-5.2%
<b>Error average:</b>		<b>-106.6%</b>		<b>-45.8%</b>		<b>-13.9%</b>		<b>-3.0%</b>

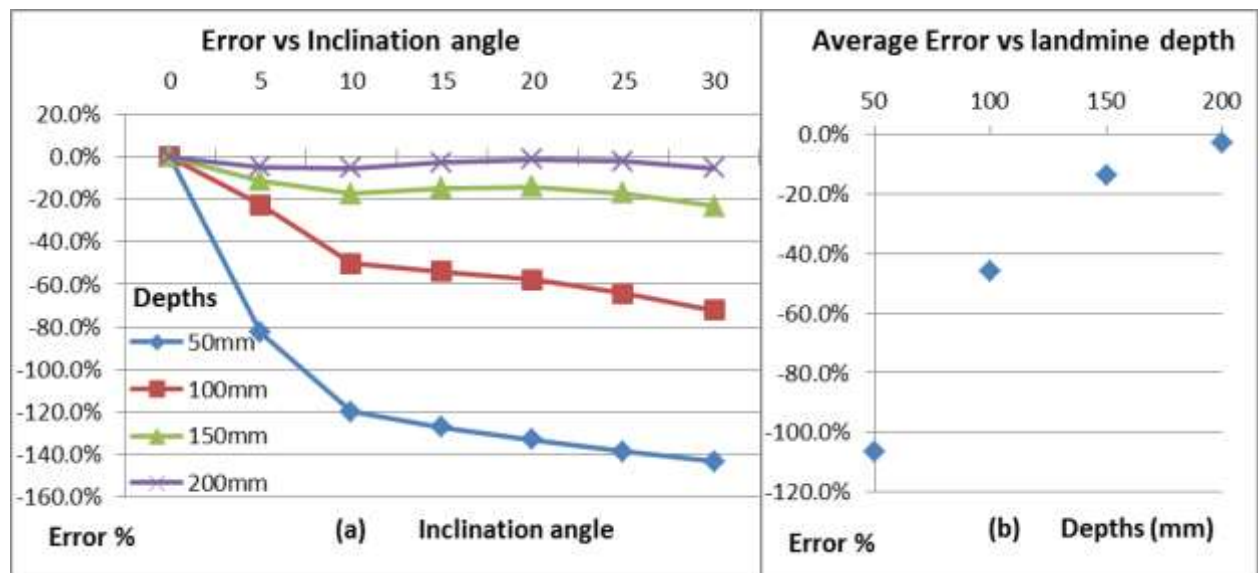


**Figure 3.14:** Inclined Landmine effect for LM02



### 3.3.2 Test Cases 2: Noise Effect on Detection

The real environment will not behave exactly the same as the finite element model does. But in fact, the sensor output will suffer from some noise. In this section, it is assumed random noise in the range of 5% to 20% of the signal average. The target is to monitor the effect of this noise on the detection rate of the NN.

Using the data of (20 validation set x 5 objects types) with random noises 5%, 10%, and 20% of each signal average, Table 3.8 compares true and false alarms percentage of LM01 and LM02. It indicates that 5% and 10% noises do not affect the true alarm percentage of LM01 and LM02, which are the same 95% and 70% respectively. But at noise 20% the true alarm decreased to 90% and 50% respectively. It is very important to mark that there is no effect of the 5%-20% noises on OnlySand detection. This indicates that the output of the NN will not give OnlySand unless it is really only sand.

The same test is done using the data of inclined landmine as shown in Figure 3.12, with random noises 5%, 10%, 20% of each signal average. Table 3.9 shows that for LM01 the true alarm is decreased at noises 5% from 100% to 96% and at noise 20% the true alarm becomes 82%. For LM02 the true alarm is decreased at noises 5% from 75% to 71% and at noise 20% the true alarm becomes 54%.

**Table 3.8:** Perceptron NN (classification) validation data analysis plus random noises 10% , 20% of each signal average

Detect Data from	LM01			LM02			TIN200			ROCK200			OnlySand		
	10000			01000 00000			00100			00010			00001		
	No Noise	With noise 10%	With noise 20%	No Noise	With noise 10%	With noise 20%	No noise	With noise 10%	With noise 20%	No noise	With noise 10%	With noise 20%	No noise	With noise 10%	With noise 20%
<b>True alarm</b>	95%	95%	90%	70%	70%	50%	100%	90%	85%	50%	55%	55%	100%	100%	100%
<b>Not Detected</b>	5%	5%	10%	30%	30%	50%	0%	10%	15%	50%	45%	45%	0%	0%	0%
<b>False alarm</b>	0%	0%	0%	11%	10%	10%	0%	6%	11%	17%	18%	20%	0%	0%	0%

**Table 3.9:** Inclination effect on alarm rate with signal noises 5%, 10%, 20%

Input Output	Data of LM01				Data of LM02			
	Without noise	with noise 5%	With noise 10%	with noise 20%	Without noise	with noise 5%	With noise 10%	with noise 20%
<b>LM01</b>	100%	96%	93%	82%	--	--	--	--
<b>LM02</b>	--	--	4%	4%	75%	71%	68%	54%
<b>TIN-200</b>	11%	18%	21%	18%	--	--	7%	18%
<b>ROCK-200</b>	32%	32%	25%	36%	25%	29%	25%	28%
<b>Sand</b>	4%	4%	4%	4%	--	--	--	--

## CHAPTER 4 : SENSOR DYNAMIC MODELING

The main target in this chapter is to utilize the application of a dynamic force to detect the ground stiffness  $k_o$ , which can be considered an indication of object presence (Ex: landmine). A complete derivation for single DOF sensor and two DOF are presented and then a detailed comparison is tabulated.

Also, this chapter focuses on the presentation of the novel contact sensor for landmine detection. The sensor principle is based on the concept of 2-DOF vibration absorber system (two spring and two masses), to detect the presence of an object (landmine) in sand which modeled as a third spring. The 3<sup>rd</sup> spring stiffness (the sand stiffness) can be measured as function of the vibration absorber frequency  $\omega_{Abs}$  (the frequency at which the 2<sup>nd</sup> mass gives zero amplitude (theoretically proven)) and the 1<sup>st</sup> mass gives near to peak. When the sand stiffness changed due to existence of the landmine, the vibration absorber frequency  $\omega_{Abs}$  changes, and subsequently the landmine can be detected. The mathematical proof of the idea is verified by simulation on Matlab and finite element COMSOL Multi-physics. The system parameters are chosen to be associated with the sand-landmine stiffness measurement range. The simulation results are optimized to give best sensitivity and linearity of the sensor output. The sensor gives sensitivity of 1559 Hz/(MN/m) and linearity better than 95%. Finally, a detailed design procedure for the contact stiffness sensor for landmine detection is developed.

## 4.1 Vibration Analysis of Difference Sensor Architecture

In this section the main target is to utilize the application of a dynamic force to detect the ground stiffness  $k_o$ , which can be considered an indication of object presence (Ex: landmine). A complete derivation for single DOF sensor and two DOF are presented and then a detailed comparison is tabulated.

### 4.1.1 Single DOF Sensor System

Single DOF system has one mass  $m_1$  and one spring  $k_1$  as shown in Figure 4.1. This system is excited from its suspension in order to detect the ground stiffness  $k_o$ . The direct relation can be derived as follows:

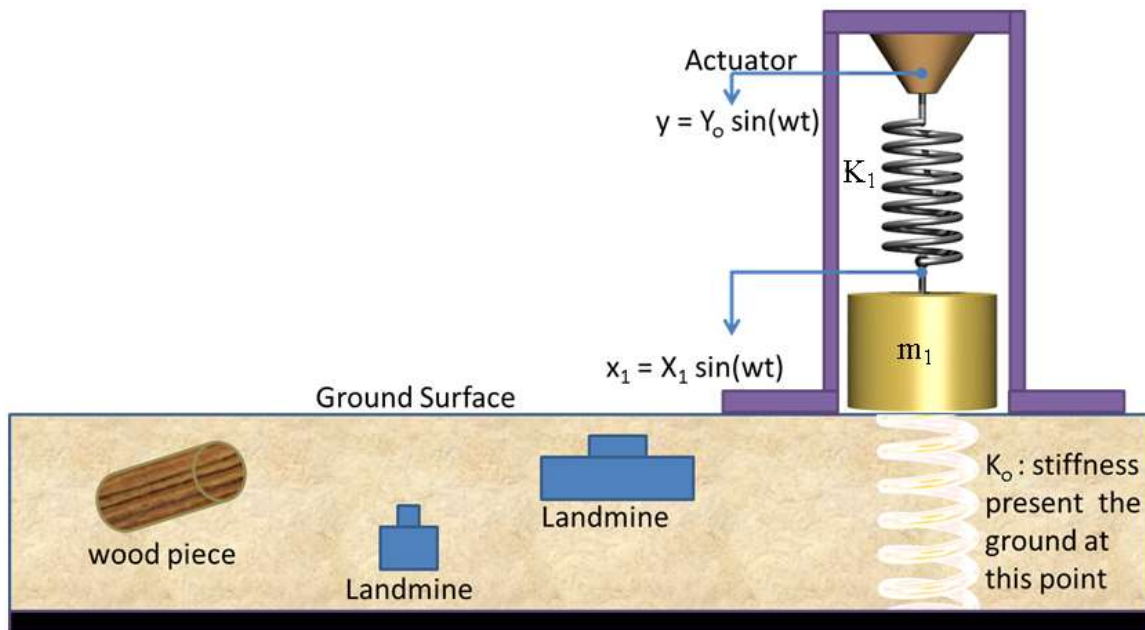


**Figure 4.1:** Single DOF sensor System

The dynamic equation:

$$m_1 \ddot{x}_1 + (K_o + K_1)x_1 = K_1 y \quad (4.1)$$

Non linear relation with  $K_o$

$$\omega^2 X_1 = \frac{K_1 Y}{-m_1 + \frac{1}{\omega^2} (K_o + K_1)} \quad (4.2)$$

$$\frac{\omega^2 Y}{\omega^2 X_1} = -\omega^2 \frac{m_1}{K_1} + \left( \frac{K_o}{K_1} + 1 \right) \quad (4.3)$$

$$R = \frac{\omega^2 Y}{\omega^2 X_1} = -\frac{\omega^2}{\omega_1^2} + \left( \frac{K_o}{K_1} + 1 \right) \quad (4.4)$$

Let :  $m_1$  and  $k_1$  selected in order to make  $\omega_1 = \omega$  ... Resonance

$$K_o = R K_1 \quad (4.5)$$

It must be noted here, this relation can be acquired only at resonance.

### 4.1.2 Two DOF Sensor System

Two DOF system has two masses  $m_1$  and  $m_2$  and two springs  $k_1$  and  $k_2$  as shown in Figure 4.2. This system is excited from its suspension in order to detect the ground stiffness  $k_o$ . The direct relation can be derived as follows:

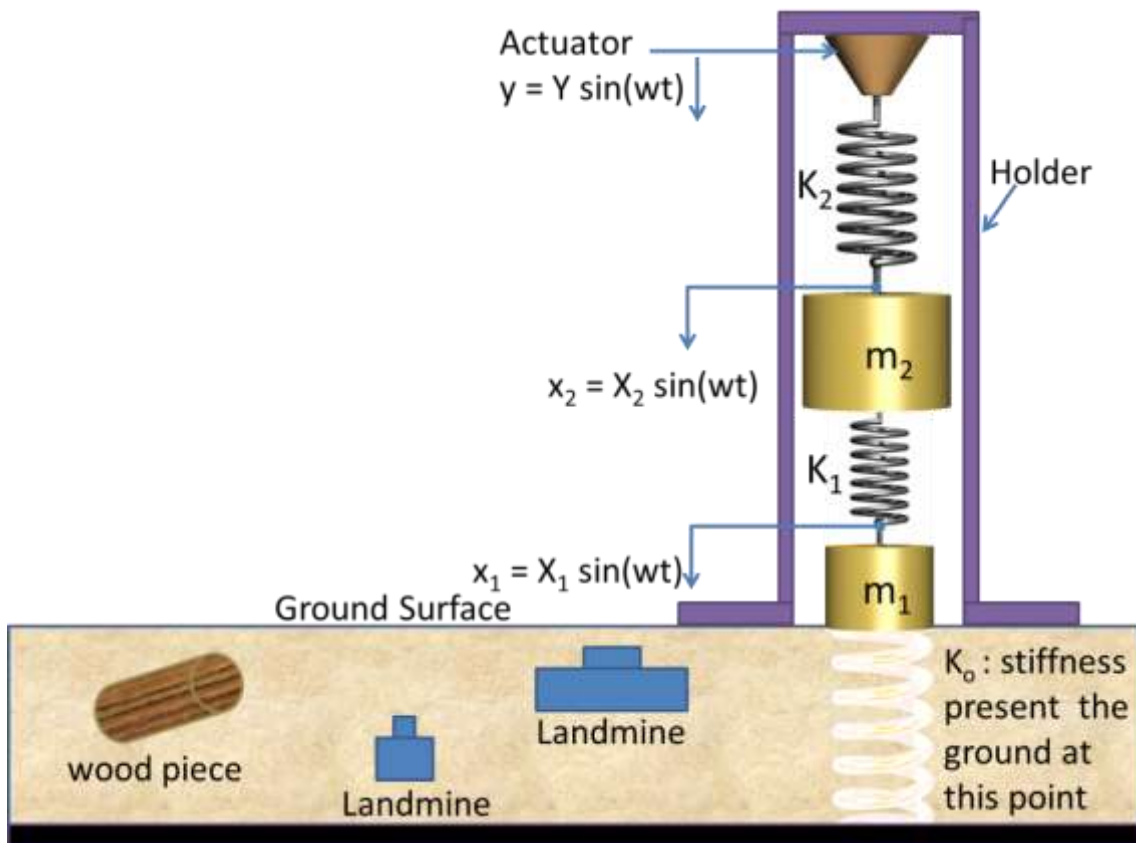


**Figure 4.2:** Two DOF sensor system

$$x_1(t) = X_1 \sin(\omega t) \quad (4.6)$$

$$\dot{x}_1(t) = \omega X_1 \cos(\omega t) \quad (4.7)$$

$$\ddot{x}_1(t) = -\omega^2 X_1 \sin(\omega t) \quad (4.8)$$

Amplitudes of the accelerations  $X_1''$ ,  $X_2''$

$$X_1'' = -\omega^2 X_1 \quad (4.9)$$

$$R = \frac{X_2''}{X_1''} = \frac{-\omega^2 X_2}{-\omega^2 X_1} = \frac{X_2}{X_1} \quad (4.10)$$

Dynamic equations:

$$m_1 \ddot{x}_1 + (K_o + K_1)x_1 - K_1 x_2 = 0 \quad (4.11)$$

$$m_2 \ddot{x}_2 - K_1 x_1 + (K_1 + K_2)x_2 = K_2 y \quad (4.12)$$

Dynamic equations in matrix form:

$$\begin{bmatrix} -m_1 \omega^2 + (K_o + K_1) & -K_1 \\ -K_1 & -m_2 \omega^2 + (K_1 + K_2) \end{bmatrix} \begin{bmatrix} X_1 \\ X_2 \end{bmatrix} = \begin{bmatrix} 0 \\ K_2 Y \end{bmatrix} \quad (4.13)$$

By solving these two equations manually or by symbolic toolbox

$$X_1 = f(Y, \omega, K_o, K_1, K_2, m_1, m_2)$$

$X_1$

$$= \frac{K_1 K_2 y}{K_1 K_2 + K_1 K_o + K_2 K_o - K_1 m_1 \omega^2 - K_1 m_2 \omega^2 - K_2 m_1 \omega^2 - K_o m_2 \omega^2 + m_1 m_2 \omega^4} \quad (4.14)$$

$$X_2 = f(Y, \omega, K_o, K_1, K_2, m_1, m_2)$$

$X_2$

$$= \frac{K_2 y (-m_1 \omega^2 + K_1 + K_o)}{K_1 K_2 + K_1 K_o + K_2 K_o - K_1 m_1 \omega^2 - K_1 m_2 \omega^2 - K_2 m_1 \omega^2 - K_o m_2 \omega^2 + m_1 m_2 \omega^4} \quad (4.15)$$

$$R = f(\omega, K_o, K_1, m_1),$$

$$R = \frac{X_2}{X_1} = 1 - \frac{m_1 \omega^2}{K_1} + \frac{K_o}{K_1} \quad (4.16)$$

$$R = f(\omega, K_o, K_1, m_1), \quad \text{not dependent on: } Y, K_2, m_2$$

Also the partial derivatives indicate the effect of each parameter.

$$\frac{\partial R}{\partial \omega} = -\frac{(2 m_1 \omega)}{K_1}, \quad \text{non linear} \quad (4.17)$$

$$\frac{\partial R}{\partial m_1} = -\frac{\omega^2}{K_1}, \quad \text{linear at certain } \omega, K_1 \quad (4.18)$$

$$\frac{\partial R}{\partial K_o} = \frac{1}{K_1}, \quad \text{linear at certain } K_1 \quad (4.19)$$

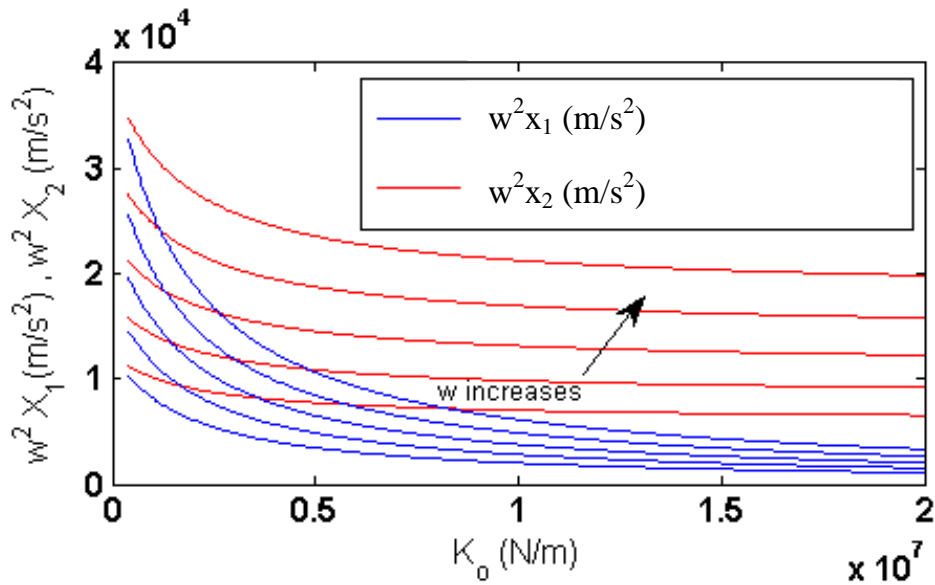
$$\frac{\partial R}{\partial K_1} = \frac{m_1 \omega^2 - K_o}{K_1^2}, \quad \text{not linear} \quad (4.20)$$

Let :  $m_l$  and  $k_l$  selected in order to make  $\omega_{ll} = \omega \dots$  Not resonance

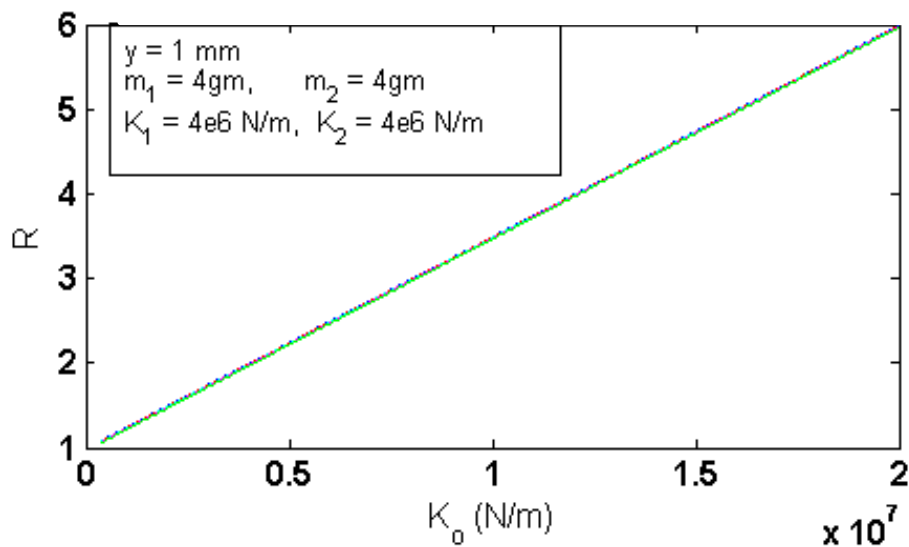
$$K_o = R K_1 \quad (4.21)$$

Figure 4.3 and Figure 4.4 study the effect of increasing the excitation freq.  $\omega$  at  $k_1 = 4$  MN/m and at two different values of  $m_1$  4gm and 40 gm. Where the acceleration amplitudes increase as the excitation frequency  $\omega$  increases. And the acceleration amplitudes decrease as the masses increase. While the amplitudes ratio  $R$  dependent only on  $k_o$  linearly.

When  $\omega = 550:100:950$  Hz,  $K_2 = 4$  MN/m (hard)



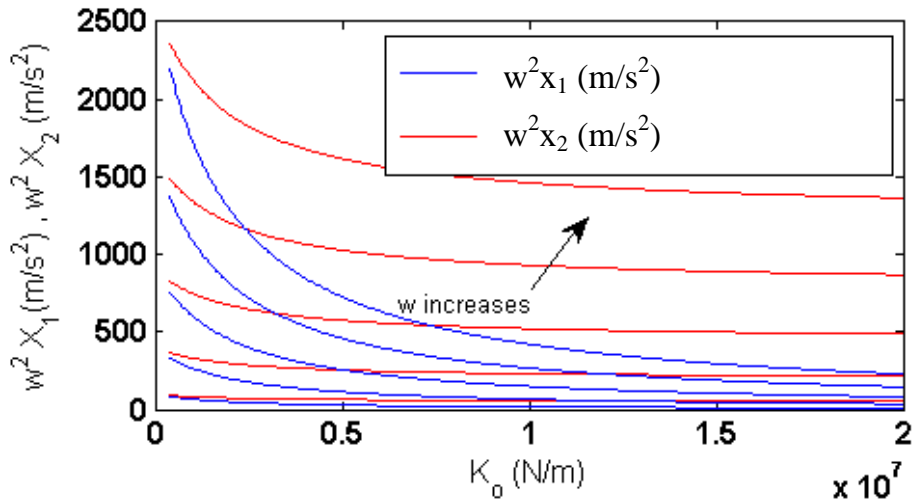
(a) Acceleration Amplitudes of the two masses versus the stiffness  $K_o$



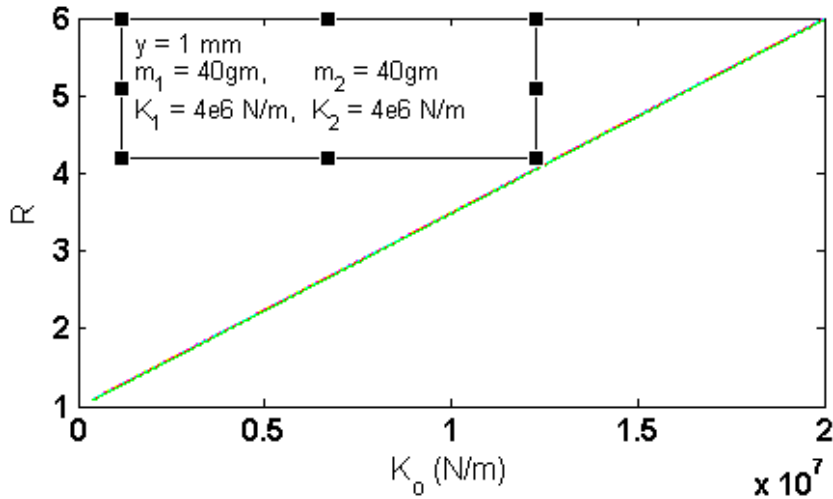
(b) Amplitudes Ratio  $R = X_2/X_1 = w^2 X_2 / w^2 X_1$  linear relation with the stiffness  $K_o$

**Figure 4.3:** Acceleration Amplitudes and ratio versus at higher excitation frequency range 550-950 Hz and at  $K_1 = 4$  MN/m and  $m_1 = 4$  gm

When  $w = 50:50:250$  Hz,  $K_2 = 4\text{MN/m}$  (hard)



(a) Acceleration Amplitudes of the two masses versus the stiffness  $K_0$

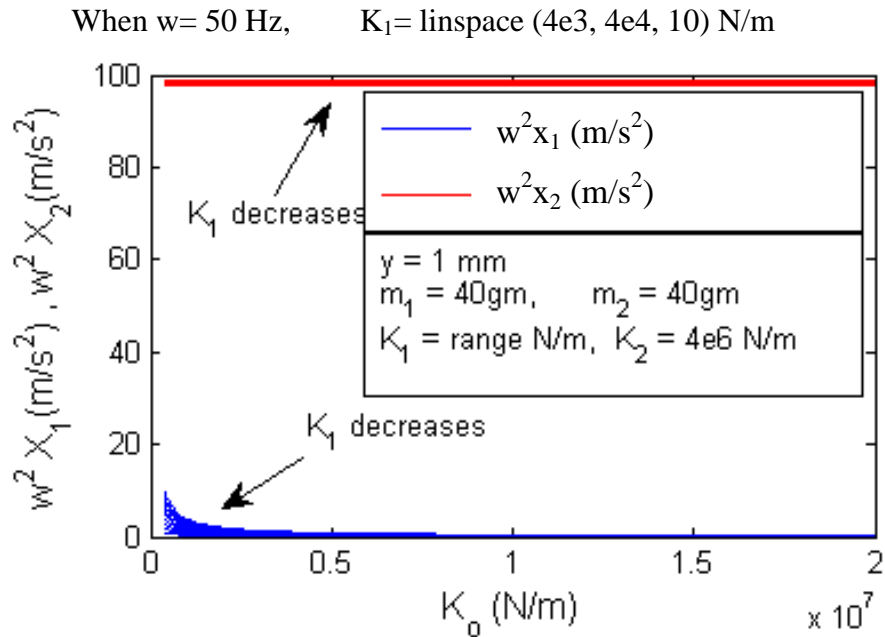


(b) Amplitudes Ratio  $R = X_2/X_1 = w^2 X_2 / w^2 X_1$  linear relation with the stiffness  $K_0$

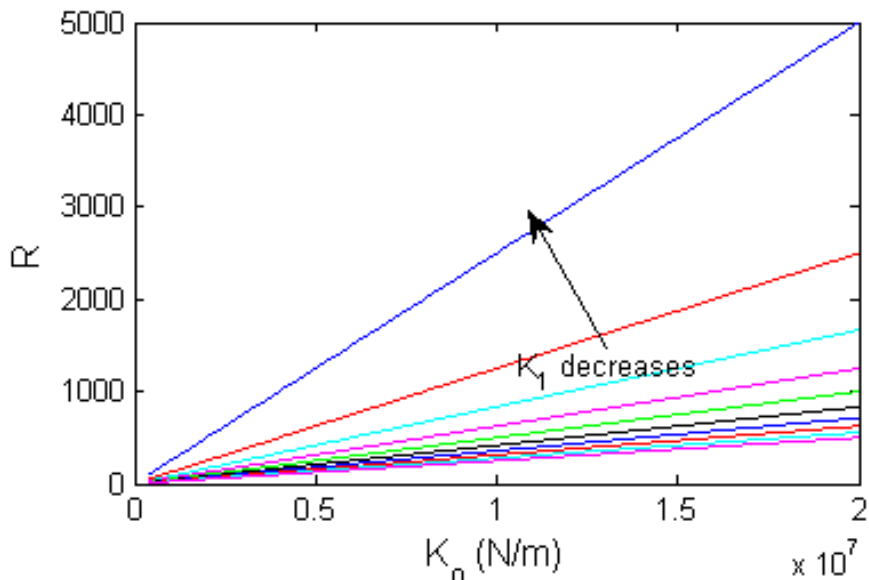
**Figure 4.4:** Acceleration Amplitudes and ratio versus at lower excitation frequency range 50-550 Hz and at  $K_1 = 4$  MN/m and  $m_1 = 40$  gm



Figure 4.5 and Figure 4.6 study the effect of decreasing the stiffness  $k_1$  while  $k_2 = 4$  MN/m and  $m_1 = m_2 = 40$  gm and  $w=50$  Hz. The acceleration amplitude  $X_1$  decreases as the stiffness  $k_1$  decreases. And the acceleration amplitudes decrease as the masses increase. While the amplitudes ratio  $R$  dependent on  $k_o$  linearly. And  $R$  increases dramatically with decreasing the stiffness  $k_1$ .



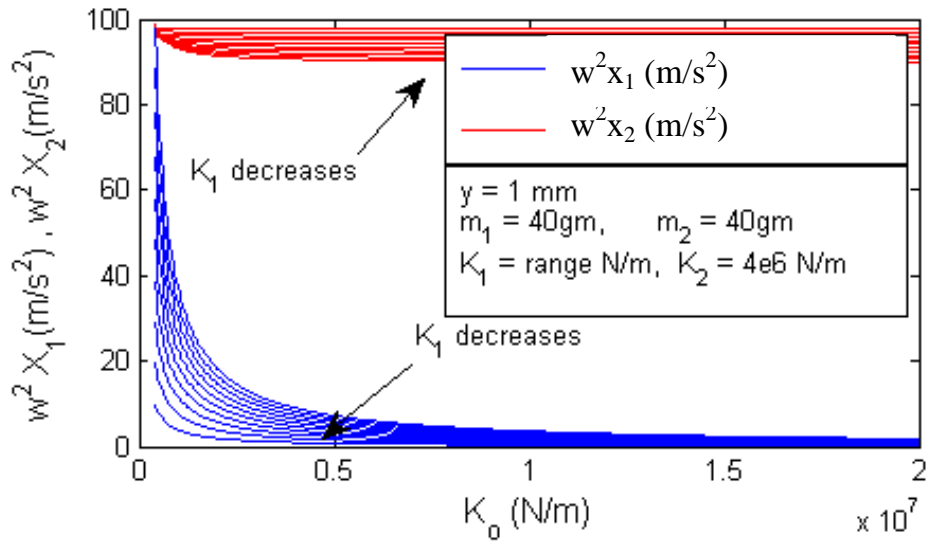
(a) Acceleration Amplitudes of the two masses versus the stiffness  $K_o$



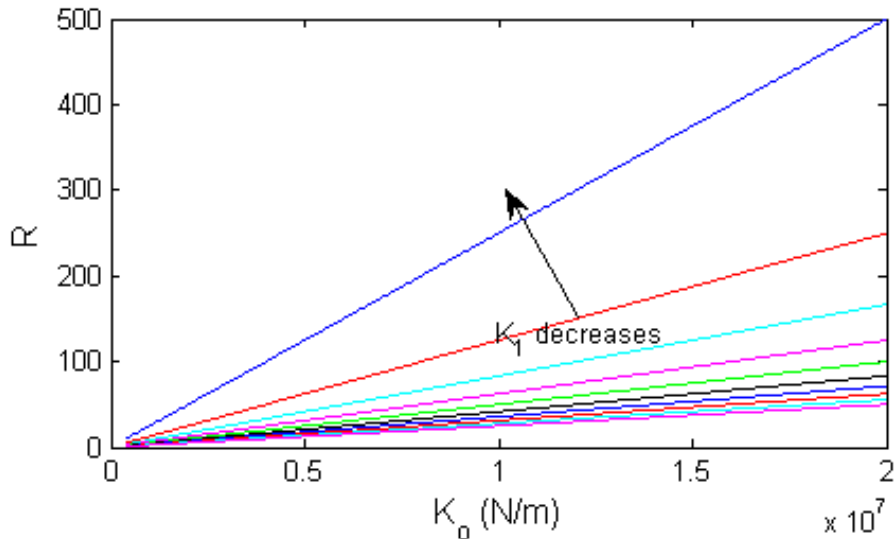
(b) Amplitudes Ratio  $R = X_2/X_1 = w^2 X_2 / w^2 X_1$  linear relation with the stiffness  $K_o$

**Figure 4.5:** Acceleration Amplitudes and ratio versus at lower range of  $k_1$  with excitation frequency 50 Hz and at  $K_2 = 4$  MN/m and  $m_1 = 40$  gm

When  $w = 50$  Hz,  $K_1 = \text{linspace}(4e4, 4e5, 10)$  N/m



(a) Acceleration Amplitudes of the two masses versus the stiffness  $K_0$

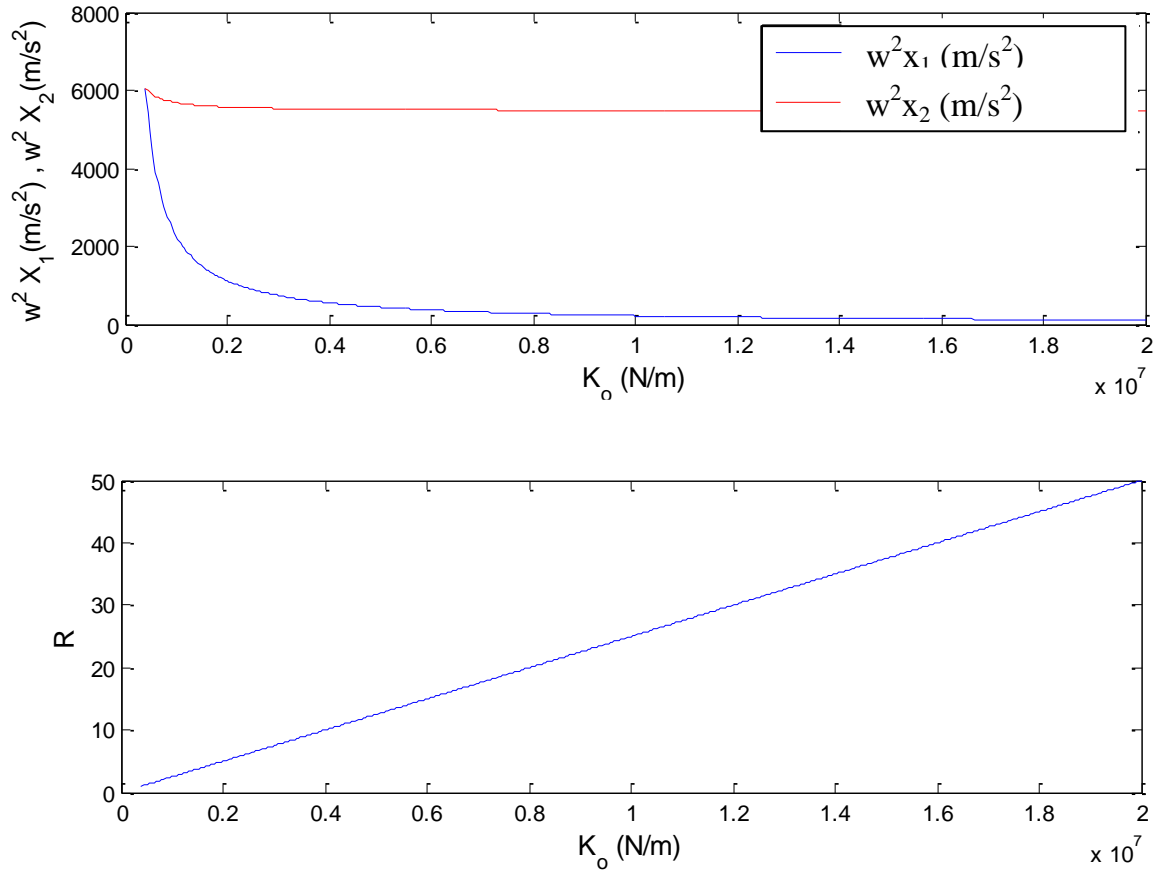


(b) Amplitudes Ratio  $R = X_2/X_1 = w^2 X_2 / w^2 X_1$  linear relation with the stiffness  $K_0$

**Figure 4.6:** Acceleration Amplitudes and ratio versus at higher range of  $k_1$  with excitation frequency 50 Hz and at  $K_2 = 4$  MN/m and  $m_1 = 40$  gm

Figure 4.7 shows the selected design in accelerometer range of 600g, where g is the gravity  $9.81 \text{ m/s}^2$  nearly  $10 \text{ m/s}^2$  and excitation frequency 380 Hz,  $m_1=m_2=40 \text{ gm}$ ,  $K_1=400 \text{ kN/m}$  (softer), and  $K_2=4 \text{ MN/m}$ (harder).

When  $w=380 \text{ Hz}$ ,  $K_1=4e5 \text{ N/m}$ ,  $K_2=4e6 \text{ N/m}$  (hard)



(b) Amplitudes Ratio  $R=X_2/X_1 = w^2 X_2 / w^2 X_1$  linear relation with the stiffness  $K_o$

**Figure 4.7:** Acceleration Amplitudes and ratio versus at lower range of  $k_1$  with excitation frequency 380 Hz and at  $K_1=400 \text{ kN/m}$  (softer),  $K_2=4 \text{ MN/m}$ (harder) and  $m_1=40 \text{ gm}$

### 4.1.3 Comparison between Single DOF and Two DOF Sensor Systems

In this section a comparison between the two sensors models and required formula, as proved earlier. The main advantage in the 2DOF sensor model is that the linear formula is obtained at  $\omega = \omega_{11} = \sqrt{K_1/m_1}$  away from resonance frequencies of the system as shown in Table 4.1.

**Table 4.1:** Comparison between 1 DOF and 2 DOF sensor systems

Modelling Method:	Requirement	Output	Advantages	Disadvantages
<b>1DOF spring only</b>	$Z = \frac{\text{output}}{\text{input}} = \frac{\omega^2 X_1}{\omega^2 Y}, \quad R = \frac{1}{Z}$ $k_o = k_1 \left( R - 1 + \frac{\omega^2}{\omega_1^2} \right)$ $k_o = f(R, \omega, \omega_1, k_1)$ <p>At  <math>\omega = \omega_1 = \sqrt{K_1/m_1}</math> ...resonance  <math>k_o = k_1 R</math></p>	$K_o$ is Linear with the ratio $I/(X/Y)$	Linear relation $R=I/Z = f(K_o, K_1)$	1- Need to work at $\omega = \omega_1$ (the resonance freq.) 2- The input vibration is transferred to the ground, which may affect the measurements.
<b>2DOF spring only</b>	$R = \frac{\text{output2}}{\text{output1}} = \frac{\omega^2 X_2}{\omega^2 X_1}$ $k_o = k_1 \left( R - 1 + \frac{\omega^2}{\omega_{11}^2} \right)$ $k_o = f(R, \omega, \omega_{11}, k_1)$ <p>At  <math>\omega = \omega_{11} = \sqrt{K_1/m_1}</math> not resonance  <math>k_o = k_1 R</math></p>	$K_o$ is Linear with the ratio $(X_2/X_1)$	- Linear relation $R = f(K_o, K_1)$ - with big $K_2$ , can be isolated from the ground - Need to work at $\omega = \omega_{11}$ (not the resonance freq.)	1- The input vibration is transferred to the ground, which may affect the measurements.

The above methods still need experimental verification. In the next chapter, another method (based on the vibration absorption phenomenon) will be presented, because the ratio  $R = X_2/X_1$  may suffer from noise in the experimental work especially if noise in  $X_1$ .

## 4.2 Novel Sensor Description

The sensor is modeled as 2-DOF system, where  $m_1$ ,  $m_2$ ,  $k_1$ , and  $k_2$  are small mass, big mass, small spring stiffness and big spring stiffness, respectively. While the ground stiffness is modeled as  $k_o$  (sensed object stiffness), as shown in Figure 4.8. The mass  $m_2$  is subjected to sinusoidal excitation force:  $f_u = F_u \sin(\omega t)$ , where  $F_u$  is the excitation force amplitude and  $\omega$  is the excitation frequency, respectively. The system is designed to satisfy the vibration absorber phenomenon where:

$$\omega_{11} = \sqrt{k_1/m_1} = \omega_{22} = \sqrt{k_2/m_2} \quad (4.22)$$

At  $k_o$  equals zero (no object is in contact) and when the system operates at  $\omega = \omega_{22} = \omega_{11}$  the vibration absorber phenomenon occurred (where the displacement of the mass  $m_2$  equals zero and the whole the excitation energy is absorbed by the mass  $m_1$ . where the absorber part ( $m_1$ ,  $k_1$ ) exerts a force equals and opposites to the acting force on  $m_2$  [56]. When the sensor contacts an object with certain stiffness  $k_o$ , the overall system natural frequencies are shifted and also the vibration absorber frequency  $\omega_{Abs}$  of the phenomenon is also shifted. There is a direct relation between  $k_o$  and that frequency as will be clarified in the following derivation.

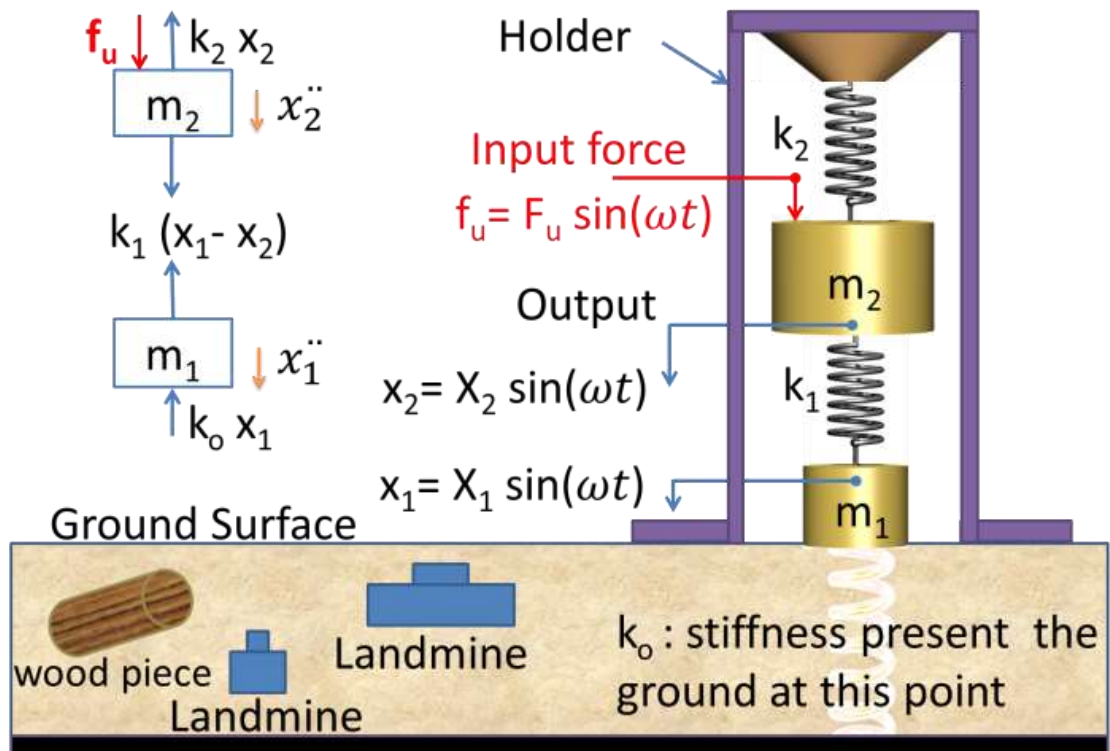


**Figure 4.8:** Sensor physical model and free body diagram.

### 4.3 Mathematical Derivation

From the free body diagram in Figure 4.8 the dynamic equations are as follow:

$$m_1 \ddot{x}_1 + (k_o + k_1) x_1 - k_1 x_2 = 0 \quad (4.23)$$

$$m_2 \ddot{x}_2 + (k_1 + k_2) x_2 - k_1 x_1 = f_u \quad (4.24)$$

By solving these differential equations, the amplitudes  $X_1$ ,  $X_2$  are:

$$X_2 = \frac{\left[ \frac{F_u}{k_2} \right] \left[ \left( 1 + \frac{k_o}{k_1} \right) - \left( \frac{\omega}{\omega_{11}} \right)^2 \right]}{\left[ \left( 1 + \frac{k_1}{k_2} \right) - \left( \frac{\omega}{\omega_{22}} \right)^2 \right] \left[ \left( 1 + \frac{k_o}{k_1} \right) - \left( \frac{\omega}{\omega_{11}} \right)^2 \right] - \frac{k_1}{k_2}} \quad (4.25)$$

$$X_1 = \frac{X_2}{\left[ \left( 1 + \frac{k_o}{k_1} \right) - \left( \frac{\omega}{\omega_{11}} \right)^2 \right]} = \frac{[F_u/k_2]}{\left[ \left( 1 + \frac{k_1}{k_2} \right) - \left( \frac{\omega}{\omega_{22}} \right)^2 \right] \left[ \left( 1 + \frac{k_o}{k_1} \right) - \left( \frac{\omega}{\omega_{11}} \right)^2 \right] - \frac{k_1}{k_2}} \quad (4.26)$$

A vibration absorber phenomenon occurs at:  $X_2=0$

$$\left[ \left( 1 + \frac{k_o}{k_1} \right) - \left( \frac{\omega}{\omega_{11}} \right)^2 \right] = 0 \quad (4.27)$$

$$X_1 = \frac{-F_u}{k_1} \quad (4.28)$$

Thus the frequency at the vibration absorber phenomenon:

$$\omega_{Abs} = \sqrt{\omega_{11}^2 \left( 1 + \frac{k_o}{k_1} \right)} \quad (4.29)$$

Thus the ground stiffness  $k_o$  and the frequency ( $\omega_{Abs}$ ), at which the vibration absorber phenomenon occurs can be expressed as follows:

$$k_o = k_1 \left( \frac{\omega_{Abs}^2}{\omega_{11}^2} - 1 \right) \quad (4.30)$$

#### 4.4 Measuring Range of Sand-Landmine Problem

Unlike Young's modulus, stiffness is not only dependent on the material property of an object, but also on its dimensions. It is assumed that, the ground material is homogeneous elastic and incompressible. If the ground is excited by a vertical load,  $F$ , acting over an indenter of radius  $r$  as shown in Figure 4.9, the local static stiffness of the land  $k_o$  can be expressed as follows [57]:

$$E = \frac{(1 - \nu^2)F}{2rd} \quad (4.31)$$

$$k_o = \frac{F}{d} = \frac{2rE}{(1 - \nu^2)} \quad (4.32)$$

Where:  $E$ ,  $\nu$ ,  $h$ , and  $d$ , are the Young's Modulus, Poisson's ratio of the ground, the ground height from rigid rock and indentation depth respectively.

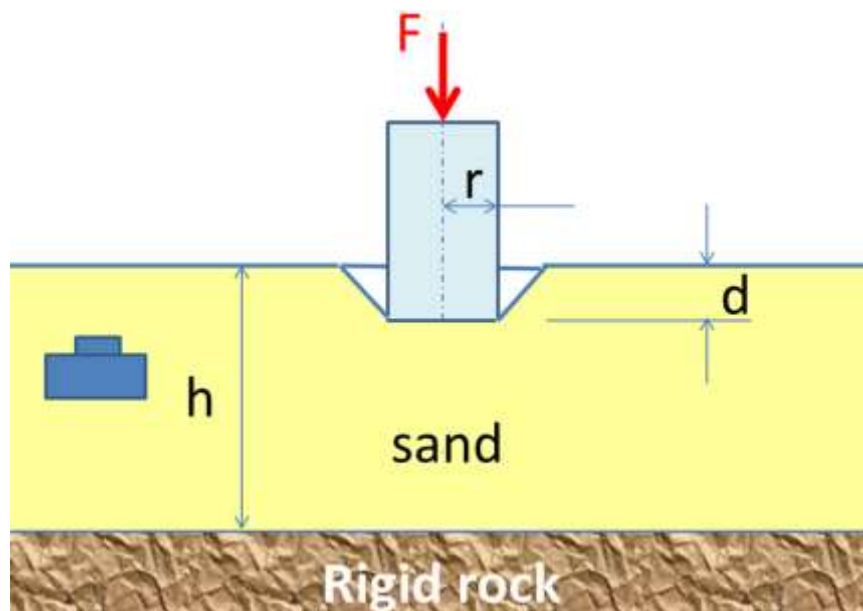


**Figure 4.9:** Indentation model parameters.

From Equation (4.32), in order to estimate the stiffness measuring range, it is required to select the Young's modulus range and the indenter radius. Table 4.2 and Table 4.3 show Young's Modulus for granular and cohesive materials [58-61]. From literature, typical medium uniform sand Young's modulus values: 30- 50 MPa. Base on the sand-landmine finite element model, the stiffness of the sand above landmine increases around three times [52]. In this model Young's Modulus range is selected be up to 150 MPa (50MPa x 3) to represent the presence of landmine with the indenter radius is 5 mm. By applying Equation (4.32), the stiffness measuring range can be estimated as 0-2 MN/m.

**Table 4.2:** Typical values of Young's modulus for granular material (MPa)

Type	Description	Loose	Medium	Dense
GW, SW	Gravels/Sand well-graded	30-80	80-160	160-320
SP	Sand, uniform	10-30	30-50	50-80
GM, SM	Sand/Gravel silty	7-12	12-20	20-30

**Table 4.3:** Typical values of Young's modulus for cohesive material (MPa)

Type	Description	Very soft to soft	Medium	Stiff to very stiff	Hard
ML	Silts with slight plasticity	2.5 - 8	10 - 15	15 - 40	40 - 80
ML, CL	Silts with low plasticity	1.5 - 6	6 - 10	10 - 30	30 - 60
CL	Clays with low-medium plasticity	0.5 - 5	5 - 8	8 - 30	30 - 70
CH	Clays with high plasticity	0.35 - 4	4 - 7	7 - 20	20 - 32
OL	Organic silts	-	0.5 - 5	-	-
OH	Organic clays	-	0.5 - 4	-	-

#### 4.5 Parameters Selection Criterion Based on Vibration Absorber System

In this section the criterion for selecting the sensor parameters ( $m_1$ ,  $k_1$ ,  $m_2$ , and  $k_2$ ) are decided:

1. First of all the ratio between the springs stiffness and the masses must satisfy the vibration absorber equality in Equation (4.22).
2. To get clear point of phenomenon occurrence (easily find zero displacement at  $m_2$ ),  $m_1/m_2 = 0.5$  is considered [56].
3. The relation between  $\omega_{Abs}-k_o$  derived in Equations (4.29, 4.30), should be linear through the working range, in order to maintain constant sensitivity along the measuring range.
4. The sensitivity value ( $d\omega_{Abs}/dk_o$ ), which is directly adapted by ( $k_1$ , and  $m_1$ ) should be as large as possible to realize high accuracy when obtaining the object stiffness  $k_o$ .
5. The masses  $m_1$  and  $m_2$  should be as small as possible in order to not activate the landmine.
6. The masses  $m_1$  and  $m_2$  should be as small as possible in order increase the frequency range at certain  $k_1$ , and  $k_2$ .



## 4.6 Modeling and Simulation

### 4.6.1 Mathematical Model

In this section the frequency responses of  $x_1$  and  $x_2$ , the displacements of the lumped masses  $m_1$  and  $m_2$ , respectively, are determined using MATLAB, based on Equations (4.25, 4.26). Then, the frequency at which the zero displacement at  $m_2$  occurs (vibration absorber phenomenon) is determined using the flowchart shown in Figure 4.10. The relation between the sand stiffness ( $k_o$ ) and the corresponding frequency ( $\omega_{Abs}$ ), at which the vibration absorber occurs is determined as for the selected design parameters:  $m_1= 0.0017$  kg,  $k_1= 1.78$  kN/m (based on the available Piezo actuator PIEZO SYSTEMS: T434-A4-201),  $m_2= 2 m_1$ , and  $k_2= 2k_1$  (criteria 1 and 2 are applied here). The normalized displacements, of the two masses vs. the excitation frequency, are presented in Figure 4.11, at certain  $k_o$  values.

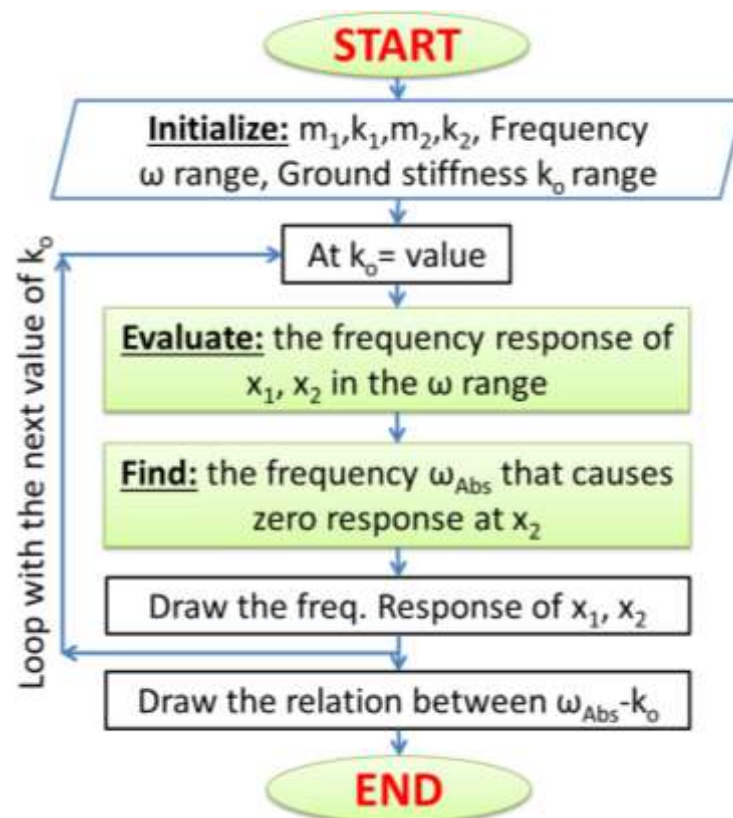
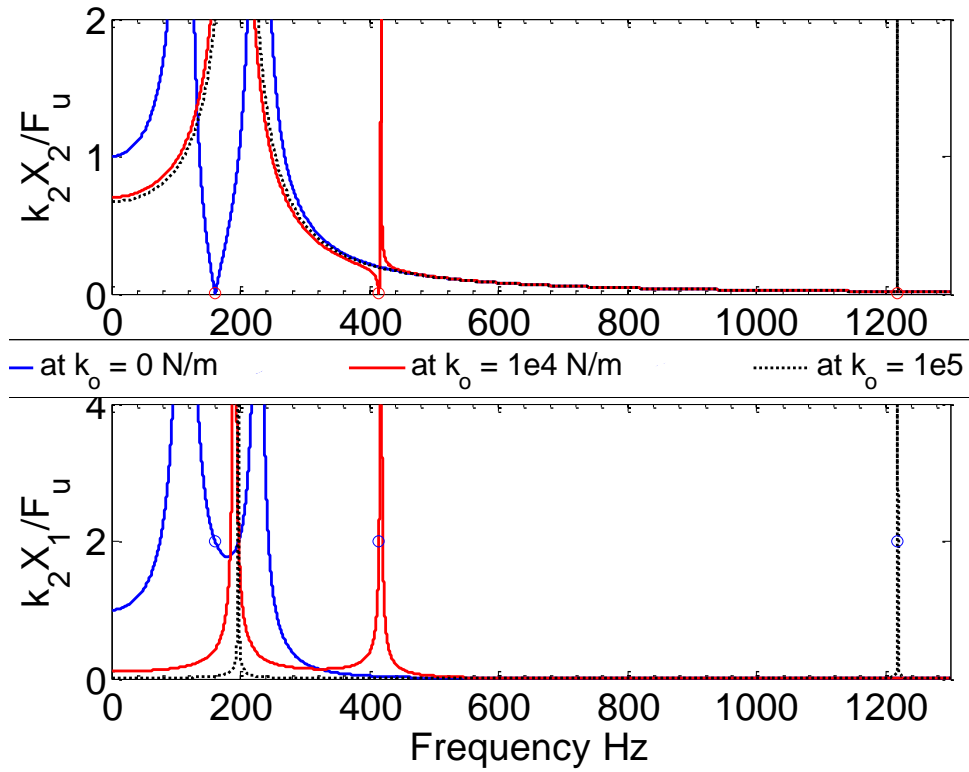
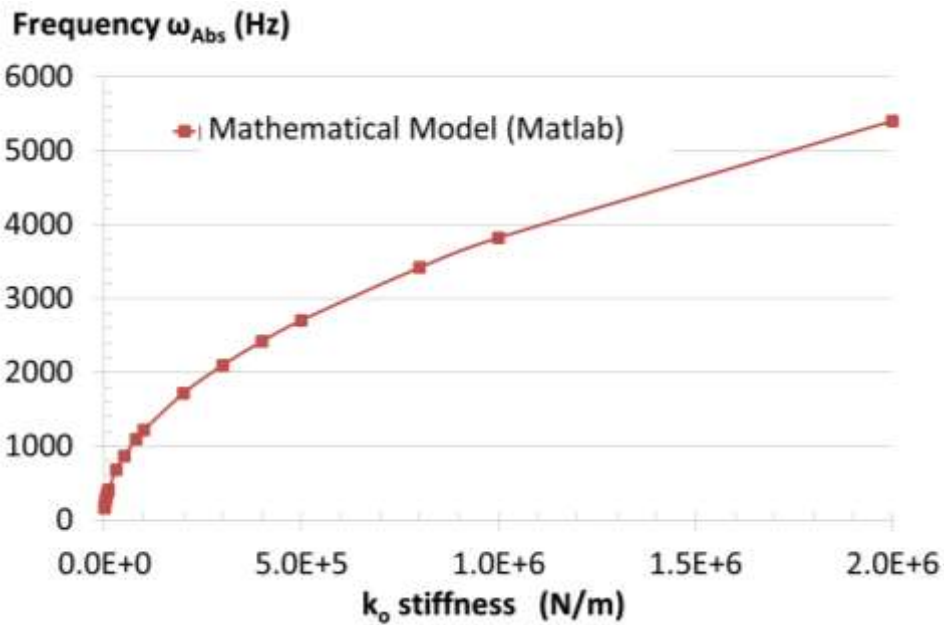


Figure 4.10: Flow chart of the mathematical model algorithm.



**Figure 4.11:** Frequency response of  $x_2$ ,  $x_1$  at certain ground stiffness  $k_o$  values, and the corresponding vibration absorber frequency  $\omega_{Abs}$ .



**Figure 4.12:** Frequency response at certain ground stiffness  $k_o$  values, and the corresponding vibration absorber frequency  $\omega_{Abs}$ .

From the Figure 4.11, and at  $k_o = 0$  N/m (blue curve), it is clear that the vibration absorber phenomenon is happened at frequency  $\omega = \omega_{Abs} = 161.2$  Hz, where the  $x_2$  response equals zero. For the same sensor parameters but at different ground stiffness values:  $k_o = \{10^4, 10^5\}$  N/m, the corresponding vibration absorber frequencies are different. As presented in Figure 4.12, it is clear that this relation is nonlinear. This is why the sensor parameters should be properly selected to fulfill the criteria in section 4.5. In the next section a finite element method will be used to determine the vibration absorber frequency of the sensor system when subjected to different land stiffness  $k_o$ . The sensor dimension will be selected to fulfill the selection criteria 3, 4, 5, and 6 in section 4.5.

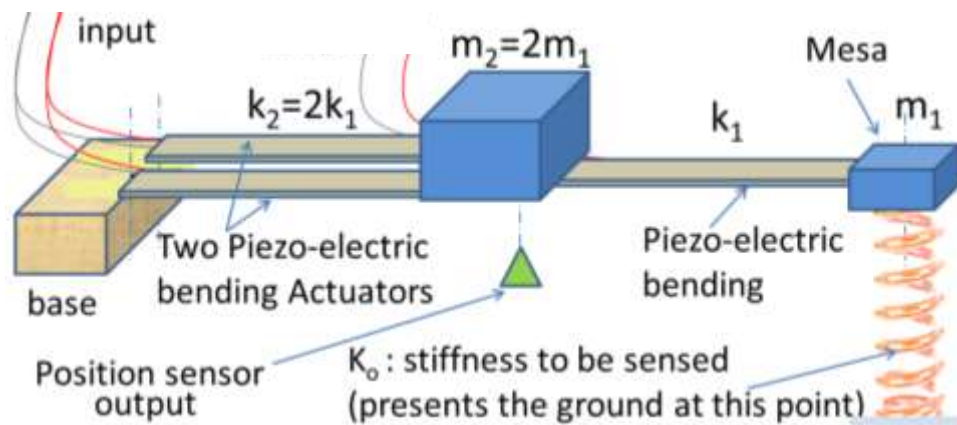


**Figure 4.13:** Piezo-electric version of the proposed sensor

#### 4.6.2 Finite Element model (with COMSOL Multiphysics)

In this section the sensor parameters ( $m_1$ ,  $k_1$ ,  $m_2$ , and  $k_2$ ) and its dimension will be selected to give the best sensitivity and linearity of the sensor. The numerical value of the sensor parameters will be based on the commercial Piezo-electric actuators cantilever system as shown in Figure 4.13. The two springs  $k_1$  and  $k_2$ , which are shown in Figure 4.8 are presented by the stiffness of the cantilever beams. The masses  $m_1$  and  $m_2$  which in Figure 4.8 is represented by the equivalent masses of the two Piezo-electric cantilever plus the concentrated masses which shown in Figure 4.13.

The Piezo-electric actuators is chosen here because it offers excitation with high frequency range more than the frequency range offered by commercial motors which used in the excitation systems such as rotating mass unbalance or cam-follower.

### 4.6.2.1 The COMSOL Model

**Model Type:** 2D Solid Mechanics

**Material:** Piezo-ceramic, Lead Zirconate Titanate, Piezo Systems Material Designation Type 5A4E (Navy Type II)

**Elastic Modulus:** 52 GPa, Poisson's: 0.38, Density: 8216 kg/m<sup>3</sup>

**Geometry:** As shown in Figure 4.14, two block for the two masses and two beams for the two springs.

Beam1 width= Beam2 width=28.6 mm,

Mass1= 1.5 gm, Mass2= 3 gm.

**Note:** the mass  $m_I$  in the mathematical modeling and MATLAB simulation is the equivalent mass [56]:

$$m_1 = Mass1 + \frac{beam1\ mass}{4} \quad (4.33)$$

Beam thickness = height (t) = n\*0.86mm,

Where n = 1 to 5. This is to increase the beams stiffness dramatically based on the stiffness relation:

$$k = \frac{Ewt^3}{L_c^3} \quad (4.34)$$

Where:  $E$ ,  $w$ ,  $t$ , and  $L_c$  are the Young's Modulus, width, height, and length. Based on this relation and the n values, the stiffness  $k_I$  is {1, 8, 27, 64, and 125} times the original spring stiffness with  $n=1$  and  $t=0.86$  mm. These values of  $k_I$  will be used to study the effect of changing its value on the sensor sensitivity and linearity.

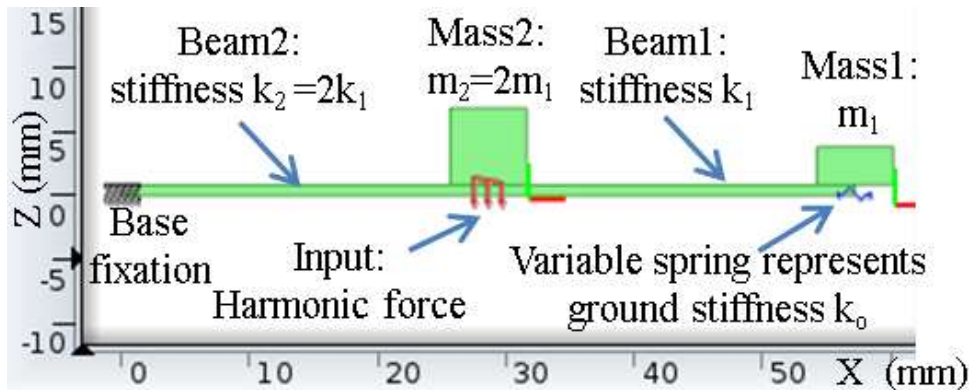


**Figure 4.14:** Finite element COMSOL model 2D beam model, load and boundary constraints

**Solid Mechanics:**

**Boundary conditions:** fixed from left.

**Boundary load:** applied at the end of the beam2, harmonic perturbation force per unit length in y direction:  $5 \times 10^2$  N/m.

Spring foundation to represent the object stiffness (the ground in our case), at each beam thickness we will find the sensor output frequency with different land stiffness:  $k_0 = \{ 0, 10^2, 5 \times 10^2, 10^3, 3 \times 10^3, 5 \times 10^3, 8 \times 10^3, 10^4, 3 \times 10^4, 5 \times 10^4, 8 \times 10^4, 10^5, 2 \times 10^5, 3 \times 10^5, 4 \times 10^5, 5 \times 10^5, 8 \times 10^5, 10^6, 1.5 \times 10^6, 2 \times 10^6 \}$  N/m.

**Meshing:** the system is meshed by:

**Type:** free Triangular. Size: extremely fine.



## **CHAPTER 5 : SIMULATION RESULTS AND PARAMETER OPTIMIZATION**

This chapter illustrates the sensor finite element model simulations results. After that it presents the optimization process and the optimum design results. The two natural frequencies, the mode shapes, and the vibration absorber frequency of the system (which composed of Piezo Systems: T434-A4-201), are determined. Finally it lists a detailed design procedure for the whole process.

### **5.1 Simulation Results**

The effect of changing the sand stiffness ( $k_o$ ) on the sensor vibration absorber frequency is shown in Figure 5.1, the simulation results is presented for ( $n=1, k_I=1.78$  kN/m).

Figure 5.1 shows that, this design dimension couldn't satisfy the required measurement range 0- 2 MN/m because saturation occurs after stiffness ( $k_o$ ) =  $2 \times 10^5$  N/m. Also another problem appears that the vibration absorber frequency ( $\omega_{Abs}$ ) is very close to the upper natural frequency of the system in the range up to  $k_o = 10^5$  N/m, as shown in Figure 5.2. This means it is difficult to distinguish the vibration absorber frequency ( $\omega_{Abs}$ ), during changing the excitation frequency. At  $k_o = 10^5$  N/m the difference between the second natural frequency and the vibration absorber frequency is very small around 14 Hz, which is one of the drawbacks of this design parameter value ( $n=1, k_I=1.78$  kN/m).

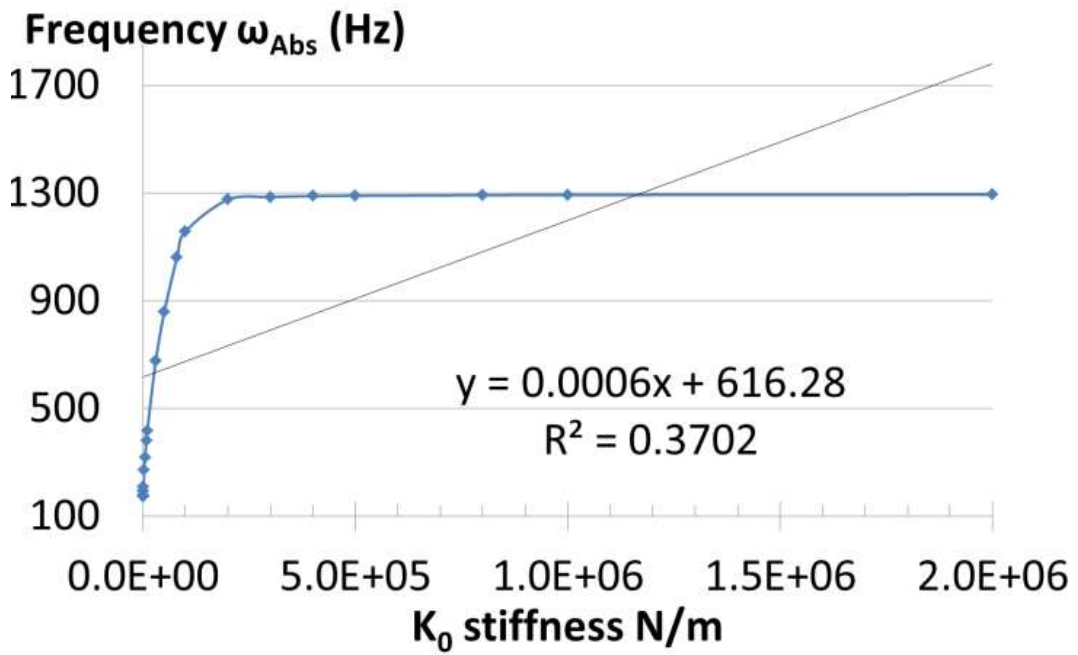


**Figure 5.1:** Linearity of the relation between  $\omega_{Abs}$ - $k_o$  (finite element model)  $k_o$  range (0 – 2 MN/m) at ( $n = 1$ ,  $k_j=1.78$  kN/m).

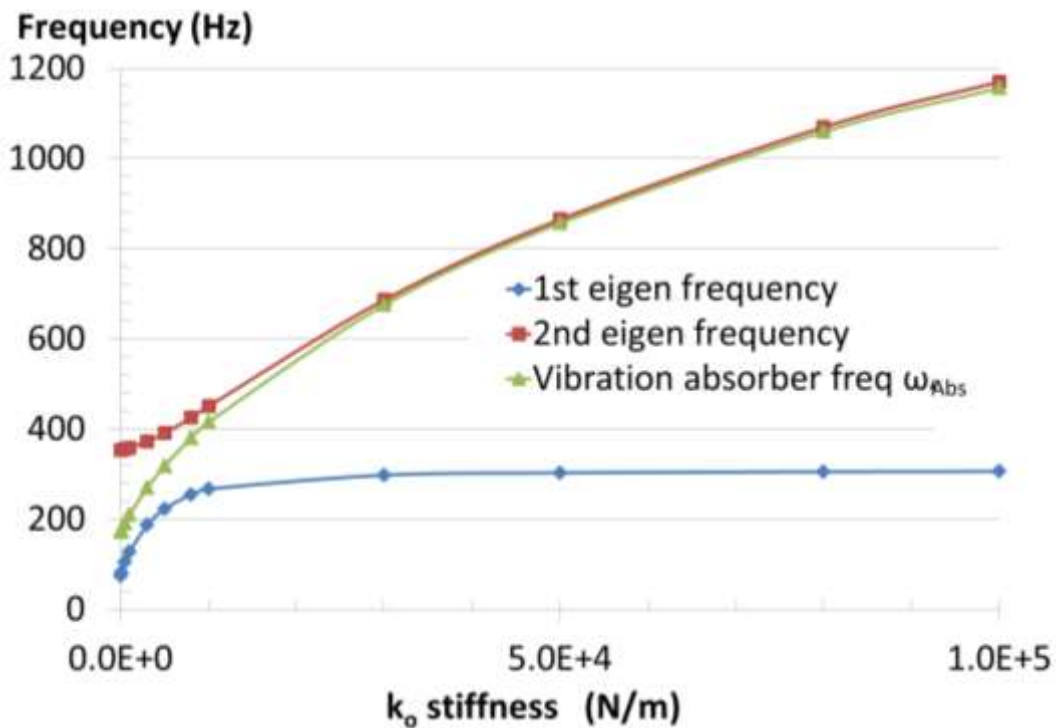


**Figure 5.2:** Sensor frequencies when changing stiffness  $k_o$  at ( $n=1$ ,  $k_j=1.78$  kN/m).



## 5.2 Parameter Optimization

In this section, it may be better to start with a question:

“How to: maximize the linearity, range and also the sensitivity?”

Figure 5.1 shows the linearity in terms of square correlation ( $R^2$ ) of the relation between  $\omega_{Abs}-k_o$  in the range (0 – 2 MN/m) at the design parameter ( $n=1, k_I=1.78$  kN/m).  $R^2=37\%$  isn't acceptable.

The design criteria 1 and 2 is used with each design configuration at  $n= 1, 2, 3, 4, 5$ . For each stiffness  $k_I$  in Table 5.1, finite element studies are carried out to find the vibration absorber frequency ( $\omega_{Abs}$ ) when the ground stiffness ( $k_o$ ) changes in the range (0 – 2 MN/m). After that the sensitivity and the linearity are calculated for each design configuration based on the selection criteria in section 4.5.

To find the best sensor stiffness  $k_I$ , the sensitivity and linearity is drawn vs.  $k_I$ , as shown in Figure 5.3. It shows also that the linearity increases as the stiffness  $k_I$  increases. On the other hand the sensitivity increases also up to a certain level and then decreases. For getting best sensitivity with acceptable linearity, one of the three optimization rules can be considered, as follows:

1. Select  $k_I$  which give max sensitivity: at  $k_I= 6.5 \times 10^4$  N/m  
Sensitivity= $3200$  Hz/ (2MN/m) = $1600$  Hz/ (MN/m)  
But linearity is not good: 91%
2. Or select the breakpoint, the best of both sensitivity and linearity (considering the importance of both is equally weighted): at  $k_I= 1.8 \times 10^5$  N/m  
Sensitivity=  $3080$  Hz / (2MN/m) =  $1540$  Hz / (MN/m)  
And linearity= 95.1%
3. Or select the best possible sensitivity that satisfy some acceptable linearity such as 95%, from the standard Piezo-electric actuator ( $n=4, k_I=1.14 \times 10^5$  N/m).  
Sensitivity=  $3118.76$  Hz/ (2MN/m)=  $1559.38$  Hz/ (MN/m)  
And linearity= 95%

By analyzing these optimization rules, and considering our target to fabricate a sensor with best performance. The 1<sup>st</sup> rule is not suitable as the linearity is not good 91%. The 2<sup>nd</sup> rule doesn't enhance the linearity too much than the 3<sup>rd</sup> rule and also lower sensitivity. Based on the ( $n = 4$ ) parameters configuration can be considered an optimum, at which:

$$k_I = 1.14 \times 10^5 \text{ N/m}, \quad k_2 = 2 * k_I = 2.28 \times 10^5 \text{ N/m}.$$

According to the design criteria 5 and 6 (to minimize the masses as possible),  $m_2$  is selected by adding the equivalent mass of the beam2 to the expected lumped mass (3gm) of a position sensor at mass2, as shown in Figure 4.13.

$$m_2 = 5 \text{ gm}, \quad m_1 = 0.5 m_2 = 2.5 \text{ gm}.$$

After determining the best sensor parameter in the range of sand stiffness, the finite element simulation is carried out to examine these parameters on the sensor behavior.

**Table 5.1:** Parameter  $k_1$  changes effect on sensitivity and linearity

n	$k_1^{(a)}$	Total equivalent mass $m_1^{(a)}$	Sensitivity	$R^2$
	N/m	kg	Hz/(2MN/m)	
1	$1.78 \times 10^3$	0.00173	1121.25	0.37
2	$1.43 \times 10^4$	0.00199	2313.72	0.68
3	$4.82 \times 10^4$	0.00224	3136.05	0.90
4	$1.14 \times 10^5$	0.00250	3118.76	0.95
5	$2.23 \times 10^5$	0.00275	2795.01	0.96

(a)  $m_1$  and  $k_1$  and are calculated based on Equations 4.33, and 4.34.

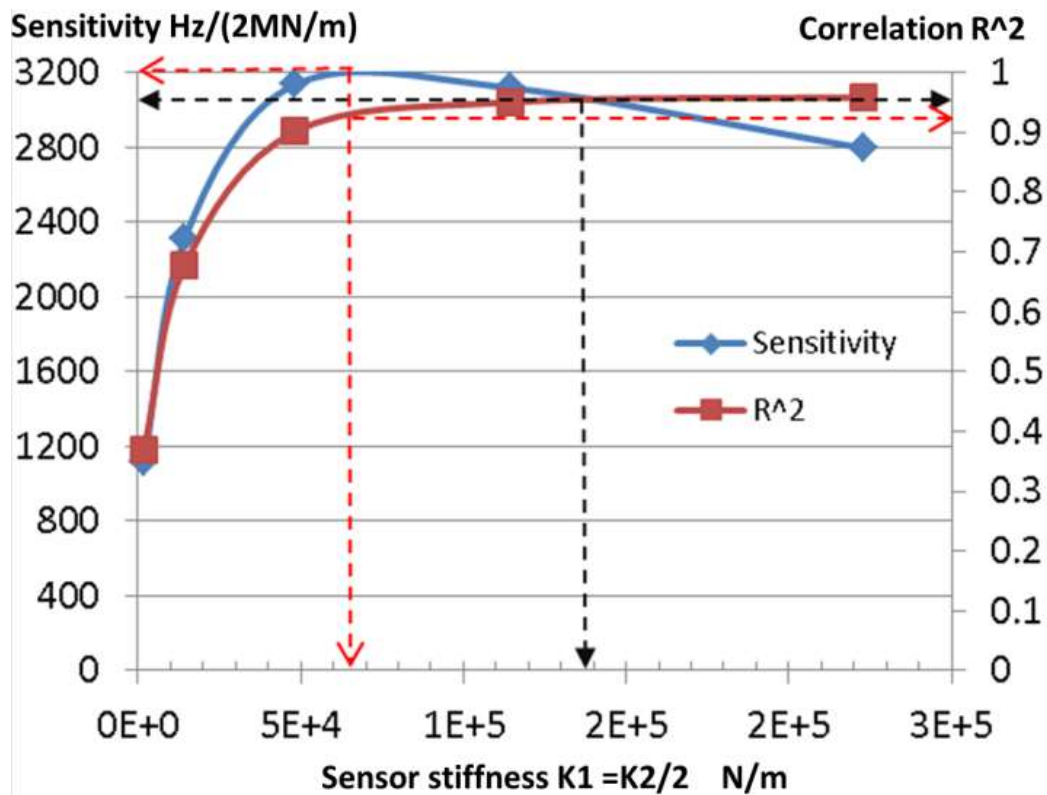


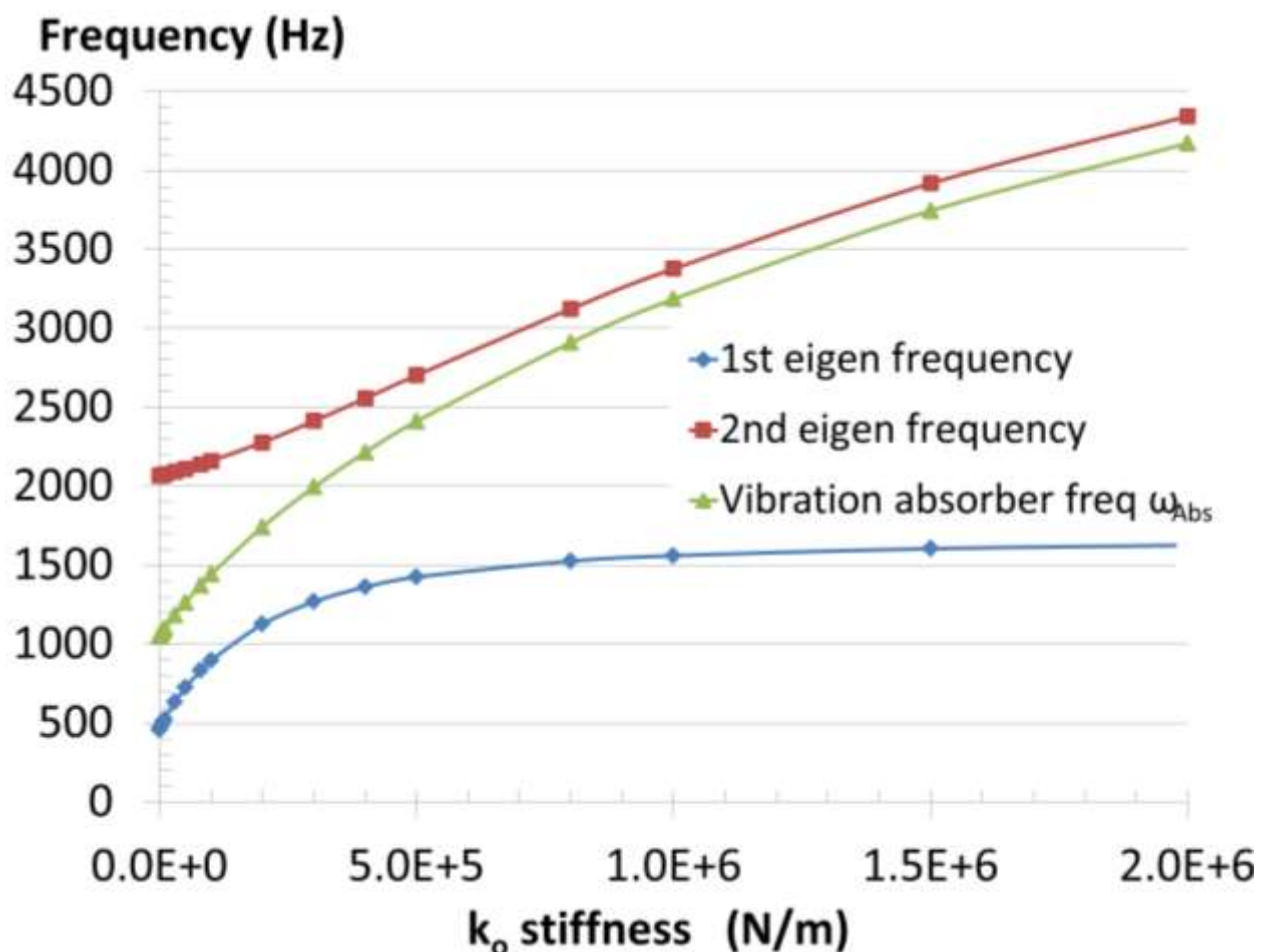
**Figure 5.3:** Optimization based on the sensor stiffness  $k_1$ .

### 5.3 Sensor Behavior with Optimum Parameter

This section will present simulation of the sensor with optimized parameters using the finite element by COMSOL, and then these results will be compared with the simplified mathematical model derived in section 4.3, using MATLAB.

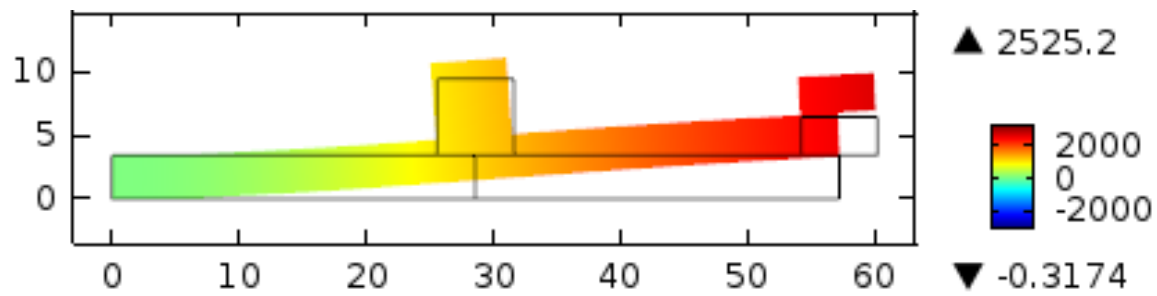
The COMSOL model here is the same as that described in section 4.6.2, as shown in Figure 4.14, except that in Geometry: Height =  $4 \times 0.86\text{mm}$ . As  $n = 4$ , so the number of actuators at beam1 is four layers and hence  $k_I = 1.14 \times 10^5 \text{ N/m}$ .

Figure 5.4 shows the vibration absorber frequency ( $\omega_{Abs}$ ), and the two natural frequencies of the sensor at different  $k_o$ . It is clear that the vibration absorber frequency ( $\omega_{Abs}$ ) can be easily distinguished from the two natural frequencies (the difference is more than 200 Hz in the worst case). The natural frequency mode shapes and the vibration absorber case of the sensor with optimum parameters are shown in Figure 5.5.

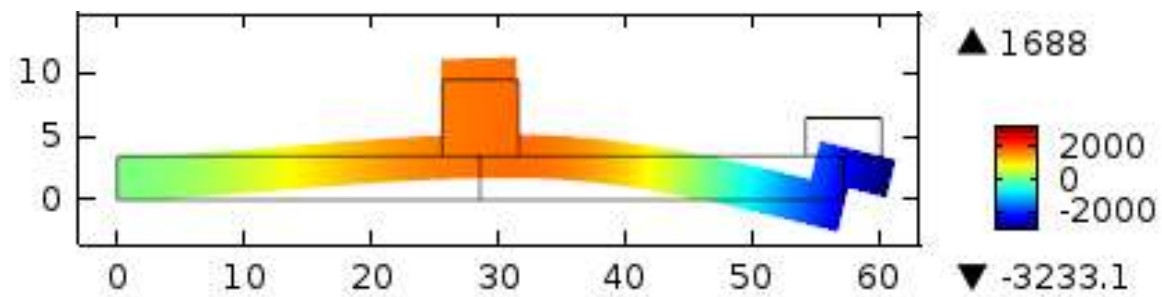


**Figure 5.4:** Optimum Sensor frequencies change when changing stiffness  $k_o$  Range (0-2 MN/m) at ( $n = 4, k_I = 1.14 \times 10^5 \text{ N/m}$ ).

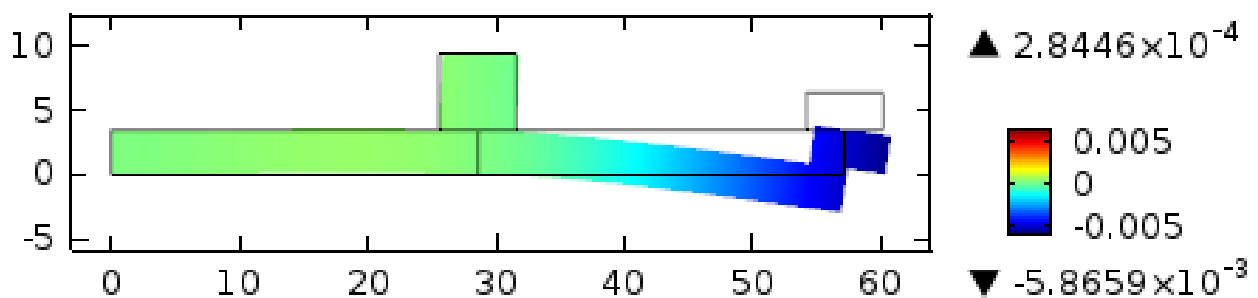
By applying the optimum parameters to the algorithm in Figure 4.10, the frequency response at the lumped masses  $m_1$  and  $m_2$  based on Equations 4.25, 4.26 can be calculated by MATLAB. Figure 5.6 shows a comparison between the mathematical results from MATLAB and the finite element by COMSOL. As shown in Figure 5.6, a difference lower than 10% is occurred between the mathematical calculation by MATLAB and finite element simulation by COMSOL.



(a) Y-displacement (mm), 1<sup>st</sup> natural frequency at 897.14 Hz



(b) Y-displacement (mm), 2<sup>nd</sup> natural frequency at 2160.42 Hz



(c) Y-displacement (mm), Vibration absorber phenomenon at frequency  $\omega_{Abs}=1441.16$  Hz when displacement =0 at  $m_2$ .

**Figure 5.5:** Finite element COMSOL model responses at ground stiffness  $k_o = 10^5$  N/m and  $(n = 4, k_I=1.14 \times 10^5$  N/m).

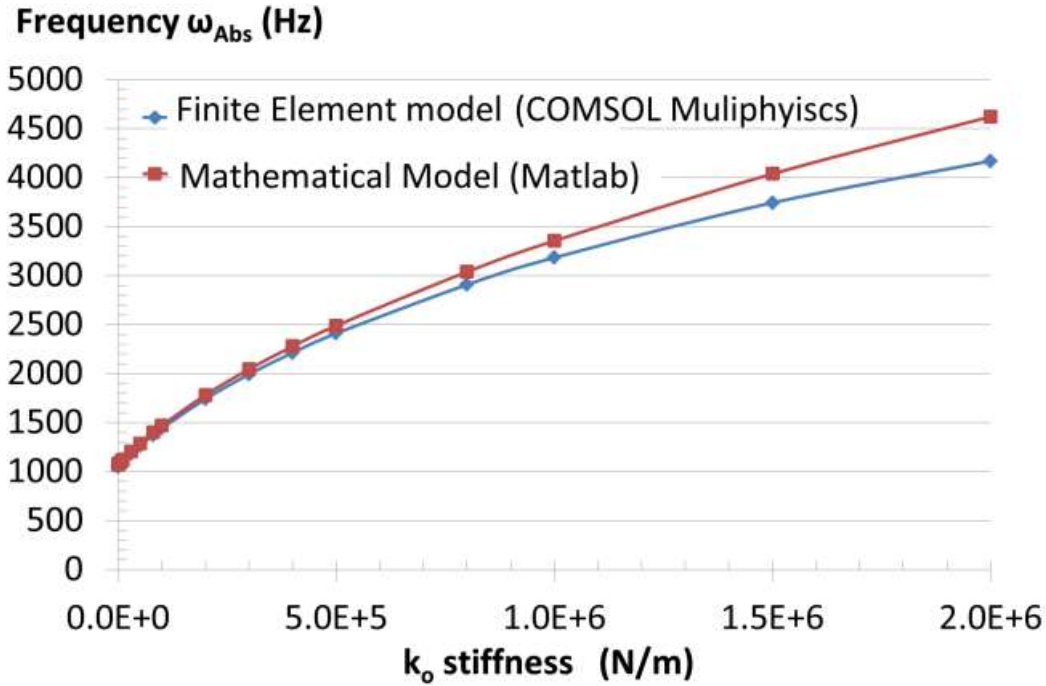


**Figure 5.6:** Optimum design comparison between the theoretical results and finite element results for stiffness  $k_o$  range (0 – 2 MN/m) at ( $n = 4$ ,  $k_I=1.14 \times 10^5$  N/m).

#### 5.4 Design Procedure of the Sensor

This concept can be applied to any application in which the stiffness measurement is needed. The measurement range may be modified according to the application. Then the following design procedure can be applied to find the best sensitivity and linearity of the sensor in the desired range as follows:

1. Start with the selection of the measuring range according the required application, see section 4.4. For sand-landmine problem a range of (0 to 2 MN/m) is selected.
2. Decide the required masses at  $m_1$  and  $m_2$ , which include some additional parts (ex: position sensor). It must be low, because increasing the masses decreases the sensitivity.
3. Use the simplified mathematical model to investigate the sensor performance from Equation (4.30). As initial guess let  $k_I$ = one-twentieth max range of  $k_o$ .
4. If the sensor performance is good, in terms of linearity and sensitivity. Then the fine tuning can be done.
5. Use a finite element modeling tool, to verify the simplified mathematical model and to find the relation between the vibration absorber frequency  $\omega_{Abs}$  and the sand stiffness  $k_o$ .
6. Find the sensitivity and linearity at each  $k_I$ .

7. Repeat 4, 5, and 6 at number of points around the correct guess of  $k_I$ . Then draw the sensitivity and linearity against  $k_I$  (e.g. Figure 5.3). Then apply the suitable optimization rules. For example, the best sensitivity with linearity measure  $R^2=95\%$ , see section 5.2, to find the best sensitivity and linearity.

## CHAPTER 6 : EXPERIMENTAL RESULTS

This chapter presents an experimental prototype for the illustration of the mathematical proven and finite element simulated sensor based on the concept of 2-DOF system vibration absorber.

### 6.1 The Need of a Prototype

For getting wide detection range 0-2 MN/m in sand-landmine problem, a large Piezo electric system (4-layers of T434-A4-201) is required as explained in the previous chapters using Matlab and COMSOL. In this chapter, the proof of concept is implemented experimentally with just one layer of the available commercial PIEZO SYSTEMS: D220-A4-503YB which is shown in Figure 6.1.

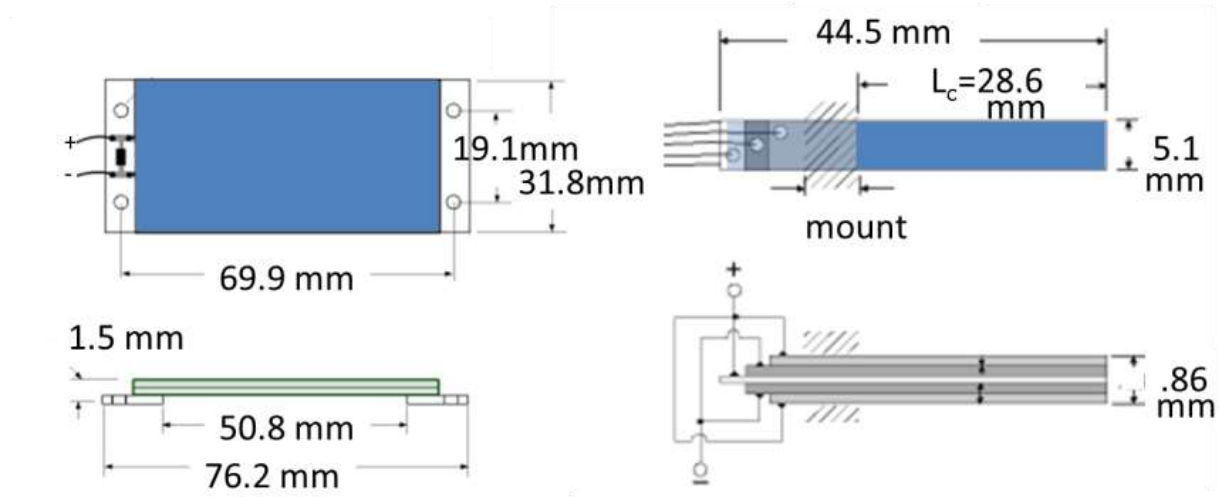


**Figure 6.1:** PIEZO SYSTEMS: D220-A4-503YB and T434-A4-201

## 6.2 Sensor Prototype

In this section a prototype is produced to validate experimentally that the contact sensor (2-DOF vibration absorber based) can be used in stiffness measurements. The experimental setup is prepared, then the sensor behavior is investigated at no contact and at contact with number of different objects stiffness  $k_o$ .

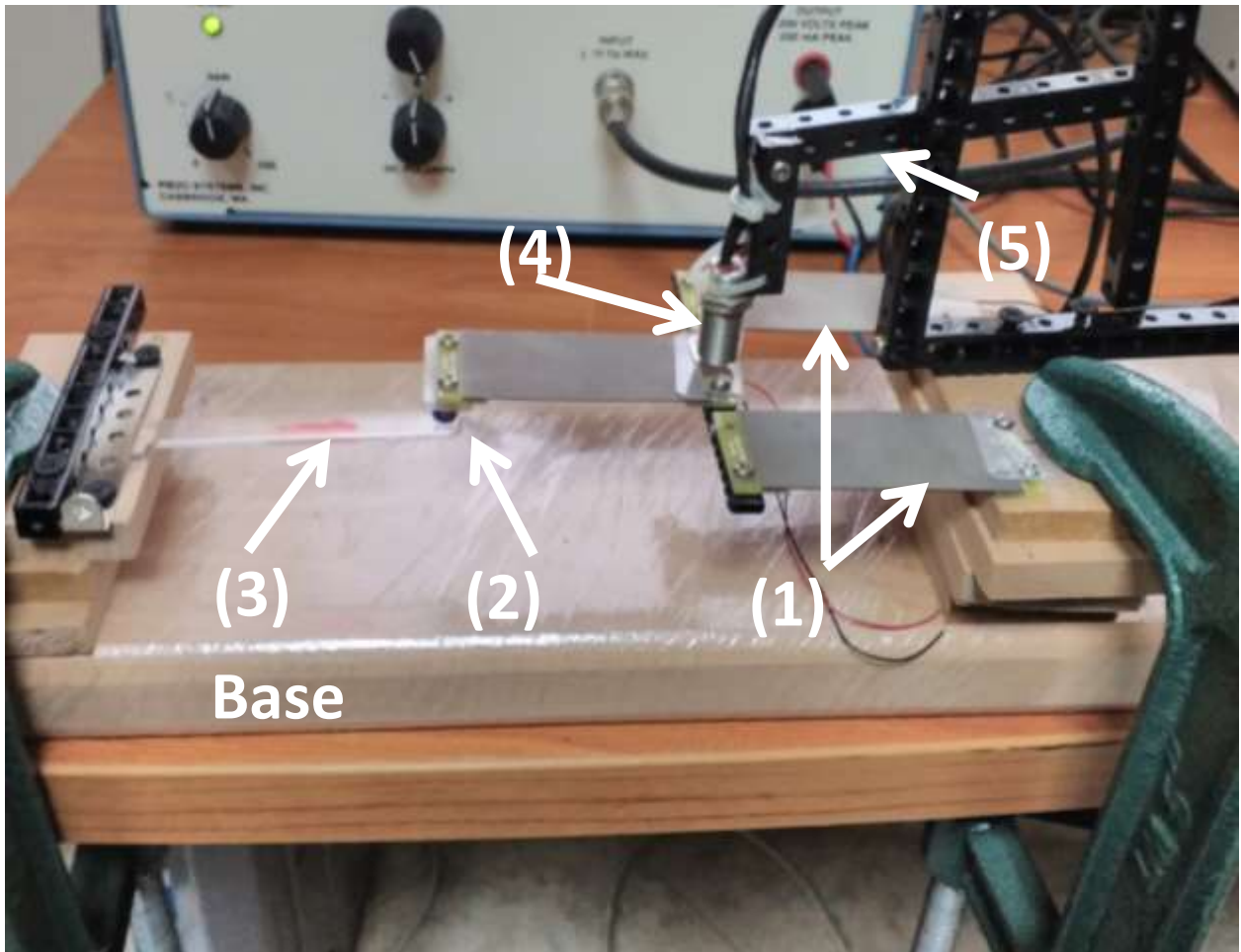
As shown in Figure 6.1, the sensor prototype consists of two cantilevers which are built to satisfy the criterion on section 4.5, using the Piezo-electric bending actuators D220-A4-503YB. Where the system parameters are:

$$k_1 = 188 \text{ N/m},$$

$$m_1 = 3.4 + 10.3/4 = 6 \text{ gm},$$

$$k_2 = 2k_1,$$

$$m_2 = 2m_1$$



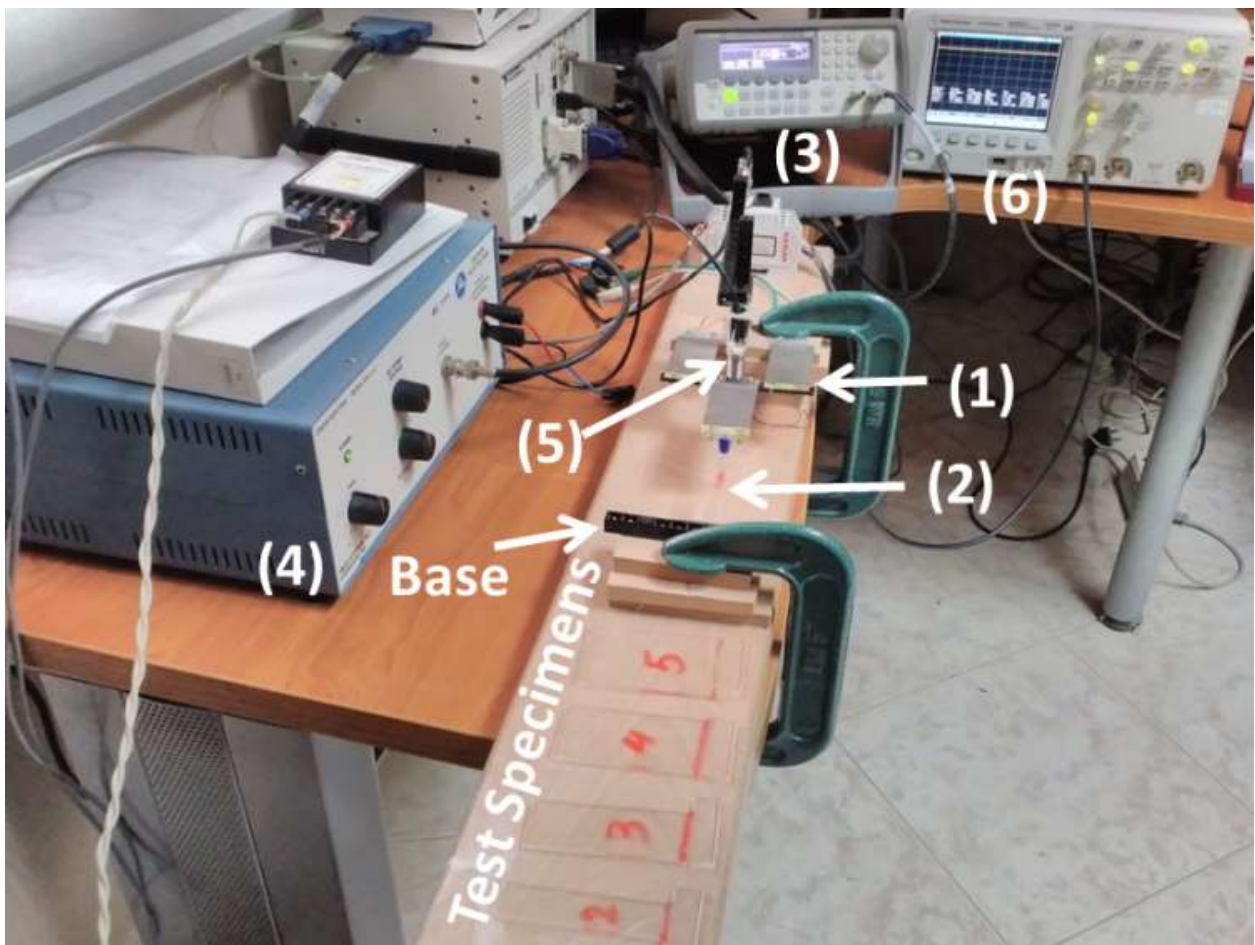
- (1) Two Piezo-electric bending Actuators
- (2) Indenter
- (3) Test specimen 1 with stiffness  $k_o$
- (4) Eddy current position sensor probe
- (5) Position sensor level adjustment mechanism

**Figure 6.2:** Sensor Prototype



### 6.3 Experimental Setup

The experimental setup consists of the sensor prototype, signal generator, amplifier, position sensor, oscilloscope and Acrylic (PMMA) cantilevers (represent the stiffness objects which are required to be measured), as shown in Figure 6.3. The stiffness  $k_o$  values are calculated for the cantilever specimens using Equation 4.13, where  $E$  equals 3 GPa for Acrylic.



- |  |                      |
|--|----------------------|
| (1) The sensor Prototype               | (2) Test specimen 1  |
| (3) Function generator                 | (4) Linear Amplifier |
| (5) Eddy current position sensor probe | (6) Oscilloscope     |

**Figure 6.3:** Experimental setup

## 6.4 Position Sensor Calibration

In this section, the eddy current position sensor is calibrated to work around 2mm, this means its output voltage is nearly zero when the metallic part is positioned 2mm away from its probe. The calibration experiment required a moving metallic plate (using digital Vernier) against the eddy current position sensor probe as shown in Figure 6.4.

The Table 6.1 states the calibration experiment result, and the Figure 6.5 shows the linear, nonlinear and saturation ranges. All our experiments after that will be executed in the linear range only.



**Figure 6.4:** Calibration experimental setup

**Table 6.1: Calibration Results**

<b>Distance (mm)</b>	<b>Voltage (V)</b>
0	-5.1
0.2	-4.61
0.4	-4.09
0.9	-2.86
1.25	-1.99
1.4	-1.63
1.6	-1.17
2.05	-0.17
2.25	0.24
2.55	0.83
2.9	1.41
3.2	1.88
3.5	2.29
3.8	2.65
4.4	3.36
5.01	3.7
5.34	3.87
5.55	4
5.82	4.07
6.13	4.2
6.6	4.33
6.95	4.39
7.22	4.44
7.83	4.5
8	4.54
8.27	4.55
8.46	4.55
8.93	4.58

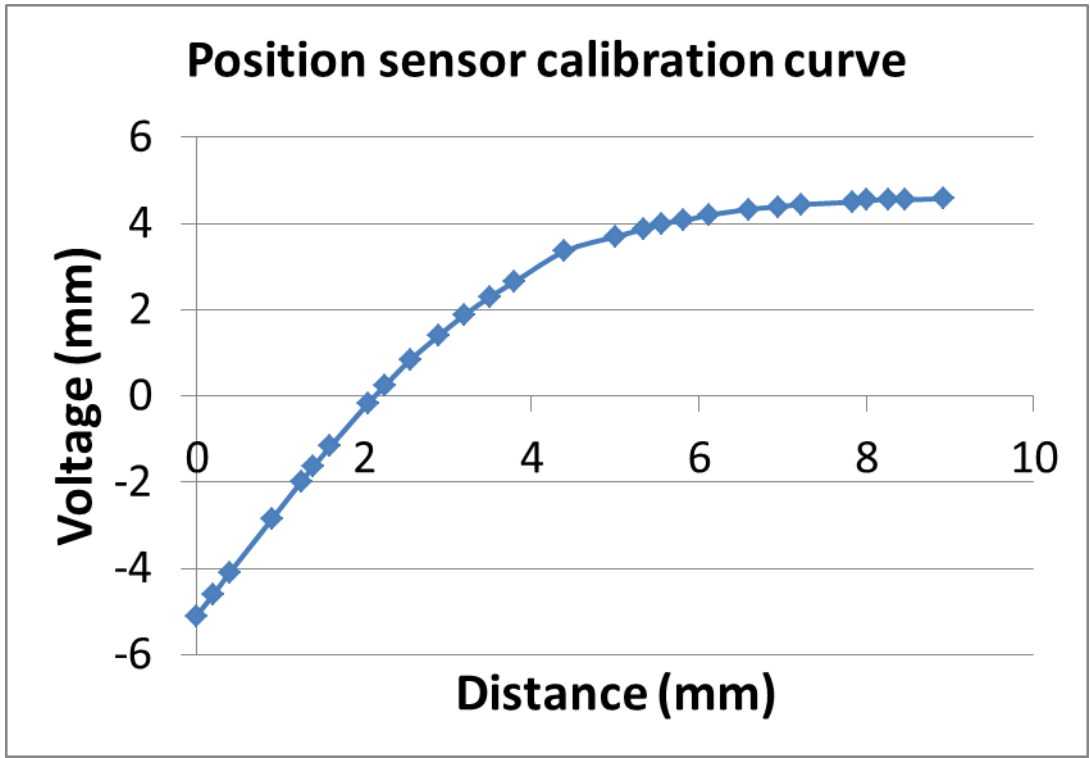


**Figure 6.5:** Eddy current position sensor calibration curve

## 6.5 Specimens Preparations

In this section, different sizes of the Acrylic (PMMA) cantilevers were fabricated using the Universal Laser-Cutting Machine as shown in Figure 6.6.

This laser cutting machine can be adjusted for cutting Acrylic with two factors: the cutting power and cutting speed.

Where:

The full cutting power = 30 Watt

And for each cutting operation, the operator adjusts the percentage of the full cutting power and full cutting speed.



**Figure 6.6:** Universal Laser Cutting Machine

Table 6.2 lists the Specimen stiffness calculation for Experiments set. In order to give almost 20 multiples of stiffness  $k_o$ . All of these 20 specimens are fabricated at the same power 50% and speed 50%.

**Table 6.2:** Experiment #3 – Specimens stiffness calculations

Experiment Set#- Specimen#	Length $L_c$	Width $w$	Thickness $t$	Young's modulus $E$	Stiffness $k_o = (E w t^3)/(4L_c^3)$
	mm	m	mm	G Pa	N/m
Exp3_SP01	75	2.05	2.48	3	55
Exp3_SP02	75	4.66	2.45	3	122
Exp3_SP03	75	7.05	2.45	3	184
Exp3_SP04	75	9.53	2.44	3	246
Exp3_SP05	75	11.99	2.46	3	316
Exp3_SP06	75	14.52	2.47	3	387
Exp3_SP07	75	16.85	2.48	3	459
Exp3_SP08	75	19.50	2.50	3	540
Exp3_SP09	75	21.89	2.52	3	620
Exp3_SP10	75	24.48	2.58	3	744
Exp3_SP11	75	27.02	2.60	3	844
Exp3_SP12	75	29.38	2.65	3	972
Exp3_SP13	75	32.07	2.70	3	1118
Exp3_SP14	75	34.35	2.74	3	1256
Exp3_SP15	75	37.13	2.79	3	1439
Exp3_SP16	75	39.53	2.83	3	1593
Exp3_SP17	75	41.96	2.87	3	1770
Exp3_SP18	75	44.57	2.88	3	1893
Exp3_SP19	75	47.00	2.96	3	2174
Exp3_SP20	75	49.57	3.01	3	2411

Figure 6.7 shows the output specimens of such cutting operation and Figure 6.8 shows specimen fixed the stiffness sensor in the final setup.



**Figure 6.7:** Twenty specimens fabricated with widths from 2.5 mm to 22.5 mm, with step 2.5 mm.



**Figure 6.8:** 5mm width specimen fixed in the final stiffness sensor setup

### 6.6 Experiment #3

In this section, the sensor response is investigated at no contact ( $k_o = 0$ ) and at contact with different stiffness. It is very important to mark that, the noise amplitude in the system is measured to be 80 mv as shown in Figure 6.9, which implies that the actual amplitude of the sensor at detection mode (vibration absorber mode) is nearly zero, as mathematically proven in Chapter 4, previously. Also Figure 6.10 shows the maximum possible displacement  $x_2$  using the Oscilloscope  $k_o=0$ , and with excitation at 1<sup>st</sup> resonance mode.

The relation between the stiffness  $k_o$  and the 3 modes (1<sup>st</sup> and 2<sup>nd</sup> resonances and vibration absorber) can be divided into three zones for each: linear zone, nonlinear zone, and saturation zone. It is clear that: The 1<sup>st</sup> resonance frequency-stiffness ( $\omega_1-k_o$ ) relation is the most critical (very high Pk-Pk) and lower sensitivity and linearity. The 2<sup>nd</sup> resonance frequency-stiffness ( $\omega_2-k_o$ ) relation has wider linearity range than the others. The vibration absorber frequency-stiffness ( $\omega_{Abs}-k_o$ ) relation has the highest sensitivity in the linear zone.



**Figure 6.9:** Oscilloscope output no excitation exist, noise only exist.





**Figure 6.10:** Oscilloscope output at  $k_o=0$ , and with excitation at 1<sup>st</sup> resonance mode.

The sensor response is investigated at no contact ( $k_o = 0$ ) and at contact with different stiffness as shown in Table 6.3 for 1<sup>st</sup> resonance mode, Table 6.4 for vibration absorber mode and Table 6.5 for 2<sup>nd</sup> resonance. The average frequency of 5 repeats of each specimen is used. The standard deviation (SD) is calculated to draw the error bar in Figure 6.11.

Figure 6.11 shows that the relation between the stiffness  $k_o$  and the 3 modes (1<sup>st</sup> and 2<sup>nd</sup> resonances and vibration absorber) can be divided into three zones for each: linear zone, nonlinear zone, and saturation zone. It is clear that: The 1<sup>st</sup> resonance frequency-stiffness ( $\omega_1-k_o$ ) relation is the most critical (very high Pk-Pk) and lower sensitivity and linearity. The 2<sup>nd</sup> resonance frequency-stiffness ( $\omega_2-k_o$ ) relation has wider linearity range than the others. The vibration absorber frequency-stiffness ( $\omega_{Abs}-k_o$ ) relation has the highest sensitivity in the linear zone. Sensitivity= 7.58 (N/m) / Hz.

**Table 6.3:** 1<sup>st</sup> resonance frequency change with stiffness  $k_o$ 

Stiff. $k_o$	1 <sup>st</sup> Resonance (Hz)							Pk-Pk Volt
	Iter.1	Iter.2	Iter.3	Iter.4	Iter.5	Avg	Std.Dev.	
N/m								
0	13.1	13.1	13.1	13.1	13.1	13.1	0.000	8
55	19	19	19	19	19	19	0.000	4.4
122	24.1	24.2	24.1	24.1	24.2	24.14	0.055	2.9
184	27.3	27.4	27.4	27.4	27.3	27.36	0.055	2.1
246	30	30	29.9	29.9	29.9	29.94	0.055	1.8
316	32.5	32.4	31.6	31.6	31.7	31.96	0.451	2
387	32.9	33.3	33.3	33.3	33.2	33.2	0.173	1.5
459	34.6	34.7	34.7	34.7	34.7	34.68	0.045	1.6
540	34.3	34.9	34.9	35	34.9	34.8	0.283	1
620	35.4	36	36	35.9	35.8	35.82	0.249	1
744	36.5	37	37	36.9	36.9	36.86	0.207	1

**Table 6.4:** Vibration absorber frequency change with stiffness  $k_o$ 

Stiff. $k_o$	Vibration Absorber mode (Hz)							Pk-Pk Volt
	Iter.1	Iter.2	Iter.3	Iter.4	Iter.5	Avg	Std.Dev.	
N/m								
0	29.4	29.5	29.4	28.9	29.6	29.36	0.270	0.076
55	34.9	34.7	34.9	35	34.6	34.82	0.164	0.078
122	42.5	42.4	42.5	42.5	42.4	42.46	0.055	0.089
184	53.2	53.6	54	53.8	53.8	53.68	0.303	0.047
246	55.2	55	55	55.2	55	55.08	0.110	0.047
316	54.6	54.8	55.5	57	57.5	55.88	1.307	0.057
387	54.2	59.1	59.8	59.8	59.8	58.54	2.445	0.08
459	61	61.5	62	61.5	61.5	61.5	0.354	0.05
540	64	60.5	60.5	60.5	61.5	61.4	1.517	0.05
620	63.1	61	62.5	64.5	64	63.02	1.370	0.065
744	66	67	67.5	67.5	67.5	67.1	0.652	0.069

**Table 6.5:** 2<sup>nd</sup> resonance frequency change with stiffness  $k_o$

Stiff. $k_o$	2 <sup>nd</sup> Resonance (Hz)							Pk-Pk
	Iter.1	Iter.2	Iter.3	Iter.4	Iter.5	Avg	Std.Dev.	
0	56.4	56.4	56.4	56.3	56.3	56.36	0.055	2.1
55	56.9	56.8	56.9	56.8	56.8	56.84	0.055	1.6
122	59.6	58.7	58.9	58.9	58.8	58.98	0.356	1.1
184	60.1	59.8	60.2	60	60.4	60.1	0.224	0.8
246	60.8	60.6	60.6	60.7	60.7	60.68	0.084	0.7
316	62.9	62.8	63.6	63.7	63.2	63.24	0.404	0.4
387	70.3	70.2	70.5	70.6	70.5	70.42	0.164	0.4
459	70.4	70.3	70.4	70.3	70.4	70.36	0.055	0.4
540	70.3	70.3	70	70	70	70.12	0.164	0.33
620	70.3	70	70	70.5	70	70.16	0.230	0.33
744	70.5	70.5	70.5	70	70	70.3	0.274	0.33

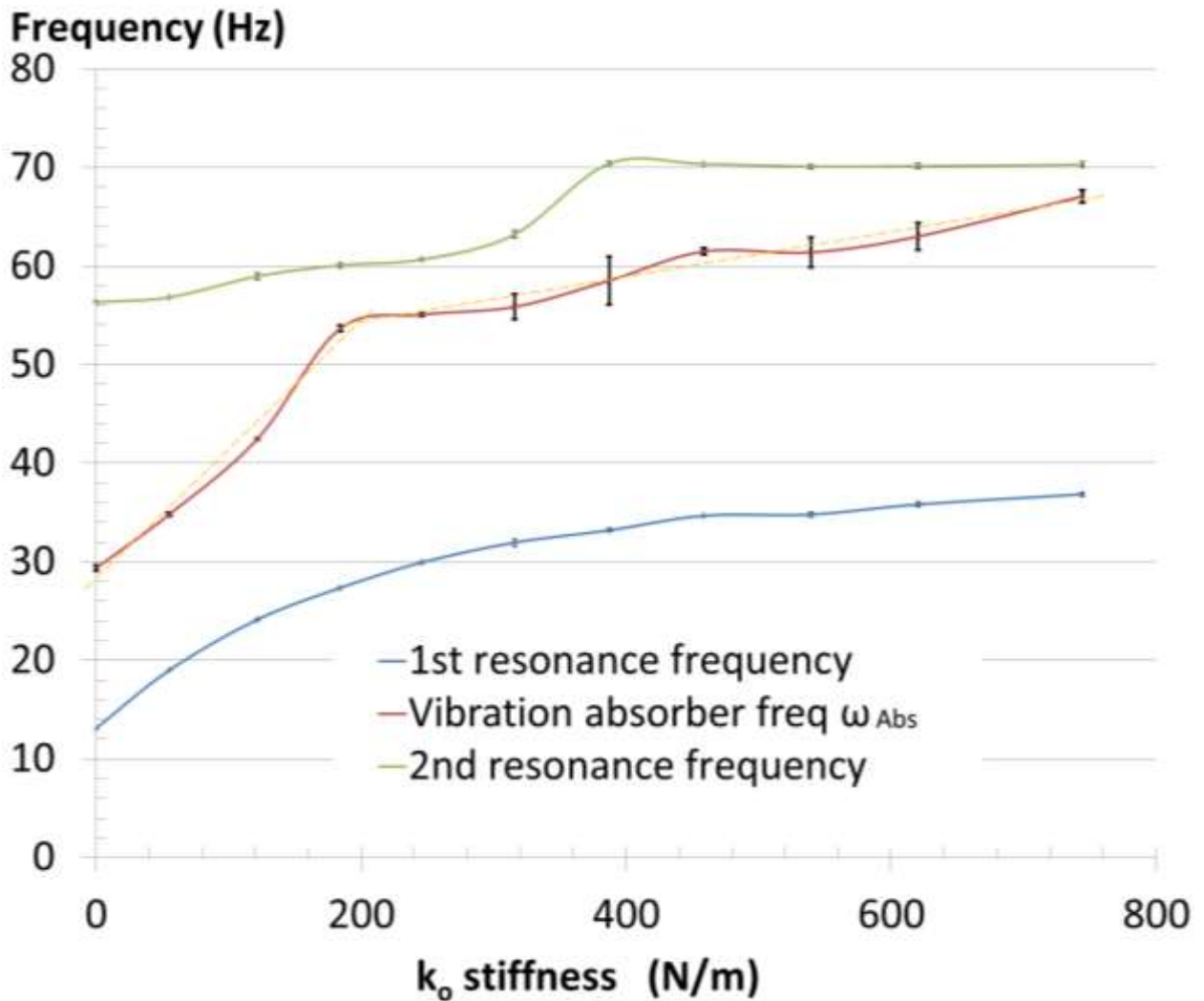


**Figure 6.11:** Experiment #3, all the specimens are form same fabrication conditions

## 6.7 Experiment #4

In this section, the sensor response is investigated at no contact ( $k_o = 0$ ) and at contact with different objects from the environment like (no object, sponge, leaves, anti-personnel landmine LM02, sand from the north coast, sand with metal part, clay from Borg Alarab, and clay with metal part) . Table 6.6 lists the 1<sup>st</sup> resonance frequency, the vibration absorber frequency and the 2<sup>nd</sup> resonance frequency of each object. Figure 6.12 locates the three frequencies of sponge as an example of soft material.

**Table 6.6:** Objects test

#	Object type	1 <sup>st</sup> resonance frequency (Hz)	Vibration absorber frequency(Hz)	2 <sup>nd</sup> resonance frequency (Hz)	Expected stiffness $k_o$ (N/m)
0	No object	13.2	29.7	56.7	0
1	Sponge	23.5	47.1	60.1	150
2	Leafs	71.2	65.5	71.2	695
3	AP landmine (LM02)	49	68.5	71.2	Out of range
4	Sand from the north coast	14.5	31.8	56.8	25
5	Sand with metal part	52	67.2	70	750
6	Clay from Borg Alarab	15	37.8	57.9	80
7	Clay with metal part	56.6	68.2	70.5	760

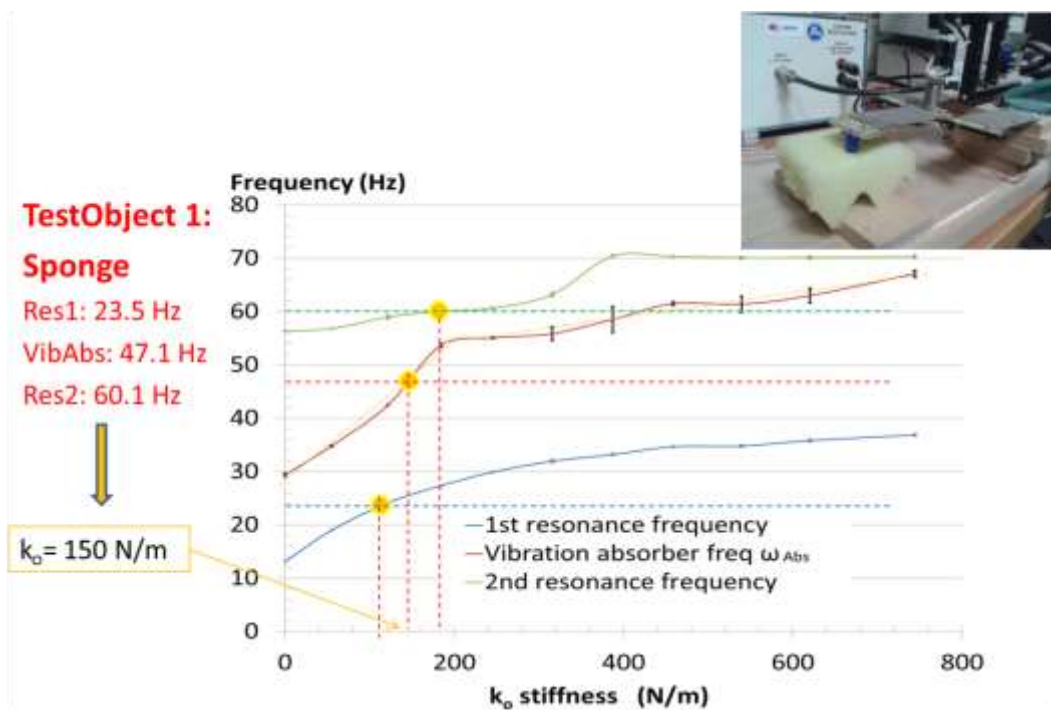


**Figure 6.12:** Test object 1, Sponge

Figure 6.13 locates the three frequencies of leaves as an example of harder material. Figure 6.14 locates the three frequencies of LM02 as an example of metal. Yellow circle indicate acceptable measure while the red circle indicate out of range. Stiffness  $k_o$  is deduced from the vibration absorber curve.

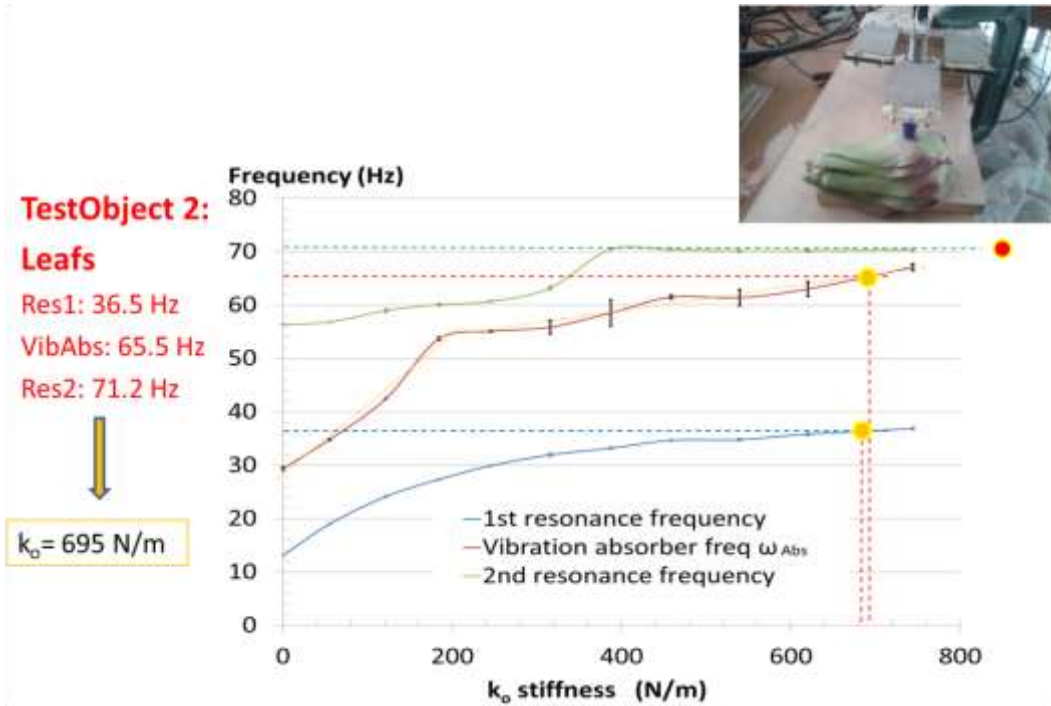


Figure 6.13: Test object 2, leaves

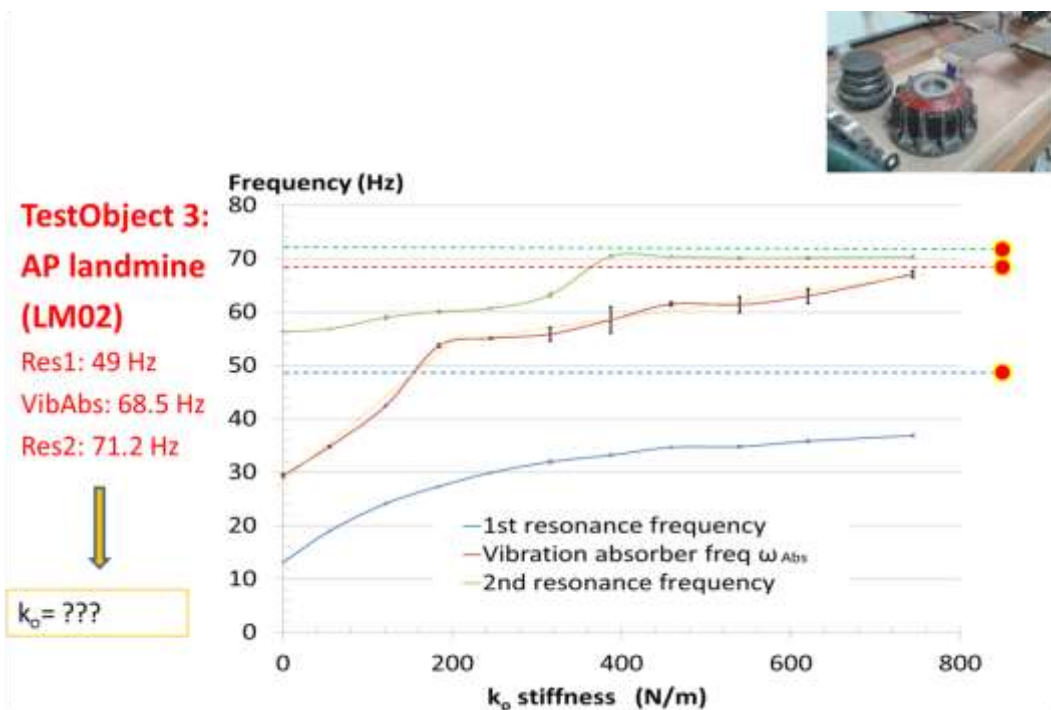


Figure 6.14: Test object 3, Anti-Personnel (LM02)

Figure 6.15 and Figure 6.16 locates the three frequencies of sand only and sand with metal.  
 Figure 6.17 and Figure 6.18 locates the three frequencies of clay only and clay with metal.

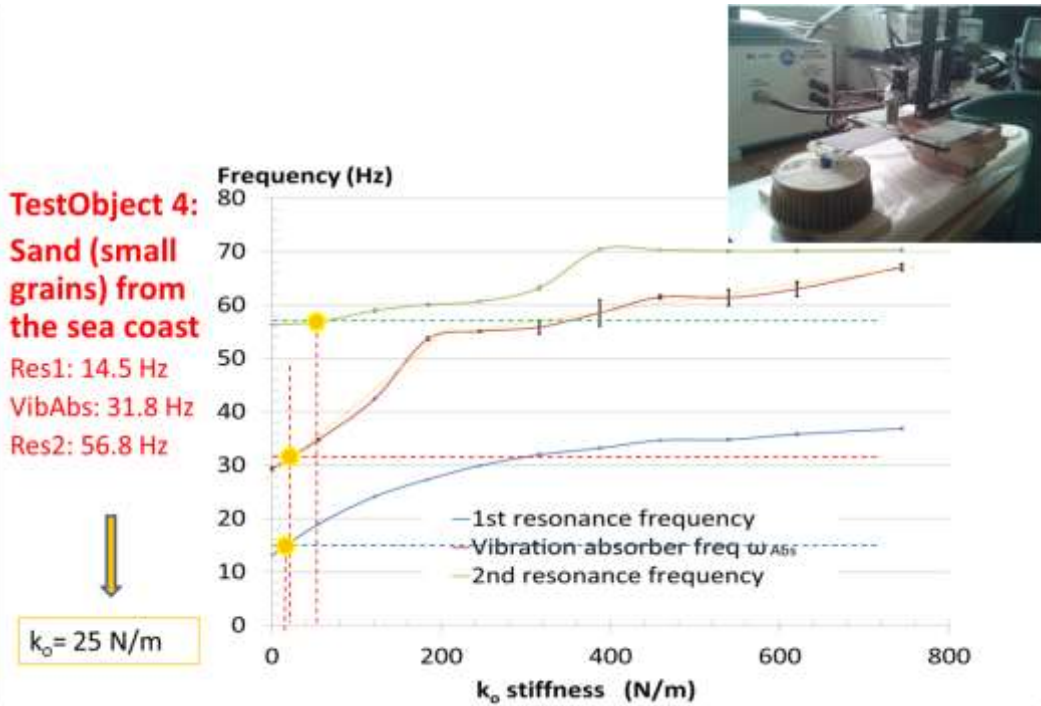


Figure 6.15: Test object 4, Sand from the sea coast

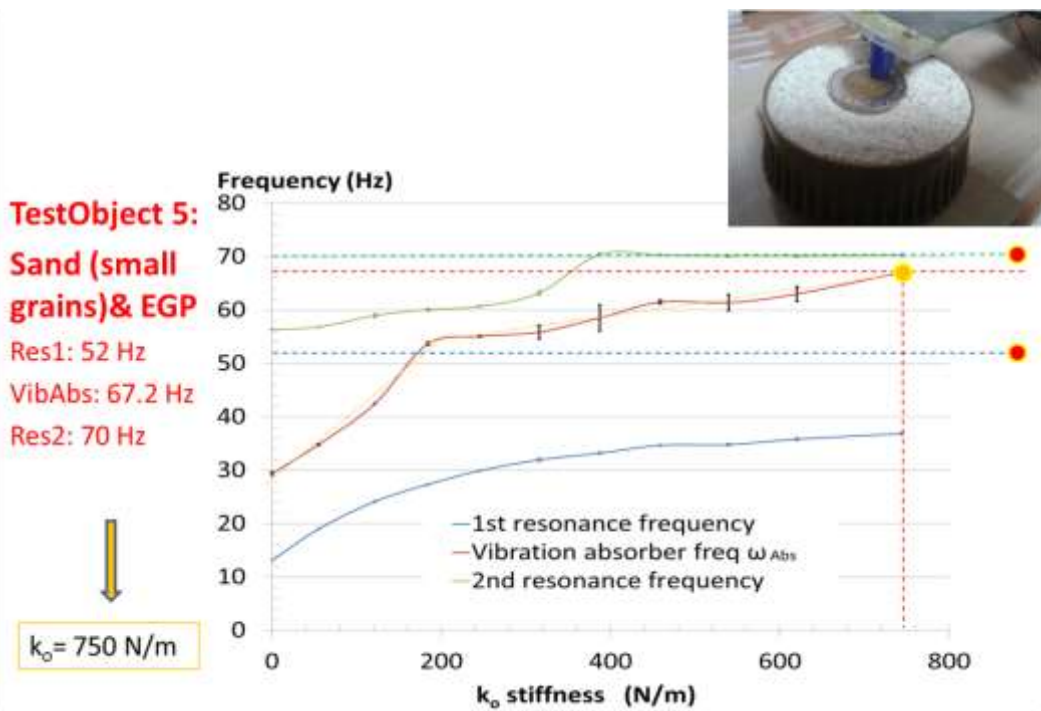


Figure 6.16: Test object 5, Sand and metal on the surface

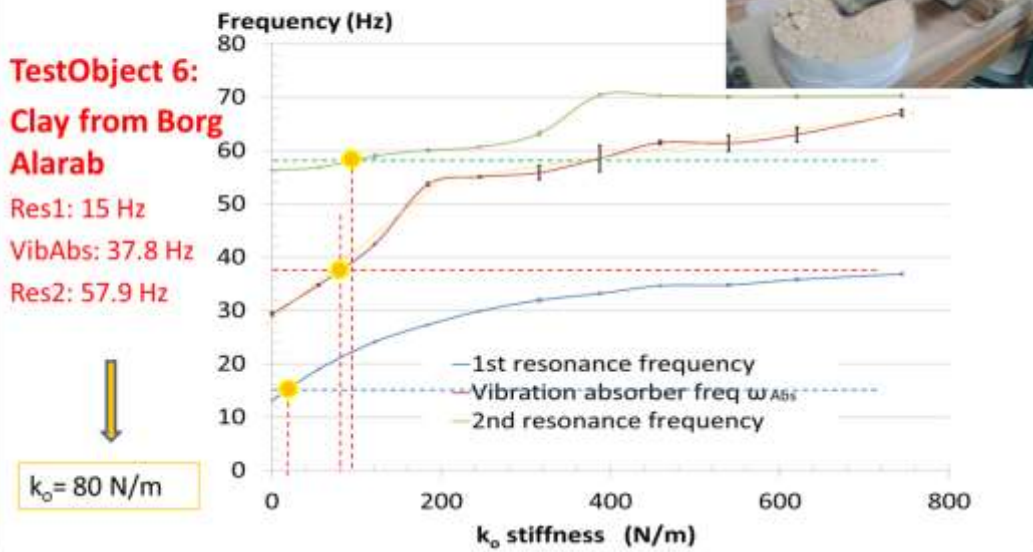


Figure 6.17: Test object 6, Clay from Borg Alarab

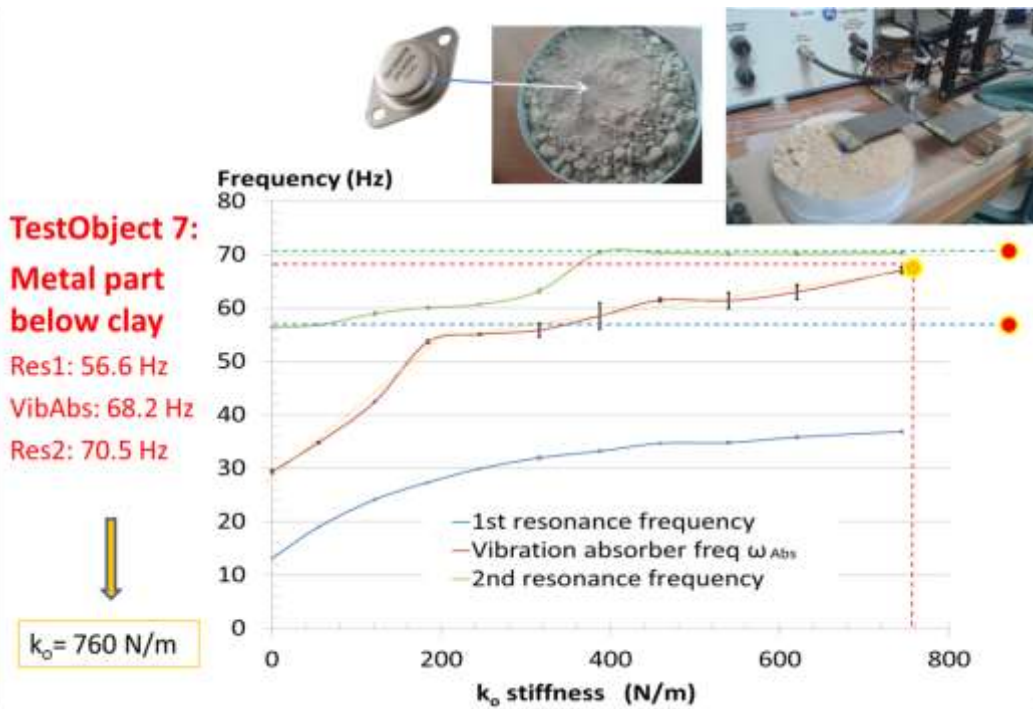


Figure 6.18: Test object 1, Metal part below clay





## **CHAPTER 7 :    STUDY SENSOR FABRICATION WITH MEMS TECHNOLOGY**

### **7.1 Miniaturization Advantages**

The proposed Stiffness Sensor using 2-DOF system based on Vibration Absorption Phenomenon is implemented with prototype in a macro-scale as shown in the previous chapter (Experimental Results). The core concept of sensing through vibration absorber mode of 2-DOF system can be utilized for many applications not only the landmine detection. Miniaturizing the sensor dimension has many advantages.

The main advantages of MEMS for engineering point of view [62]:

- Small systems tend to move or stop more quickly due to low mechanical inertia. It is thus ideal for precision movements and for rapid actuation.
- Smaller size of the systems means less space requirements. This allows the packaging of more functional components in a single device.
- Less material requirements mean low cost of production and transportation.
- Miniaturized systems encounter less thermal distortion and mechanical vibration due to low mass.
- Small systems have higher dimensional stability at high temperature due to low thermal expansion.
- Miniaturized devices are particularly suited for biomedical and aerospace applications due to their minute sizes and weight.
- Ready mass production in batches.

From the application point of view, the benefits of MEMS design of the sensor can be acquired with smart prodder (for landmine detection) and also for biomedical application.

## 7.2 MEMS Design

In MEMS design it is important to compact the architecture. For this reason, instead of building similar cantilevers to those in Figure 6.2 another more compact architecture is selected as shown in Figure 7.1.

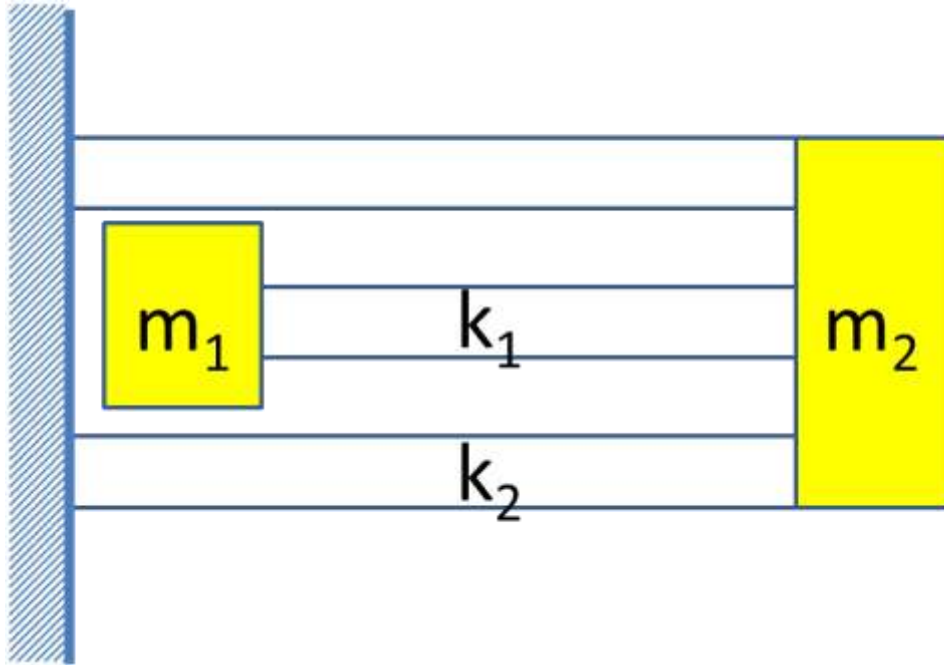


**Figure 7.1:** Layout 1 of the proposed sensor in MEMS.

In MEMS design the stiffness high or low can be acquired easily and the mass can be minimized also. But the mass  $m_1$  is limited by the indenter size.

So that starting from the indenter radius 5 mm, let the height = working stroke = 1 mm  
Silicon density =  $2.3 \text{ gm/cm}^3$ . This implies  $m_1$  at least = 0.18 gm.

Thus  $m_2 = 2 m_1 = 0.36 \text{ gm}$ ,

$$k_1 = 1.14 \times 10^5 \text{ N/m}, \quad k_2 = 2.28 \times 10^5 \text{ N/m},$$

$$\omega_{11} = \omega_{22} = 4.005 \text{ kHz}$$

And from the optimization process in Chapter 5,

$$k_1 = 1.14 \times 10^5 \text{ N/m}, \quad k_2 = 2.28 \times 10^5 \text{ N/m},$$

$$m_1 = 2.5 \text{ gm}, \quad m_2 = 2 m_1 = 5 \text{ gm}$$

$$\omega_{11} = \omega_{22} = 1.075 \text{ kHz}$$

Stiffness  $k_1 = 1.14 \times 10^5 \text{ N/m}$  can be obtained by many dimensions of the Silicon ( $E = 2 \times 10^{11} \text{ N/m}^2$ ) as follows in Table 7.1:

**Table 7.1:** Cantilever dimensions options to satisfy stiffness  $k_I=1.14 \times 10^5$  N/m

$k_1$	length $L_c$	width $w$	thickness $t$	Silicon E	$K= E w t^3 / (4L_c^3)$
#	mm	mm	mm	N/m <sup>2</sup>	N/m
1	15	2	1.565	2.00E+11	1.14E+05
2	15	7.7	1	2.00E+11	1.14E+05
3	12	2	1.255	2.00E+11	1.14E+05
4	12	3.95	1	2.00E+11	1.14E+05
5	10	1	1.318	2.00E+11	1.14E+05
6	10	2.28	1	2.00E+11	1.14E+05
7	5	1	0.658	2.00E+11	1.14E+05
8	5	0.285	1	2.00E+11	1.14E+05

### 7.3 Fabrication Process

Based on Table 7.1 the selected thickness is 1 mm and the length of cantilever1 is 10 mm and the length of cantilevers2 is 15 mm as shown in Figure 7.2. Also Figure 7.3 represents the schematic of the sensor on silicon wafer.

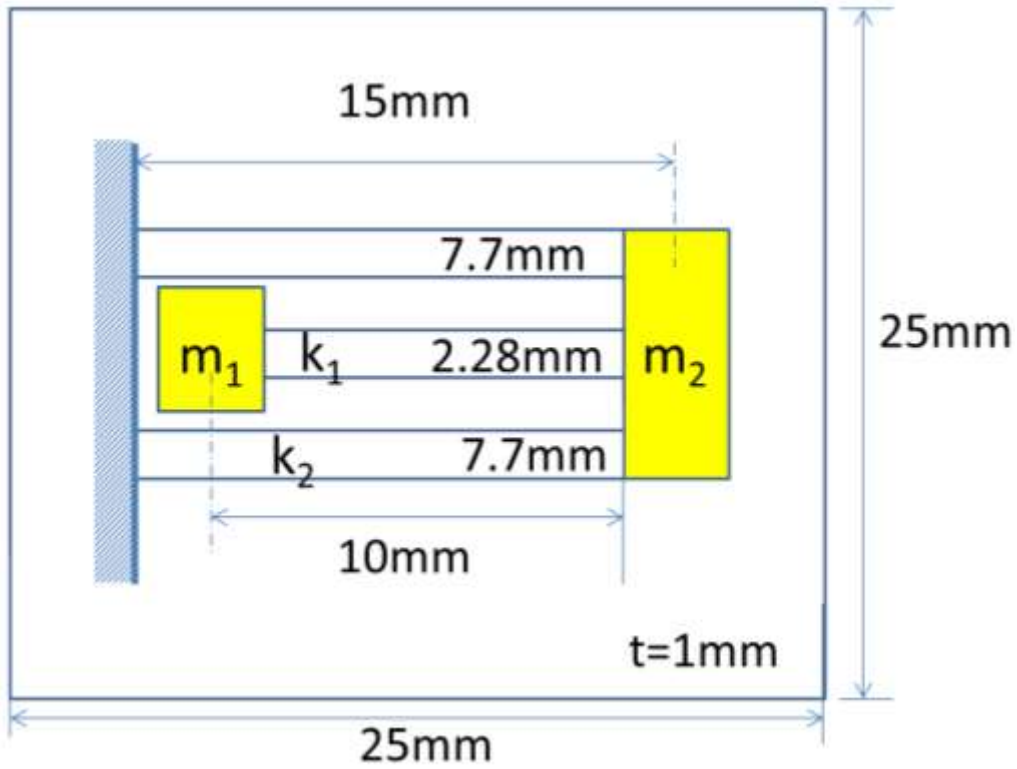


**Figure 7.2:** Layout of the proposed sensor in MEMS with dimensions.

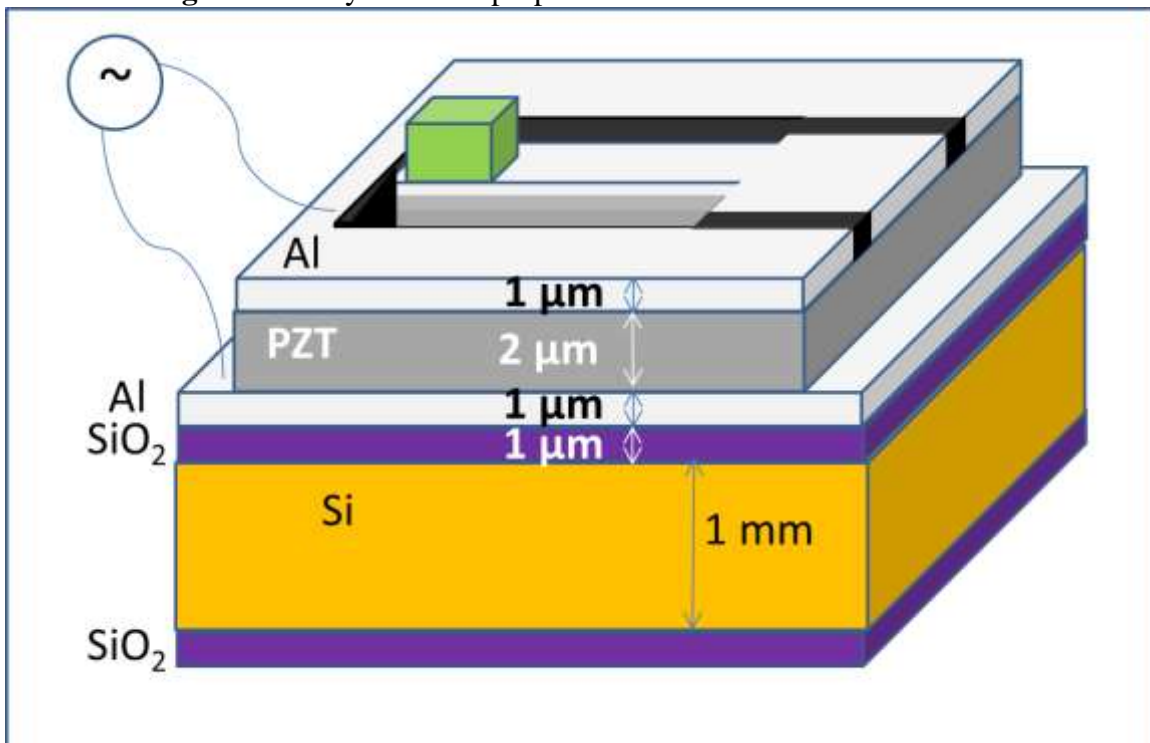


**Figure 7.3:** Schematic representation proposed sensor in MEMS.

As Figure 7.4 shows, the fabrication process of the stiffness sensor using 2-DOF vibration absorber system starts with silicon substrate of thickness 1 mm. then oxidation with  $O_2$  gas at  $110^\circ C$  that results around  $1 \mu m$  layer of Silicon dioxide ( $SiO_2$ ). In order to deposit by

sputtering the piezoelectric Lead Zirconate Titanate (PZT) layer, two layers of Aluminium (Al) must be deposited (one layer before the PZT and the other after). That is to supply the charge to the PZT through the two Al layers. A pattern is used before the Deep Reactive Ion Etching (DRIE). Finally, the cantilevers are formed by etching using KOH (potassium hydroxide) or TMAH (Tetramethyl Ammonium Hydroxide) to remove the SiO<sub>2</sub>, and Si.

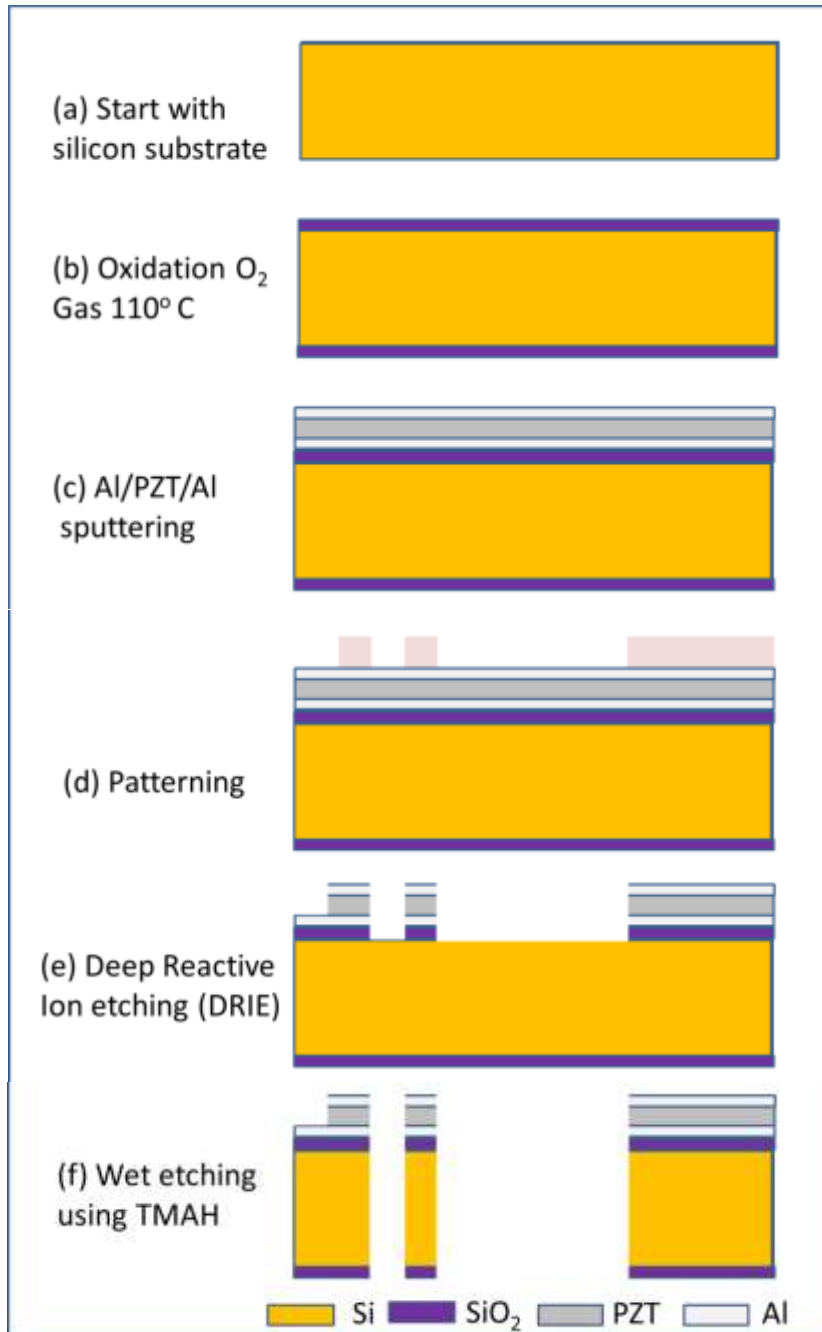


**Figure 7.4:** Fabrication process flow of stiffness sensor based on vibration absorber



## CHAPTER 8 : CONCLUSIONS AND FUTURE WORK

This work presents contact sensor design for landmine detection. Two main modeling perspectives, static loading and dynamic loading, are investigated.

The static loading model was developed to study the effect of landmine presence inside sand we applying 1 kPa. Neural networks are trained to distinguish between 5 kinds of objects and also to detect the depth. More over intensive studies and analysis are presented of landmine inclination angles effect and 20% noise effect to the detection rates.

The Dynamic loading models are also investigated for single DOF sensor and two DOF sensor detailed derivations and simulation are executed. Novel Stiffness Sensor using 2-DOF system based on Vibration Absorption Phenomenon is presented. Detailed finite element analysis is development in order to investigated the direct relation between the stiffness  $k_o$  and the vibration absorber frequency  $\omega_{Abs}$ . Experimental prototype is developed and its performance is evaluated.

### 8.1 Conclusions

The outcome of this work could be concluded in the followings:

- 1- Buried objects give different pressure distribution at the sand surface when exposed to pressure loading 1 kPa. 2D FEMs are studied for different objects in sand at different depths. The proposed inverse approach based on NN is a reliable and efficient tool for LM detection.
- 2- PNN is used to detect the object type. The true alarm rates for training LM01 is 100%, and for LM02 is 67%, while, for validation LM01 is 95%, LM02 is 70%.
- 3- The effect of LM inclination angles ( $0^\circ$ - $30^\circ$ ) is studied at depths (50, 100, 150, 200mm). The results show same detection rates as those at no inclination.
- 4- At inclination angle  $0^\circ$ , there is no error in the FFNN when detecting the depth. The error increases as the inclination angle increases. And the error of the inclination angle is dominant as the LM is closer to the sand surface.
- 5- The effect of random noises 5%, 10%, and 20% of the signal average is studied. 10% noise doesn't affect the true alarms of LM01 and LM02, which are the same 95% and 70% respectively as in validation data with no noise.

- 6- Novel contact stiffness sensor has been introduced with a detailed design procedure for landmine detection, based on the concept of 2-DOF vibration absorber system.
- 7- Simplified mathematical model has been introduced and simulated with MATLAB and verified with finite element with COMSOL.
- 8- The measuring range of the sensor is chosen to be associated with typical sand Young's modulus values: up to 150 MPa and at indenter radius 5 mm. This gives the stiffness range (0-2 MN/m).
- 9- The sensor design parameters are selected to satisfy the vibration absorber phenomenon, and optimized to give high sensitivity and good linearity. It can give as high sensitivity as 1559 Hz / (MN/m) and linearity ( $R^2 = 95\%$ ).
- 10- The main advantage of this idea is that the frequency ( $\omega_{Abs}$ ) searching is done away from the resonance points of the system. Also comparing with the 1<sup>st</sup> and 2<sup>nd</sup> natural frequency the relation between  $\omega_{Abs}$  and  $k_o$  has highest sensitivity and good linearity.
- 11- Experimental prototype is developed to prove the concept which indicates that:
  - The 1<sup>st</sup> resonance is the worst: lower sensitivity, lower linearity and high deflection amplitude which may cause failure,
  - while the 2<sup>nd</sup> resonance has wider linearity range.
  - On the other hand, the ( $\omega_{Abs}-k_o$ ) relation has the highest sensitivity in the linear zone. The Sensitivity is as high as 7.58 Hz/(N/m).



## 8.2 Future Work

The following are some of the problems that may be attempt in the future research work:

1. Study the electromechanical coupling in the piezoelectric transducers.
2. Development of real scale sensor prototype (the vibration absorber based stiffness sensor) for sand-landmine problem (stiffness range 0-2 MN/m).
3. Extending the proposed measurement concept (the vibration absorber based stiffness sensor) to other applications like the tissue compliance sensing.
4. Automate the searching process of the three frequency modes (1<sup>st</sup> natural frequency, vibration absorber frequency, and the 2<sup>nd</sup> natural frequency) for example with NI-DAQ system and LAB-VIEW software.
5. Utilization of artificial intelligence techniques like (Fuzzy logic and Neural Networks) to gain the best stiffness detection using the three frequency modes.
6. Enhance the MEMS design of the propose vibration absorber based sensor model. Then fabricate and test.



## REFERENCES

- [1] “Landmine Monitor 2015”, International Campaign to Ban Landmines – Cluster Munition Coalition (ICBL-CMC), 2015.  
ISBN: 978-2-8399-1707-0
- [2] S.M. Megahed, H.F.M. Ali and A.H. Hussein, “Egypt Landmine Problem: History, Facts, Difficulties and Clearance Efforts”, International Symposium Humanitarian Demining 2010, Šibenik, Croatia, 2010.
- [3] K. Furuta, J. Ishikawa (Eds.), “Anti-personnel Landmine Detection for Humanitarian Demining”, Springer, 2009.  
ISBN: 978-1-84882-346-4
- [4] “Detectors and Personal Protective Equipment Catalogue 2009”, GICHD: Geneva International Centre for Humanitarian Demining, Geneva, 2009.
- [5] J. Macdonald, J.R. Lockwood, J. Mcfee, T. Altshuler, T. Broach, L. Carin, R. Harmon, C. Rappaport, W. Scott, and R. Weaver, “Alternatives for Landmine Detection” (Pittsburg, PA: RAND), 2003.
- [6] M. Habib, “Humanitarian Demining Innovative Solutions and the Challenges of Technology”, ARS Publisher, 2008.
- [7] H.F.M. Ali, “Requirements and Design Constraints of a Demining Robot Prototype with its Kinematic Modeling, Simulation and Experimentation”, M.Sc. Thesis, Cairo University, 2011.
- [8] K.M. Dawson-Howe and T.G. Williams, “The Detection of Buried Landmines Using Probing Robots” *Robot. Auto. Syst.*, vol. 23, no. 4, pp. 235-243, 1998.
- [9] N. Furihata and S. Hirose, “Development of Mine Hands: Extended Prodder for Protected Demining Operation” *Auto. Robots*, vol. 18, no. 3, pp. 337-350, 2005
- [10] S.M. Megahed, H.F.M. Ali, “Remotely Operated Robots with Application to Landmines Removal in Egypt”, 43<sup>rd</sup> Intl. Symp. on Robotics (ISR2012), Taipei, Taiwan, 2012.

- [11] A.K. Sinha and S.D. Mehta, "Detection of Landmines", Defence Science Journal, vol. 51, pp. 115-131, 2001.
- [12] S. Baglio, G. Muscato and N. Savalli, "A Smart Tactile Piezo Sensor for Material Recognition", in The 14<sup>th</sup> European Conference on Solid-State Transducers, EURO-SENSORS XIV, Copenhagen, 2000.
- [13] S. Baglio, G. Muscato and N. Savalli, "Tactile Measuring Systems for the Recognition of Unknown Surfaces", IEEE Transaction on Instrumentation and Measurement, vol. 51, no. 3, pp. 522-531, 2002.
- [14] S. Baglio, G. Muscato and N. Savalli, "Hybrid Tactile Probe for Damage Detection and Material Recognition", in Smart Nondestructive Evaluation and Health Monitoring of Structural and Biological Systems conference at SPIE's Smart Structures and Materials and NDE for Health Monitoring and Diagnostics 2003 co-located meetings, 2003.
- [15] D. Antonic and M. Zagar, "Method for Determining Classification Significant Features from Acoustic Signature of Mine-like Buried Objects", in 15<sup>th</sup> World Conference on Non-Destructive Testing, Rome, 2000.
- [16] D. Antonic, "Creating ROC by Altering Classification Rule", in 3<sup>rd</sup> European-American Workshop on Reliability of NDE and Demining, Berlin, 2002.
- [17] D. Melville, "User Evaluation Report: SmartProbe Instrumented Prodder", in Land Forces Trials and Evaluation Unit, Oromocto, 1999.
- [18] H.F. Research Inc, "Force and Temperature Compensation for the Instrumented Prodder", in Contract Report, CR 2002-114, Suffield, Defence R&D Canada, 2002.
- [19] A.J. Schoolderman, S.G.M. Van Dijk and D. Deurloo, "Instrumented Prodder: Results from Tests under Controlled Conditions", in Technical Report TNO, 2003.
- [20] A.J. Schoolderman, S.G.M. Van Dijk and D. Deurloo, "Instrumented Prodder: Preliminary Results of the Technology Demonstrator Evaluation", Proc. of the International Conference on Requirements and Technologies for the Detection, Removal and Neutralization of Landmines and UXO, vol. 2, pp. 673-679, 2003.
- [21] M.A. Borza and F.G. DeWitt, "Acoustic Landmine Prodding Instrument with Force Feedback", U.S. Patent 6,109,112, 2000.
- [22] M.A. Borza, "Prodder with Force Feedback", U.S. Patent 6,386,036, 2002.
- [23] R. Gasser and T. Thomas, "Prodding to detect mines: a technique with a future", in 2<sup>nd</sup> IEE International Conference on Detection of Abandoned Landmines, Edinburgh, 1998.

- [24] R. Gasser, "Technology for Humanitarian Demining", PhD Thesis, University of Warwick, 2000.
- [25] R. Gasser, "Feedback Prodders: A Training Tool to Improve Deminer Safety", 2001. Available Online: <http://www.maic.jmu.edu/journal/5.2/features/prodders.html>.
- [26] D. Antonic, "Analysis and Interpretation of Ultrasonic Prodder Signal", in MATEST 2003 - Achievements & Challenges / Krstelj, Vjera(ed), Brijuni, Pula, 2003.
- [27] J. Stepanic, G. Maric and Z. Schauerperl, "Improving Integration of Ultrasonic Sensor and Hand Probe", in ECNDT European Federation of Non-Destructive Testing, 2006.
- [28] A. Bulletti, S. Valentini, F. Cioria, G. Borgioli, M. Calzolari, L. Capineri and L. Masotti, "Silicon Micromachined Accelerometers for the Detection of Compliant Anti-personnel Landmines", IEEE SENSORS 2008 Conference, 2008.
- [29] D.M. Donskoy, A. Reznik, A. Zagrai, and A. Ekimov, "Nonlinear Vibrations of Buried Landmines", J. Acoust. Soc. Am. 117 (2), 2005.
- [30] D.M. Donskoy, "Nonlinear Vibro-acoustic Technique for Land Mine Detection", SPIE's Proceedings on Detection and Remediation Technologies for Mines and Minelike Targets III, Vol. 3392, 1998.
- [31] D.M. Donskoy, A. Ekimov, N. Sedunov, and M. Tsionskiy, "Nonlinear Seismo-acoustic Land Mine Detection and Discrimination", J. Acoust. Soc. Am. 111(6), 2705-2714, 2002.
- [32] D.M. Donskoy, A. Ekimov, N. Sedunov, and M. Tsionskiy, "Nonlinear Seismo-acoustic Land Mine Detection: Field Test", SPIE's Proceedings on Detection and Remediation Technologies for Mines and Minelike Targets VII, Vol. 4742, pp. 685-695, 2002.
- [33] C.T. Schröder and W.R. Scott, "A Finite-Difference Model to Study the Elastic-Wave Interactions with Buried Land Mines", IEEE Transactions on Geoscience and Remote Sensing, vol. 38, no. 4, 2000.
- [34] W.R. Scott, J.S. Martin, and G.D. Larson, "Experimental Model for a Seismic Landmine Detection System", IEEE Transactions on Geoscience and Remote Sensing, vol. 39, no. 6, 2001.
- [35] J.S. Martin, G.D. Larson, and W.R. Scott, "Surface-Contacting Vibrometers for Seismic Landmine Detection", Proc. of SPIE Vol. 5794 (SPIE, Bellingham, WA), 2005.  
DOI: 10.1117/12.603923

- [36] J.S. Martin, G.D. Larson, and W.R. Scott, "An Investigation of Surface-contacting Sensors for the Seismic Detection of Buried Landmines", *J. Acoust. Soc. Am.*, Vol. 120, No. 5, 2006.
- [37] J. Ishikawa, and A. Iino, "A Study on Prodding Detection of Antipersonnel Landmine Using Active Sensing Prodder", *International Symposium: Humanitarian Demining 2010*, Šibenik, Croatia, 2010.
- [38] S. Baglio, L. Cantelli, C. Costantino, F. Giusa and G. Muscato, "A Survey on Instrumented Prodding Techniques for Landmine Recognition" *Proc. 10th Int. Symp. Humanitarian Demining Coupled (IARP WS HUDEM)*, Šibenik, Croatia, 2013.
- [39] S. Baglio, G. Muscato and N. Savalli, "Tactile measuring systems for the recognition of unknown surfaces", *IEEE Trans. Instrum. Meas.*, vol. 51, no. 3, pp. 522-531, 2002.
- [40] S. Baglio, L. Cantelli, F. Giusa, G. Muscato and A. Noto, "A Novel Smart Prodder with Sensor Feedback for Material Recognition in Humanitarian Demining Applications" *Proc. IEEE SENSORS*, pp. 779-782, Valencia, Spain, 2014.
- [41] S. Baglio, L. Cantelli, F. Giusa, and G. Muscato, "Intelligent Prodder: Implementation of Measurement Methodologies for Material Recognition and Classification With Humanitarian Demining Applications", *Instrumentation and Measurement, IEEE Transactions on*, vol.64, no.8, pp.2217,2226, 2015.  
DOI: 10.1109/TIM.2014.2386917
- [42] J.M. Muggleton, M.J. Brennan, and C.D.F. Rogers, "Point vibration measurements for the Detection of Shallow-buried Objects", *Tunnelling and Underground Space Technology* (39) 27–33, 2014.
- [43] F. Pennec, H. Achkar, D. Peyrou, R. Plana, P. Pons, and F. Courtade, "Verification of Contact Modeling with Comsol Multiphysics Software", *Rapport LAAS n07604*. 2007.  
<hal-00180257>
- [44] "Structural Mechanics Module Verification Manual", Comsol Multiphysics, © Copyright 1994–2008.
- [45] Y. Matriche, M. Feliachi, A. Zaoui, and M. Abdellah, "An EMI Inversing Problem For Landmine Characterization Based On Improved Particle Swarm Optimization And Finite Element Analysis", *Progress In Electromagnetics Research B*, Vol. 49, 411–428, 2013.

- [46] Z. Zyada, T. Matsuno and T. Fukuda, “Fuzzy Template Based Automatic Landmine Detection from GPR Data”, the 7th IARP International WS HUDEM'2008, AUC, Cairo, 2008.
- [47] K. O’Neill, F. Shubitidze, I. Shamatava, and K.D. Paulsen, “Accounting for the Effects of Widespread Discrete Clutter in Subsurface EMI Remote Sensing of Metallic Objects”, IEEE Transactions on Geoscience and Remote Sensing, Vol. 44, No. 1. 32–46, 2006.
- [48] J.T. Miller, T.H. Bell, J. Soukup, and D. Keiswetter, “Simple Phenomenological Models for Wideband Frequency-domain Electromagnetic Induction”, IEEE Transactions on Geoscience and Remote Sensing, Vol. 39, No. 6, 1294–1298, 2001.
- [49] M.W. Asten, “On the Time-domain Electromagnetic Response of a Conductive Permeable Sphere”, Journal of Applied Geophysics, Vol. 67, 63–65, 2009.
- [50] K. Moustafa, and K.F.A. Hussein, “Aperture Sensor GPR System for Land Mine Detection”, Progress In Electromagnetics Research, Vol. 72, 21–37, 2007.
- [51] M. Nishimoto, K. Nagayoshi, S. Ueno, and Y. Kimura, “Classification of Landmine-Like Objects Buried under Rough Ground Surfaces Using a Ground Penetrating Radar”, IEICE Transactions on Electronics, Vol.E90-C, No.2, pp.327-333, 2007.
- [52] H.F.M. Ali, Z. Zyada, A.M.R. Fath El-Bab, and S.M. Megahed, “Inclination Angle Effect on Landmine Detection Estimation in Sandy Desert using Neural Networks”, The 10<sup>th</sup> Asian Control Conference, IEEE (ASCC 2015), 2015.  
DOI: 10.1109/ASCC.2015.7244615
- [53] Jaeger Platoon Website, <http://www.jaegerplatoon.net/landmines2.htm>, last checked Dec-2015.
- [54] AbsoluteAstronomy Website,  
[http://www.absoluteastronomy.com/topics/List\\_of\\_landmines](http://www.absoluteastronomy.com/topics/List_of_landmines), last checked Dec-2015.
- [55] H.V. Kamat, D.H. Rao, “Direct Adaptive Control of Non-linear Systems using a Dynamic Neural Network”, IEEE Trans. Automat.Contr. 1995; 39: 987–991, 1995.
- [56] W.T. Thomson, “Theory of Vibration with Applications”, Springer US, 1993.
- [57] J.W. Harding, I.N. Sneddon, “The Elastic Stresses Produced by the Indentation of the Plane Surface of a Semi-infinite Elastic Solid by a Rigid Punch”, Mathematical Proceedings of the Cambridge Philosophical Society, Volume 41, Issue 01, pp.16-26, 1945.

- [58] R. Obrzud and A. Truty, “The Hardening Soil Model - A Practical Guidebook”, Z Soil. PC 100701 report, revised 31.01.2012.
- [59] A. Kezdi, “Handbook of Soil Mechanics”, Elsevier, Amsterdam, 1974.
- [60] M. Prat, E. Bisch, A. Millard, P. Mestat, and G. Cabot, “La Modelisation des Ouvrages”, Hermes, Paris, 1995.
- [61] Geotechdata.info, “Soil Young's Modulus”, site:  
<http://www.geotechdata.info/parameter/soil-young's-modulus.html> (09.2013), check 3-2016.
- [62] T.R. Hsu, “MEMS and Microsystems: Design, Manufacture, and Nanoscale Engineering,” 2<sup>nd</sup> Edition, John Wiley & Sons, Inc., Hoboken, New Jersey, 2008.  
ISBN: 978-0-470-08301-7



## APPENDIX A: SENSORS TECHNOLOGIES COMPARISON

The table A.1 compares the known technologies in the field of demining sensors [4].

**Table A.1:** Summary of the Detection Technologies Reviewed

#	Technology	Operating Principle	Strengths	Limitations	Potential for Humanitarian Mine Detection
	<b>Electromagnetic</b>				
1	Electromagnetic Induction	Induces electric currents in metal components of mine	Performs in a range of environments	Metal clutter; low metal mines	<b>Established technology</b>
2	Ground-penetrating Radar	Reflects radio waves off mine/soil interface	- Metallic/non-metallic - has the capability of imaging the target shape	Roots, rocks, water pockets, other natural clutter; extremely moist or dry environments	<b>Established technology</b>
3	Electrical impedance Tomography	Determines electrical conductivity distribution	Detects all anomalies, even if nonmetal	Dry environments; can detonate mine	Unlikely to yield major gains
4	X-ray backscatter	Images buried objects with x rays	Advanced imaging Ability	Slow; emits radiation	Unlikely to yield major gains
5	Infrared/hyperspectral	Assesses temperature, light reflectance differences	Operates from safe standoff distances and scans wide areas quickly	Cannot locate individual mines	Not suitable for close-in detection

**Table 1: Summary of the Detection Technologies Reviewed (cont'd)**

#	Technology	Operating Principle	Strengths	Limitations	Potential for Humanitarian Mine Detection
<b>Acoustic/Seismic</b>					
6	Acoustic/Seismic	<b>Reflects sound or seismic waves</b> off mines	Low false alarm rate; not reliant on electromagnetic Properties	Deep mines; vegetation cover; frozen ground	<b>Promising</b>
<b>Advanced Prodders/Probes (touch sensors)</b>					
7	Advanced Prodders/ Probes	Provide <b>feedback</b> about nature of probed object and amount of force applied by probe	Could deploy almost any type of detection Method	Hard ground, roots, rocks; requires physical contact with mine	<b>Promising</b>
<b>Bulk Explosives</b>					
8	Nuclear quadrupole Resonance	Induces <b>radio freq. pulse</b> that causes the <b>chemical bonds in explosives to resonate</b>	Identifies bulk Explosives	TNT; liquid explosives; radio freq. interference; quartzbearing and magnetic soils	Promising
9	Neutron	Induces <b>radiation emissions</b> from the atomic nuclei in Explosives	Identifies the elemental content of bulk explosives	Not specific to explosives molecule; moist soil; ground surface fluctuations	Unlikely to yield major gains

**Table A.1:** Summary of the Detection Technologies Reviewed (cont'd)

#	Technology	Operating Principle	Strengths	Limitations	Potential for Humanitarian Mine Detection
	<b>Explosive Vapor</b>				
<b>10</b>	Biological (dogs, bees, bacteria)	Living organisms detect explosive vapors	<b>Confirms presence of Explosives</b>	Dry environments	Basic research needed to determine potential (dogs are widely used)
<b>11</b>	Fluorescent	Measures changes in polymer <b>fluorescence</b> in presence of explosive vapors		Dry environments	Basic research needed to determine operational potential
<b>12</b>	Electrochemical	Measures changes in polymer <b>electrical resistance</b> upon exposure to explosive vapors		Dry environments	Basic research needed to determine operational potential
<b>13</b>	Piezoelectric	Measures shift in <b>resonant frequency</b> of various materials upon exposure to explosive vapors		Dry environments	Basic research needed to determine operational potential
<b>14</b>	Spectroscopic	Analyzes <b>spectral response</b> of sample		Dry environments	Basic research needed to determine operational potential

## LIST OF PUBLICATIONS

### Journals:

- 1- **Hussein F.M. Ali**, Ahmed M. R. Fath El Bab, Zakarya Zyada, and Said M. Megahed "Estimation of Landmine Characteristics in Sandy Desert using Neural Networks", Journal of Neural Computing and Applications, Springer, (Accepted: Dec 21, 2015). DOI: 10.1007/s00521-015-2153-z (Impact factor: 1.6)

### Conferences:

- 2- **Hussein F.M. Ali**, Ahmed M. R. Fath El Bab, Zakarya Zyada, and Said M. Megahed "Novel Contact Sensor Concept and Prototype based on 2-DOF Vibration Absorber System", Intelligent Systems, Modelling and Simulation, IEEE 7<sup>th</sup> International Conference, ISMS 2016. DOI 10.1109/ISMS.2016.70
- 3- **Hussein F.M. Ali**, Zakarya Zyada, Ahmed M. R. Fath El-Bab, and Said M. Megahed "Inclination Angle Effect on Landmine Detection Estimation in Sandy Desert using Neural Networks", The 10<sup>th</sup> Asian Control Conference, IEEE (ASCC 2015). DIO: 10.1109/ASCC.2015.7244615

---

### Patents:

- 4- **Hussein F.M. Ali**, Ahmed M. R. Fath El-Bab, Zakarya Zyada, and Said M. Megahed, "Stiffness Sensor Design for landmines detection using 2-DOF system based on Vibration Absorption Phenomenon" Egypt Patent No. 1782/2015, filed on 10 Nov 2015.

---

### Under review:

- 5- "Novel Contact Sensor Prototype using 2-DOF Vibration Absorber for Landmine Detection"
- 6- "Parameter Optimization of a Novel Contact Sensor Based on Frequency Response of 2-DOF Vibration Absorber System for Landmine Detection"



## مجس تلامس مستحدث للكشف عن الألغام

إعداد

حسين فؤاد محمد على

رسالة علمية مقدمة الى المدرسة التخصصية للدراسات العليا  
فى هندسة التصميم الإبداعي  
الجامعة المصرية اليابانية للعلوم والتكنولوجيا  
كاستيفاء جزئي لمتطلبات الحصول على درجة دكتوراه الفلسفة  
فى

هندسة الميكاترونيات والروبوتات

مارس 2016

## مجس تلامس مستحدث للكشف عن الألغام

مقدمة من

حسين فؤاد محمد على

للحصول على درجة دكتوراه الفلسفة

فى

هندسة الميكاترونيات والروبوتات

### لجنة الاشراف على الرسالة

- | التوقيع   | جهة العمل  | الاسم:                             |
|---|--|------------------------------------|
|    | جامعة القاهرة - كلية الهندسة<br>(مشرف رئيسي)                   | 1. أ.د/ سعيد محمد مجاهد            |
|   | الجامعة المصرية اليابانية للعلوم والتكنولوجيا<br>(مشرف مساعد)  | 2. أ.م.د/ أحمد محمد رشاد فتح الباب |
|  | جامعة طنطا - مصر، الجامعة التكنولوجية بماليزيا<br>(مشرف مساعد) | 3. أ.م.د/ زكريا على زيادة          |

### لجنة المناقشة والحكم على الرسالة

- | التوقيع   | جهة العمل  | الاسم:                             |
|---|--|------------------------------------|
|  | كلية الهندسة - جامعة بنها - مصر<br>(رئيس اللجنة - ممتحن خارجي) | 1. أ.د/ أحمد العسال                |
|  | كلية الهندسة - جامعة الإسكندرية - مصر<br>(ممتحن خارجي)         | 2. أ.د/ سهير فتحى رزيقة            |
|  | جامعة القاهرة - كلية الهندسة<br>(مشرف رئيسي)                   | 3. أ.د/ سعيد محمد مجاهد            |
|  | الجامعة المصرية اليابانية للعلوم والتكنولوجيا<br>(مشرف مساعد)  | 4. أ.م.د/ أحمد محمد رشاد فتح الباب |

قائم بأعمال نائب رئيس الجامعة للتعليم والشئون الأكاديمية

أ.د. / منى جمال الدين



## ملخص الرسالة

تعاني مناطق كثيرة في العالم من مشكلة الألغام الأرضية والتي تعيق إستغلال الموارد بشكل كبير. وبناءً على الكثير من الأبحاث الحديثة يتأكد للباحث الإمكانات الواعدة لأجهزة الاستشعار التي تعتمد على التلامس. ولضمان إعتمادية عالية لأنظمة استشعار الألغام يستلزم هذا التحليل العميق والكثير من حالات الإختبار والتجارب العملية.

يستند البحث المقترح على تحميل سطح الأرض بضغط ثابت قيمته (1kPa - أقل من ضغط تفجير اللغم) وبناءً على شكل رد الفعل الناتج على سطح الأرض يمكن تحديد نوع الجسم المطمور وكذلك تحديد عمقه تحت الرمال. تم تدريب شبكات عصبية (NN) لبحث إمكانية إيجاد حل عكسي لمسألة وجود لغم تحت الرمال. بمعنى أنه عندما يكون رد فعل الضغط معلوم التوزيع، يمكن للشبكة العصبية تقدير حجم ونوع وعمق الجسم. تم في هذا البحث دراسة وتحليل وجود لغم في الرمال باستخدام النمذجة متناهية الصغر (FE). ومن ثم أُسُخِدم توزيع الضغوط الناتجة عن وجود خمسة أنواع مختلفة من المجسمات داخل الرمال في تدريب الشبكات العصبية (NN). تم تطوير ثلاث شبكات عصبية (NN) لتقدير خصائص الألغام الأرضية. الأولى من النوع الإدراكي (PNN) والتي دُرِبَت لِتُصَنَّفِ الأجسام المطمورة في الرمال، أما الأثنين الأخرين فهما من نوع التغذية الأمامية (FFNN) والتي دُرِبَت لِتَقْوِمَ بتقدير عمق نوعين من الألغام تحت الأرض.

وعلى مستوى التحقق من أداء الشبكات العصبية (NN) كانت معدلات التصنيف الصحيح 95% للألغام المضادة للدبابات و70% للألغام المضادة للأفراد. وتم عمل مجموعتين من حالات الإختبار: المجموعة الأولى للألغام مائله بزوايا مختلفة ( $0^{\circ}$ - $30^{\circ}$ ) والمجموعة الثانية بها إضافة نسبة (10%-20%) ضوضاء عشوائية من متوسط الإشارة.

في هذا البحث تم تقديم تصور جديد للكشف عن الألغام بجهاز إستشعار تلامس. الأساس العلمي لهذا الجهاز يعتمد على ظاهرة إمتصاص الإهتزازات لمنظومة ثنائية درجات الحرية (كتلتين وزنبركين) وذلك لتستشعر وجود جسم (لغم على سبيل المثال) في الرمال والمُؤمَدَج بزنبك ثالث. يمكن التعبير عن درجة صلابة الرمال (الزنبرك الثالث) كدالة في تردد ظاهرة إمتصاص الإهتزازات ( $\omega_{Abs}$ ) وهو التردد الذي تكون عنده إزاحة الكتلة الثانية (صفر - كما أُثْبِتَت نظرياً). وعندما تتغير درجة صلابة الرمال نتيجة لوجود لغم تحتها يتغير تبعاً لهذا تردد إمتصاص الإهتزازات ( $\omega_{Abs}$ ) وبالتالي يمكن إكتشاف وجود اللغم. تم التحقق من العلاقة ( $\omega_{Abs}-k_0$ ) المثبتة نظرياً ببرامج محاكاة على الـ (Matlab) وكذلك نماذج العناصر المحدودة (FE) على برنامج (COMSOL Multi-physics). تمكنت المنظومة من قياس معامل صلابة الرمال في مدى (0-2 MN/m). وتم التنفيذ العملي والتجارب لنموذج مصغر وفي مدى أقل محققاً درجة حساسية (7.58 Hz / (N/m)). وأيضاً تم تحديد خطوات إجراء التصميم لجهاز إستشعار الصلابه بالتلامس للكشف عن الألغام.

وأخيراً، تم عمل دراسة تصنيع جهاز الإستشعار بواسطة تقنية النظم الكهروميكانيكية الدقيقة (MEMS) بما في ذلك خطوات التصميم والتصنيع.



مجس تلامس مستحدث للكشف عن الألغام

إعداد

حسين فؤاد محمد علي

رسالة نظمية مقدمة الى المدرسة التخصصية للدراسات العليا  
في هندسة التصميم الإبداعي  
الجامعة المصرية اليابانية للعلوم والتكنولوجيا  
كاستيفاء جزئي لمتطلبات الحصول على درجة دكتوراه الفلسفة  
في

هندسة الميكاترونيات والروبوتات

مارس 2016





NOVEL CONTACT SENSOR FOR LANDMINE  
DETECTION

by

Hussein Fouad Mohamed Ali

A Thesis Submitted to the  
Graduate School of Innovative Design Engineering,

Egypt-Japan University of Science and Technology (E-JUST)

In Partial Fulfillment of the Requirements for the Degree of  
Doctor of Philosophy

in

Mechatronics and Robotics Engineering

March 2016